# Modeling and Analysis of Chromosome Attachment Error Correction and Congression During Mitosis

A DISSERTATION
SUBMITTED TO THE FACULTY OF THE
UNIVERSITY OF MINNESOTA
BY

**Emily S. Tubman**

IN PARTIAL FULFILLMENT OF THE REQUIREMENTS
FOR THE DEGREE OF
DOCTORY OF PHILOSOPHY

Written under the advisement of Professor David J. Odde
May 2016

## Acknowledgements

I would first like to thank my advisor, David Odde, who has provided me with more opportunities to develop as a scientist and leader than I ever expected upon entering graduate school. From using dance to deconstruct mathematical models to inviting me to be his teaching assistant at the Marine Biological Laboratory Physiology Course where I was exposed to the world's best and brightest scientists, not once but twice, I will be eternally grateful. I thank members of the Odde lab: Dominique Seetapun, Brannon McCullough, Brian Castle, Becky Markovitz, Ben Bangasser, Louis Prahl, Ghaidan Shamsan, Mahya Hemmat, and Horacio Estabridis for helpful discussions. I thank undergraduate students: Allison Claas, Kelsey McCoy, and Teahl Banner, whose dedication to their projects while juggling full course loads was truly admirable. To Tom Hays and members of the Hays' lab, especially Yungui He, I am very grateful for patiently teaching me molecular biology techniques. To Sue Biggins, I am grateful for expert guidance in helping me develop a realistic model of yeast mitosis.

I thank my family for always believing in me and supporting me, yet never pushing me. To my best friend Heidi, I am grateful for endless encouragement and even capturing my projects on film ("Sister chromatids: you gotta keep 'em separated!"). Finally, I thank my husband Rodrigo, for his quiet, supportive presence, for constantly telling me how proud he is of me, and for reminding me daily, "Yes, you can!"

Funding for this project was provided by the National Institute of General Medical Sciences of the National Institutes of Health under award numbers R01GM071522 and R01GM076177 to David Odde and award RO1GM044757 to Tom Hays, by the University of Minnesota Interdisciplinary Doctoral Fellowship awarded to Emily Tubman, and by the University of Minnesota Undergraduate Research Opportunities Program awarded to Kelsey McCoy.

## Dedication

I dedicate this dissertation to my family: Rodrigo López, Karen Hopkins, Doug Tubman, and Behn, Nicole, and London Tubman.

## Abstract

Mitosis is the part of the cell cycle in which replicated chromosomes segregate on the mitotic spindle. Improper segregation results in aneuploidy, abnormal chromosome number, which is a hallmark of both cancer and birth defects. Chromosomes attach through kinetochores, built on centromeric DNA, to microtubules that make up the mitotic spindle. Proper attachment requires that kinetochores "biorient," or make attachments to microtubules from opposite spindle poles, which generates tension in the kinetochore-microtubule attachment. By contrast, initial and improper attachments lack tension and are eliminated by Aurora B/Ipl1 kinase-mediated, tension-sensitive phosphorylation (human: Aurora B, yeast: Ipl1). Thus, how initial tension-lacking attachments transition to stable tension-generating attachments, the "the initiation problem of biorientation (IPOB)," remains an enigma. A kinetochore-microtubule error correction model of budding yeast mitosis was developed using a well-established model of yeast metaphase microtubule dynamics and integrating kinase-mediated error correction. The model illuminates how improper kinetochore-microtubule attachments are destabilized and replaced by correct kinetochore-microtubule attachments within twenty minutes, solving the IPOB. Following biorientation, chromosomes align or "congress" at the mitotic spindle equator. In the fungi *S. cerevisiae* and *C. albicans*, chromosome congression is facilitated by the motor protein kinesin-5, which promotes length-dependent depolymerization of kinetochore microtubules (microtubules within the spindle attached to kinetochores). Spindle length is controlled by the motor protein kinesin-8, which promotes length-dependent depolymerization of interpolar microtubules (microtubules within the spindle not attached to kinetochores). However in human cells, congression has been linked to kinesin-8. Kinesin-5 and kinesin-8 were tested in the fly *Drosophila melanogaster* S2 cells using

RNAi-induced gene silencing. As with fungi, kinetochore microtubules were longer, and kinetochores less congressed in kinesin-5 knockdown spindles compared to control. Knocking down kinesin-8 levels resulted in longer spindles overall. These results are consistent with those from fungi, indicating that kinesin-5, and not kinesin-8, has a major role in promoting chromosome congression. These studies are potentially relevant medically in light of the fact that both Aurora B and kinesin-5 are targets for anticancer drugs. Altogether, these studies use *in silico* modeling in yeast and experimentation in animal cells to obtain a better understanding of how cells elegantly segregate chromosomes in mitosis in order to maintain proper ploidy.

# Table of Contents

## List of Tables

## List of Figures

## List of Supplemental Figures

## List of Supplemental Movies

## List of Abbreviations

MT=microtubule

kMT=kinetochore microtubule

iMT=interpolar microtubule

df=degrees of freedom

RNAi=RNA interference

dsRNA=double stranded RNA

NEB=nuclear envelope breakdown

AO=anaphase onset

# Chapter 1: General Introduction

## Microtubules, mitosis, and disease

Microtubules are self-assembled, linear polymers consisting of 13 protofilaments made up of αβ-tubulin heterodimers. The dimers align within a polymer lattice such that the microtubule forms a hollow cylinder 25 nm in outer diameter that has a polarity with α-tubulin at the minus end and β-tubulin at the plus end (Figure 1.1A)(1–4). A remarkable feature of microtubules is that they undergo dynamic instability, where they stochastically switch between periods of growth to shortening, a process called "catastrophe," and between periods of shortening to growth, a process called "rescue." Four parameters characterize dynamic instability: catastrophe frequency ($k_c$), rescue frequency ($k_r$), growth velocity ($V_g$), and shortening velocity ($V_s$) (Figure 1.1B) (5).

In mitosis, faithful chromosome segregation relies on dynamic microtubules to organize and segregate replicated chromosomes (consisting of two identical sister chromatids), ensuring that proper ploidy is maintained at each division cycle. "Kinetochore microtubules" attach to and position kinetochores, "interpolar microtubules" reside within the spindle and aid in the structural maintenance of the bipolar spindle, and "astral microtubules" extend beyond the spindle poles and aid in spindle positioning (Figure 1.2). Microtubule motors control spindle length, promote kinetochore positioning, and establish the bipolar spindle (Figure 1.2). In prometaphase, the plus ends of microtubules search for and capture kinetochores, proteinaceous structures built on centromeric DNA, while the microtubule minus ends remain anchored at the spindle poles (Figure 1.2A). Proper attachments require that replicated chromosomes "biorient" on the mitotic spindle, such that each kinetochore attaches to kinetochore microtubules from opposite spindle poles. In metaphase, kinetochore microtubules align kinetochores

of the replicated chromosomes at the mitotic spindle equator to achieve “chromosome congression” (Figure 1.2B), and finally in anaphase, the cohesion tethering the sister chromatids is dissolved, the microtubules depolymerize, pulling the chromosomes to opposite spindle poles, and the spindle lengthens, completing the segregation of the replicated chromosomes (Figure 1.2C).

Aneuploidy, aberrant chromosome number, results from incorrect chromosome segregation; it is prevalent in cancer and associated with multiple birth defects (6–8). Several cancer drugs have been designed to target the mitotic machinery of rapidly dividing cancer cells. The most successful are taxanes and vinca alkaloids which target microtubules, however, these drugs lead to negative side effects such as peripheral neuropathies, because they also interfere with microtubule dynamics in non-cancer cells, such as neurons (9). Therefore, there has been an effort to design drugs that target proteins involved in mitosis beyond microtubules; however, there are still many unanswered questions regarding mitosis. In this work, we have addressed two of these questions which are 1) how attachment errors between kinetochores and microtubules are corrected so that kinetochores biorient on the mitotic spindle, and 2) how chromosomes achieve chromosome congression in metaphase.

**Error correction in yeast and animal spindles**

When kinetochores on a replicated chromosome make attachments to microtubules emanating from opposite poles of the mitotic spindle, kinetochore biorientation is accomplished. The kinetochore microtubules pull on the chromatids, generating poleward forces which are resisted by cohesion proteins “cohesins” (Smc1p, Smc3p, and Scc1p in yeast) that hold the two sister chromatids together until anaphase (10). At anaphase onset, the anaphase-promoting complex (APC) ubiquitinates the

protein securin to target it for degradation (11). Securin proteolysis then activates the protease separase which cleaves cohesin, and anaphase proceeds (11). In animal spindles, there are on the order of tens of kinetochore microtubules per kinetochore, but in yeast cells, there is only a single kinetochore microtubule per kinetochore (12–14). With full kinetochore occupancy, kinetochore-microtubule attachment errors occur when both kinetochores attach to microtubules from the same spindle pole or, in the case of animal spindles, when a kinetochore attaches to microtubules from both spindle poles. Without full kinetochore occupancy, attachment errors occur when only a single kinetochore makes attachments to microtubules or when the kinetochore pair is completely unattached. When attachment errors are not corrected, chromosomes mis-segregate, which results in aneuploidy.

The Aurora B kinase in human cells, Ipl1 kinase in yeast, has been shown to be critical for establishing biorientation of kinetochores and proper chromosome segregation (15–18). Aurora B/Ipl1 promotes kinetochore-microtubule detachment when under low chromatin tension such as when both kinetochores are attached to microtubules from the same spindle pole (17–19). Detachment of microtubules from one of the kinetochores then allows that kinetochore to be captured by microtubules (or single microtubule in the case of yeast) from the opposite spindle pole to establish correct biorientation. Additionally, tension stabilizes attachments, whether the tension is generated *in vivo* following biorientation from kinetochore microtubules or *in vitro* due to a microneedle or laser trap pulling on a kinetochore attached to a microtubule (20–22). Therefore, tension is necessary to evade kinetochore-microtubule detachment, yet initial attachments lack tension. A paradox emerges, where it is unclear how nascent low-tension bioriented attachments maintain attachment before they generate the tension

that protects them from Aurora B/Ipl1-driven detachment, so called “the initiation problem of biorientation” (23, 24).

A qualitative reaction/diffusion model of Aurora B-driven error correction in animal cells was developed to explain how Aurora B, which localizes to the inner centromere, selectively phosphorylates its outer kinetochore protein targets. In the model, phosphorylated (hence active) Aurora B molecules diffuse away from the inner centromere. Cytoplasmic protein phosphatases dephosphorylate Aurora B molecules, deactivating them and generating a gradient of phosphorylation, as well as directly dephosphorylating Aurora B targets (25). If the active Aurora B molecules reach their outer kinetochore targets before deactivation, then those targets are phosphorylated and the kinetochore-microtubule attachments weakened; however, if the active Aurora B molecules are deactivated before reaching the targets, then the kinetochore-microtubule attachments remain strong (25). Although this reaction/diffusion model provides an explanation for the spatial dependence of Aurora B phosphorylation in large animal spindles, in small spindles where the space between neighboring kinetochores is much shorter, such as budding yeast, this would lead to inadvertent detachment of even correct, bioriented attachments, hence this is not a model that can be applied universally to explain error correction. Furthermore, this model is not supported with a mathematical framework.

Another model of error correction in animal spindles relies on the geometric constraints of back-to-back kinetochores with “indiscriminate” kinetochore-microtubule detachment (detachment independent of tension) to promote proper biorientation (26). In this model, the back-to-back kinetochore configuration favors replacement of incorrect attachments with correct attachments from the appropriate spindle pole, so that throughout time, all of the incorrect attachments are replaced by correct attachments

(26). The problem with this model is that it completely neglects Aurora B tension-sensitive error correction, even though Aurora B has been shown to be crucial for establishing proper attachments (18).

A mathematical model of error correction in fission yeast balances forces on the centromere, kinetochore-microtubule attachment site, and spindle pole bodies, and includes error correction by Aurora B and the geometric constraints of back-to-back kinetochores (27). When kinetochores are under tension, they are outside of the Aurora B range and the rate of kinetochore-microtubule detachment is lower than the rate of kinetochore-microtubule attachment (27). The opposite occurs when kinetochores lack tension, hence incorrect attachments are destabilized and replaced by correct attachments, similar to the previous model (27). The biggest problem with this model is that it completely neglects microtubule dynamics, which are known force generators, and relies solely on motor proteins and tension at the kinetochores to generate forces.

Finally, a model of error correction in budding yeast uses a combination of differential equation/stochastic modeling with “erasers” (Aurora B) that repress attachment of microtubules to kinetochores and tension that represses erasers (24). Two steady states on a phase plane of attachments represent loose attachment and strong attachment, separated by a separatrix (24). Passage across the separatrix to strong attachments can be acquired by stochastic fluctuations of attachment strength in both kinetochores long enough to generate tension (repress the erasers) and cross the separatrix. Hence, this model addresses the “initiation problem of biorientation” by requiring stochasticity in attachment strength to “buy time” for the kinetochores to generate tension, inhibit the erasers, and form strong, bioriented attachments (24). Although the model elegantly offers a solution to the initiation problem of biorientation for a single, bioriented kinetochore pair it has several shortages: 1) it does not explain how

a kinetochore that has lost a microtubule regains attachment, 2) it does not explain how erroneous attachments are corrected, 3) it does not explicitly model microtubule dynamics, 4) and it does not explain how *all* kinetochore pairs establish and maintain bioriented attachments on the yeast mitotic spindle.

Overall, although models of error correction have been developed in both yeast and animal spindles, they either lack a mathematical framework, specific features known to promote biorientation and correction of improper attachments, or they do not model all kinetochore pairs and attachment possibilities. Thus, they do not account for the high degree of error correction responsible for the high level of fidelity of chromosome segregation observed experimentally in both yeast and animal cells. In chapter 1, we develop a model for spindle-attachment error correction in budding yeast based on a metaphase microtubule model to explain how erroneous attachments are corrected and how all kinetochores biorient on the yeast mitotic spindle, which solves the initiation problem of biorientation.

**Chromosome congression in yeast and animal spindles**

Metaphase is characterized by chromosome congression, the aligning of chromosomes at the mitotic spindle equator. The exact purpose for congression is unclear. One proposal is that it serves as a "quality control mechanism," ensuring that all chromosomes have the same initial starting positions before the replicated chromosomes are finally separated at anaphase onset, which would be beneficial in very short mitoses, to ensure that no chromosomes are left behind; additionally, it was thought of as a checkpoint for progression to anaphase (28). However, more recently the checkpoint is believed to monitor kinetochore attachment and/or tension, rather than congression (29). Despite the lack of understanding about why chromosome

congression occurs, it is widely observed in both animal and yeast mitosis, therefore, a bigger question is how it occurs.

Kinetochore microtubules and motor proteins generate poleward forces on kinetochores; however, they must be antagonized by anti-poleward forces to align the kinetochores at the mitotic spindle equator (30–32). Overwhelmingly, this anti-poleward force has been attributed to the polar ejection force, originally discovered when mono-oriented chromosomes on monopolar spindles moved away from the pole (33). The original source of the polar ejection force was proposed to be a high density of microtubules emanating from the microtubule aster, preventing chromosome movement into it (33, 34); however, it is now believed to be due primarily to plus-end directed chromokinesins, motor proteins on chromosome arms that bind to, and walk along, astral microtubules thereby shuttling chromosomes away from the poles (35). Although the polar ejection force offers a conceptually attractive mechanism to promote chromosome congression, it is weakly supported experimentally, both because kinetochores still congress without chromokinesins and because kinetochores still congress without the chromosome arms on which chromokinesins reside and supposedly act (36–40).

Alternatively, the plus-end directed motor proteins kinesin-8 and kinesin-5 have shown activity facilitating chromosome congression in both human cells and yeast. Kinesin-8 depleted HeLa cells had a reduced rate of kinetochore microtubule switching (growth to shortening and shortening to growth) and increased kinetochore microtubule velocity, which led to increased chromosome oscillations and poorer chromosome congression, indicating that kinesin-8 contributed to chromosome congression through control of kinetochore microtubule dynamics (41). In yeast, on the other hand, kinesin-8 did not show evidence of regulating kinetochore microtubule dynamics to influence

chromosome congression but instead showed evidence of regulating interpolar microtubule dynamics to control spindle length (42). Specifically, kinesin-8 mutants had longer spindle lengths demonstrating that kinesin-8 promoted length-dependent depolymerization of interpolar, instead of kinetochore, microtubules (42). However, in yeast, tetrameric kinesin-5 was found to control kinetochore microtubule length to facilitate chromosome congression; kinesin-5 mutants had longer and more variable kinetochore microtubule lengths, demonstrating that kinesin-5 promoted length-dependent depolymerization of kinetochore microtubules to promote chromosome congression (42).

The differences in activity were due to the motors' ability or inability to crosslink, where dimeric kinesin-8, unable to crosslink, remained mainly on the longer interpolar microtubules, controlling interpolar microtubule length and spindle length, while tetrameric kinesin-5, able to crosslink yet frustrated on antiparallel microtubules which led to unbinding, remained primarily in the highly parallel environment of kinetochore microtubules, controlling kinetochore microtubule length and chromosome congression (42).

The same results were found in the infectious yeast, *Candida albicans*, indicating that kinesin-5, and not kinesin-8, controls kinetochore microtubule lengths to promote chromosome congression in fungi (43). Kinesin-5 mediated chromosome congression has not yet been demonstrated in animal cells; therefore, it is unknown whether this mechanism is specific to fungi or ubiquitous in eukaryotes. In chapter 2, we test the roles of both kinesin-5 and kinesin-8 in the fruit fly *Drosophila melanogaster* S2 cells to determine if either or both motors are involved in chromosome congression in animal cells.

## Figures

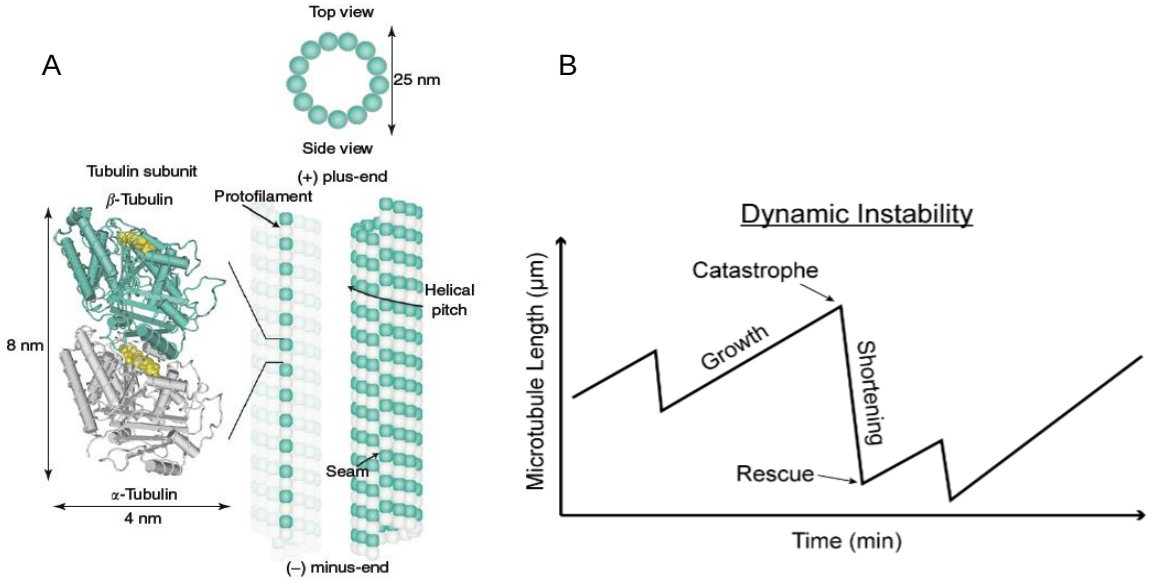


**Figure 1.1. Microtubules and dynamic instability**
A) Microtubule structure. B) Dynamic instability showing periods of growth, shortening, and switching between states. Reprinted from Encyclopedia of Cell Biology, 4, Brian T. Castle and David J. Odde, Dynamics of microtubule assembly, 36-43, 2015, with permission from Elsevier.

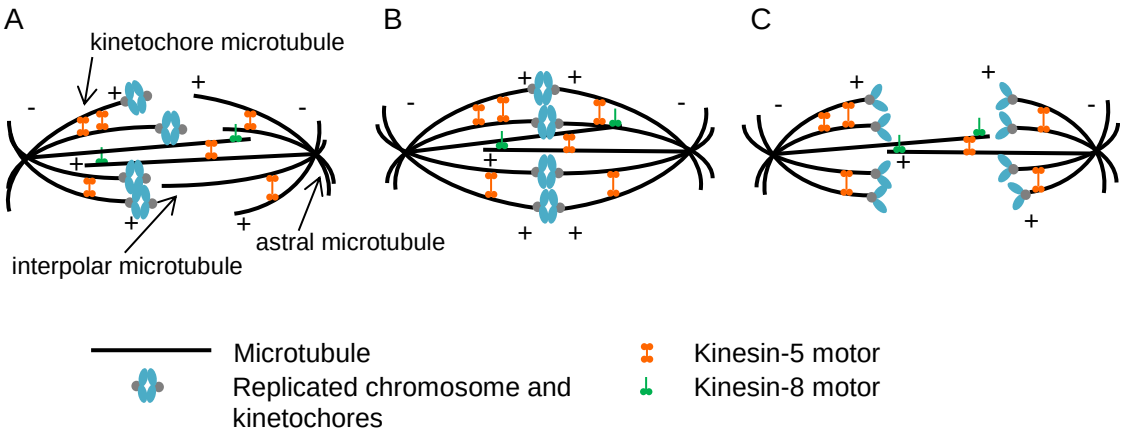


**Figure 1.2. Mitosis**
A) Prometaphase. B) Metaphase. C) Anaphase.

# Chapter 2: Model for kinetochore-microtubule error correction in budding yeast mitosis

Authors: Emily S. Tubman[1], Sue Biggins[2], David J. Odde[1]

Affiliations:

[1]Department of Biomedical Engineering, University of Minnesota, Minneapolis, MN 55455

[2]Howard Hughes Medical Institute, Division of Basic Sciences, Fred Hutchinson Cancer Research Center, Seattle, WA, 98109

## Summary

Proper segregation of the genome requires that kinetochores form and maintain bioriented, amphitelic attachments to microtubules from opposite spindle poles and eliminate erroneous, syntelic attachments in which kinetochores attach to microtubules from the same spindle pole. Ipl1/Aurora B kinase-mediated phosphorylation destabilizes incorrect kinetochore-microtubule attachments when chromatin tension is low. Correspondingly, tension stabilizes bioriented, amphitelic attachments. Thus, it remains unclear how nascent, low-tension amphitelic attachments build tension to stabilize, without first detaching from kinetochore microtubules. This has been termed the "initiation problem of bi-orientation." We developed a stochastic mathematical model for kinetochore-microtubule error correction in budding yeast. The model reveals two key requirements: 1) that in in a multisite phosphorylation model under low chromatin tension, a high critical phosphorylation for detachment provides a delay before detachment, and 2) that kinetochore-induced microtubule depolymerization generates tension in amphitelic, but not syntelic, attachments. With these requirements, the model provides a simple biophysical solution to the "initiation problem of biorientation" and predicts the high degree of amphitely observed experimentally for wild-type cells under optimal conditions.

## Introduction

Proper chromosome segregation requires that replicated chromosomes biorient on the mitotic spindle in metaphase, making amphitelic attachments in which kinetochores on centromeric DNA attach to the plus ends of dynamic kinetochore microtubules emanating from opposite spindle poles (Figure 2.1A, Metaphase) (44). This requirement ensures that when the cohesion linking the sister chromatids is degraded at anaphase onset, sister kinetochores are pulled via disassembling kinetochore microtubule plus ends toward opposite spindle poles so that ideally each daughter cell receives exactly one copy of each chromosome (10, 45). Attachment errors arise in prometaphase when kinetochores are attached to microtubules from the same spindle pole (syntelic attachment), one kinetochore is attached to microtubules from both spindle poles (merotelic attachment), one kinetochore is attached to microtubules and the other unattached (monotelic attachment), or both kinetochores are unattached (Figure 2.1A, Prometaphase) (18, 19, 29). If left uncorrected before metaphase, the attachment errors lead to segregation defects resulting in aneuploidy, aberrant chromosome number, which is a hallmark of both cancer and birth defects (6–8).

In budding yeast, in which one kinetochore is attached to a single kinetochore microtubule, four attachment states are possible and categorized based on how many sister kinetochores are occupied by kinetochore microtubule plus ends (Figure 2.1B).The Ipl1 protein kinase (Aurora B in humans) has been identified as a key regulator in error correction in budding yeast (15–17, 19, 46). Aurora B is overexpressed in certain cancers, and inhibitors are currently in clinical trials for cancer treatment (9, 47–49). It is well-accepted that the Ipl1/Aurora B kinase executes its error-correction activity by phosphorylating sites on kinetochore proteins when chromatin lacks tension (such as in

syntelic attachments) which destabilizes the kinetochore-microtubule attachment and allows the free kinetochore another opportunity to properly biorient before anaphase (17, 18, 46, 50–54). Conversely, tension stabilizes attachments, protecting sites on kinetochore proteins from kinase-mediated phosphorylation and subsequent kinetochore-microtubule detachment (17, 20–22). This suggests that the attachments with two kinetochore microtubules in budding yeast (i.e. syntelic and amphitelic) can be subdivided into low-tension attachments (vulnerable to kinase-mediated phosphorylation) and high-tension attachments (protected from kinase-mediated phosphorylation) (Figure 2.1B). Additionally, high-tension amphitelic attachments, once achieved, are relatively stable due to net disassembly of kinetochore microtubules that prevents low-tension amphitelic attachments from occurring (Figure 2.1B). Finally, the budding yeast protein phosphatase 1 catalytic subunit Glc7, which has numerous roles in the cell, antagonizes the Ipl1 kinase by dephosphorylating kinetochore phosphorylation sites, however, unlike Ipl1, it has no known tension-sensitivity (55–57). Altogether, Ipl1 kinase-mediated phosphorylation drives kinetochore-microtubule detachment and Glc7 phosphatase-mediated dephosphorylation drives kinetochore-microtubule attachment (Figure 2.1B).

Despite the wealth of experimental support for kinase-driven error correction, there are still conceptual problems regarding the mechanism. Most importantly, kinase-mediated phosphorylation promotes kinetochore-microtubule detachment when chromatin tension is low yet tension inhibits kinase-mediated phosphorylation. Thus, it is unclear how nascent, low-tension amphitelic attachments progress to a stable high-tension amphitelic state without first detaching, a paradox termed, “the initiation problem of biorientation” (23, 24, 58). Preventing unattached kinetochores requires slow kinase-mediated detachment relative to microtubule attachment, suggesting a delay before

detachment, so that monotelic attachments transition to low-tension amphitelic attachments rather than unattached kinetochores (Figure 2.1B) (58). However, this disparity in detachment-attachment time alone is insufficient to solve the initiation problem of biorientation. The kinase-mediated detachment must *also* be slow relative to the time required for amphitelic attachments to generate tension (again suggesting a delay before detachment) so that low-tension amphitelic attachments transition to stable high-tension amphitelic attachments rather than reverting to monotelic attachments (Figure 2.1B). Overall, it appears that a delay before detachment would solve the initiation problem of biorientation, although how a delay might be achieved remains relatively unknown (58).

Both conceptual and mathematical models of error correction have been developed to attempt to explain the tension conundrum in yeast and animal cells, but each has limitations. In a budding yeast conceptual model, the kinase promotes detachment of incorrect end-on rather than lateral attachments, which provides a delay before detachment; however, when one kinetochore has a lateral attachment and the other an end-on attachment, it does not explain how the end-on attachment avoids detachment, nor is the model supported with a mathematical framework (23). In a mathematical model of error correction in budding yeast, the initiation problem of biorientation is recognized by two attraction basins representing low-tension and high-tension amphitelic attachments separated by a separatrix (24). Solving the initiation problem of biorientation requires overcoming the separatrix through stochastic fluctuations of attachment strength (24). This model addresses the transition between low and high-tension amphitelic attachments but ignores all other attachment states (Figure 2.1B). Additionally, it lacks microtubule dynamics, which are the source of tension generation in bioriented attachments (20, 59). In a mathematical model of error

correction in fission yeast, proper attachment is driven by a kinetochore orientation effect and tension-sensitive kinetochore-microtubule detachment relative to attachment (27). However, this model also lacks microtubule dynamics, and it is unclear how the model overcomes the initiation problem of biorientation. Finally, other yeast or animal error correction models either lack a mathematical framework or focus on geometric constraints and kinetochore-microtubule detachment independent of chromatin tension, rather than Ipl1/Aurora B-facilitated, tension-sensitive detachment (25, 26, 60). Overall, we lack a physically-based mathematical model that accounts for the tension-sensitive kinase activity and the microtubule dynamics to then predict the error rate. As a result, how cells solve the initiation problem of biorientation, even theoretically, remains an enigma.

To address the conceptual problems posed by a tension-sensitive detachment mechanism, we sought to build a physically-based error correction model. Using a well-established model for the amphitelic metaphase kinetochore microtubules of the budding yeast spindle as a starting point, we added the possibility of kinetochore-microtubule attachment/detachment and kinase/phosphatase-mediated phosphorylation/dephosphorylation to the model so that hypothetical error correction mechanisms could be explored theoretically (42, 61, 62). The advantages of modeling budding yeast are that the number of chromosomes, kinetochores, kinetochore microtubules, and interpolar microtubules are known (16 chromosomes, 32 kinetochores, 32 kinetochore microtubules, and ~8 in wild-type metaphase haploid cells, respectively), there is only a single kinetochore microtubule per kinetochore, and dynamics occur only at the microtubule plus ends (no microtubule flux) (12, 63).

## Model Description

The model embodies three main components: 1) microtubule dynamics, 2) Ipl1 (referred to as “kinase”) and Glc7 (referred to as “phosphatase”) activity, and 3) kinetochore-microtubule attachment and detachment. All microtubule dynamics occur at the plus ends where microtubules grow (polymerize) and shorten (depolymerize) at constant velocity and stochastically switch between periods of growth and shortening (42, 61–64). Microtubule catastrophe (switch from growth to shortening) is length dependent, where the longer a microtubule is, the more likely it is to catastrophe (Figure 2.1C) (61, 62). The tetrameric bipolar motor protein kinesin-5 was found to promote length-dependent depolymerization of kinetochore microtubules and the dimeric motor protein kinesin-8 was found to promote length-dependent depolymerization of interpolar microtubules in both budding yeast and the infectious yeast *Candida albicans* (42, 43, 65, 66). Kinetochore microtubule rescue (switch from shortening to growth) is tension-dependent, where chromatin tension promotes growth (Figure 2.1D) (62, 67–69). Lastly interpolar microtubule rescue is constant and high (Figure 2.1D), consistent with very long interpolar microtubules observed in electron tomograms of budding yeast spindles (12, 42). The strong catastrophe gradient combined with the weak rescue frequency for kinetochore microtubules results in net depolymerization of kinetochore microtubules while the high rescue frequency for interpolar microtubules results in net polymerization of interpolar microtubules, such that the length of kinetochore microtubules (~1/4 spindle length) is much shorter than the length of interpolar microtubules (~4/5 spindle length). The length difference ($L_{kMT} << L_{iMT}$) promotes kinetochore capture by microtubules from the opposite spindle pole, and short kinetochore microtubules generate tension in amphitelic attachments, thus the length difference promotes amphitelic attachments.

Ipl1 kinase and Glc7 phosphatase rates were unknown and therefore both given constant values of 1 $s^{-1}$, within the range of reasonable values from 0.1-100 $s^{-1}$ (70), with the kinase active at only low chromatin tension, ($T_k \leq 0.5$ pN) and the phosphatase constitutively active (Figure 2.1E) (17, 19, 57). Chromatin is modeled as a Hookean spring where the chromatin tension is calculated by

$$T_c = k_{chrom}(\Delta x - x_{eq}) \tag{2.1}$$

where $k_{chrom}$ is the experimentally estimated chromatin spring constant, $\Delta x$ is the difference in the kinetochore positions, indicating the chromatin stretch, and $x_{eq}$ is the chromatin rest length (20, 42, 61, 62). Thus, the separation between low-tension and high-tension syntelic and amphitelic attachments (Figure 2.1B) is based on whether the chromatin tension is above or below $T_k$.

If kinetochore-microtubule detachment occurs, the chromatin relaxes to its rest length, $x_{eq}$, with the free kinetochore opposite the occupied kinetochore, and the kinetochore microtubule becomes an interpolar microtubule. Interpolar microtubules capture free kinetochores when their plus ends are within the root mean squared displacement from the kinetochore, given by

$$d = \sqrt{\langle \sigma^2 \rangle} = \sqrt{\frac{k_B T}{k_{chrom}}} \tag{2.2}$$

($k_B$ is Boltzmann's constant, and T is the absolute temperature) (20).

All simulated spindles start in a prometaphase-like attachment state, with four syntelic attachments and twelve monotelic attachments at the mother spindle pole and no attachments at the daughter spindle pole (17, 71, 72), short microtubules (100 nm

long (73)), and random phosphorylation of 0-1 for each Ipl1 kinase phosphorylation site. Simulations end one second after the spindle assembly checkpoint protein Mad2 is satisfied by a minimum tension of 5 pN in all chromosome pairs (estimated values) (74, 75). Minimum simulation times are 10 minutes, and maximum simulation times are 20 minutes (maximum simulation time estimated by doubling minimum simulation times) (61, 74, 76). Parameters are listed in Table 1 and additional model details are in the supplement.

## Results

### Adjusting the kinase activity in a single site phosphorylation model changes the stability of kinetochore-microtubule attachments

Overall, our objective was to determine how the initiation problem of biorientation might be solved, such that monotelic attachments transition to low-tension amphitelic attachments, low-tension amphitelic attachments transition to stable high-tension amphitelic attachments, and erroneous syntelic attachments are corrected. We predicted that this would require a delay before detachment even at low tension with an active kinase.

To start with a simple case, we maintained balanced kinase and phosphatase rates and assumed a single Ipl1 phosphorylation site (substrate) on kinetochores, which we called a “single site phosphorylation model.” In this model, phosphorylation of the single site immediately resulted in detachment, and thus a kinetochore had a probability of 0.5 of being detached even when under low chromatin tension. We expected that a single phosphorylation site would be insufficient to produce “complete amphitely,” in which all kinetochore pairs were amphitelic by the end of the simulation, because the

delay before detachment would be too short ($1/k_k$=1 s) and hence kinetochore-microtubule detachment would occur too often. The simulation started with maximal attachment of kinetochores to the mother spindle pole (4 pairs syntelic and 12 pairs monotelic) (Figure 2.2A) (17, 71, 72). In all monotelic attachments, one kinetochore microtubule (one horizontal line) attaches to a single kinetochore (kinetochore not shown); and in all syntelic and amphitelic attachments, two kinetochore microtubules (two horizontal lines) attach to two kinetochores (kinetochores not shown) (Figure 2.2) Within one minute, several changes occurred in kinetochore-microtubule attachments: 1) kinetochore microtubules released kinetochores in monotelic attachments to become interpolar microtubules resulting in unattached kinetochores (orange to black), 2) interpolar microtubules from opposite spindle poles captured free kinetochores in monotelic attachments, resulting in amphitelic attachments (black to green and orange to green), 3) kinetochore microtubules released kinetochores in syntelic attachments to become interpolar microtubules, resulting in monotelic attachments (blue to black and blue to orange), and 4) interpolar microtubules captured free kinetochores of unattached kinetochores becoming kinetochore microtubules, resulting in monotelic attachments (black to orange) (Figure 2.2B, 1 minute). By five to ten minutes, the number of amphitelic attachments increased, but so too did the number of unattached kinetochores and monotelic attachments (Figure 2.2B, 5 and 10 minutes). By the simulation end, complete amphitely was not achieved (Figure 2.2C and Movie 2.S1).

Because the base parameter case of $k_k = k_{ph} = 1\ s^{-1}$ resulted in an unrealistically high level of monotelic and unattached kinetochores, it seemed that complete amphitely, in which all kinetochores made amphitelic attachments by the end of the simulation, could potentially be achieved by decreasing the kinase rate. This is because when detachment occurs immediately following phosphorylation with a single phosphostate,

the only way to obtain a delay before detachment to solve the initiation problem of biorientation is to delay phosphorylation itself by decreasing the kinase rate constant. As the kinase rate constant decreases, the delay before detachment increases reciprocally.

As expected, decreasing the kinase rate constant 100-fold ($k_k$=0.01 $s^{-1}$) to increase the delay before detachment to 100 s led to an overall increase in attachment throughout all time points as well as an increase in amphitelic attachments at five and ten minutes (Figure 2.2D). As observed in the 5 minute and 10 minute time points, the kinetochore microtubules in amphitelic attachments were short relative to the entire spindle, thus the reason that amphitelic attachments were stable relative to syntelic attachments was due to the length-dependent disassembly of kinetochore microtubules that prevents low tension states from occurring in amphitelic, but not syntelic attachment states. By the simulation end, complete amphitely was achieved (Figure 2.2E and Movie 2.S2).

Decreasing the kinase rate constant another 100-fold ($k_k$=0.0001 $s^{-1}$) to further increase the delay before detachment to 10000 s (almost 3 hours) led to such slow phosphorylation and detachment that incorrect syntelic attachments were not corrected (Figure 2.2F). By the simulation end, complete amphitely was not achieved (Figure 2.2G and Movie 2.S3). In this case the time scale of the kinase reaction ($1/k_k$ = 10000 s) was longer than mitosis itself (20 min = 1200 s).

In summary, we found that balanced kinase and phosphatase activity determining the phosphostate of a single phosphorylation site in the kinetochore was partially successful in error correction, but generally resulted in incomplete amphitely (Figure 2.2B and C). We also found that complete amphitely required very weak kinase

activity relative to phosphatase activity ($k_k<k_{ph}$), providing the delay before detachment that we predicted would solve the initiation problem of biorientation (Figure 2.2D and E). Finally, we found that weakening the kinase 100-fold further ($k_k<<k_{ph}$) prevented correction of improper attachments (Figure 2.2F and G).

**An optimum of complete amphitely in a single site phosphorylation model requires very slow kinase activity relative to phosphatase activity to create a delay before detachment**

To assess the variability of outcomes over many cells, we simulated 1000 spindles per condition with a range of kinase rates and with a constant phosphatase rate ($k_k$=1 $s^{-1}$-0.0001 $s^{-1}$; $k_{ph}$=1 $s^{-1}$). We found that the fraction of cells with complete amphitely (all pairs amphitelic by simulation end) rose, reaching an optimum of 0.991 at an intermediate delay before detachment ($1/k_k$=100 s) and decreasing thereafter ($X^2$=4000, df=4, $p<10^{-100}$, Figure 2.3A) as predicted to occur if a short delay before detachment results in unattached kinetochores and monotelic attachments, a longer delay solves the initiation problem of biorientation, and a delay that is too long prevents correction of syntelic attachments.

The biphasic trend was reversed for the total time to complete mitosis, and all of the times were statistically different ($p<10^{-100}$ by Kruskal-Wallis, followed by multiple comparisons with α=0.05 by Tukey-Kramer, Figure 2.3B). In the two extreme cases of delays before detachment ($1/k_k$=1 s and $1/k_k$=10000 s) the average time to complete mitosis was the maximum allowed time (20 minutes), indicating that the tension requirement for the spindle assembly checkpoint was only satisfied at the intermediate delay before detachment ($1/k_k$=100 s).

The distribution of pooled kinetochore attachment states at anaphase onset revealed the expected attachments, where a short delay before detachment ($1/k_k$=1 s) resulted in high levels of unattached kinetochores and monotelic attachments, a longer delay ($1/k_k$=100 s) resulted in nearly perfect amphitelic attachments, and an overly-prolonged delay ($1/k_k$=10000 s) resulted in high levels of syntelic attachments ($X^2$=12000, df=2, $p<10^{-100}$ (amphitelic versus not amphitelic), Figure 2.3C). Interestingly, in all cases, amphitelic attachments accounted for at least 46% of all kinetochore attachments. For a short delay before detachment ($1/k_k$=1 s), this indicates that if high-tension amphitelic attachments were made, they were relatively stable. For an unrealistically prolonged delay before detachment ($1/k_k$=10000 s), high levels of amphitely still occurred because there were not enough microtubules from a single pole to make syntelic attachments with all kinetochores in prometaphase, which allowed amphitelic attachments to be made with the remaining monotelic kinetochores.

The average attachments over time during the first ten simulation minutes showed how the final attachments were eventually reached. For a short delay before detachment ($1/k_k$=1 s), the initial peak in unattached kinetochores indicates that most initial monotelic attachments failed, the second peak in monotelic attachments indicates that re-attachment was relatively fast, and the peak in amphitelic attachments indicates that interpolar microtubules from the opposite spindle pole grew across the spindle and captured free kinetochores (Figure 2.3D, $1/k_k$=1 s). However, eventually amphitelic attachments steadily decreased and monotelic attachments and unattached kinetochores increased throughout time, as expected due to a short delay before detachment (Figure 2.3D, $1/k_k$ =1 s). For a longer delay before detachment ($1/k_k$=100 s), amphitelic attachments rose for the same reason as the previous case but because the delay before detachment was longer, low-tension amphitelic attachments transitioned to

stable high-tension amphitelic attachments rather than reverting to monotelic attachments (Figure 2.3D, $1/k_k$=100 s). In contrast, syntelic attachments decreased more slowly, again because of the longer delay before detachment (Figure 2.3D, $1/k_k$=100 s). For an overly-prolonged delay before detachment ($1/k_k$=10000 s), amphitelic attachments rose for the same reason as the previous two cases, yet syntelic attachments remained high because the delay before detachment was too long, which inhibited most of the syntelic attachments from reverting to monotelic attachments, a prerequisite for subsequent transitioning to amphitelic attachments (Figure 2.3D, $1/k_k$=10000 s).

To explain the behavior of the system from a thermodynamic perspective, we obtained the forward and reverse rate constants for each of the transitions between attachment states, $k_f$ and $k_r$, as outputs of the simulation (77) and calculated the standard molar Gibbs free energy change, $\Delta G^0$, for each transition shown in Fig. 1B,

$$\Delta G^0 = -k_B T \ln\left(\frac{k_f}{k_r}\right). \tag{2.3}$$

The energy changes were calculated at ten simulation minutes and plotted relative to a monotelic zero energy. Positive energy changes indicate unfavorable progression toward the right in Fig. 1B, while negative energy changes indicate favorable progression toward the right in Fig. 1B. For a short delay before detachment ($1/k_k$=1 s), a global minimum occurred for the energy change from low-tension to high-tension amphitely, as evidenced by the large negative value for $\Delta G^0_{lh}$ (Figure 2.3E, $1/k_k$=1 s $\Delta G^0_{lh}$ green). However, the energy change from monotely to low-tension amphitely, $\Delta G^0_{ml}$, was positive and thus served as an energy barrier to high-tension amphitely (Figure 2.3E,

1/$k_k$=1 s $\Delta G^0_{ml}$ green). Because of the high energy barrier, nascent low-tension amphitely was unstable and often reverted back to monotely. For a longer delay before detachment (1/$k_k$=100 s), the global minimum for the energy change from low-tension amphitely to high-tension amphitely, $\Delta G^0_{lh}$, was approximately the same as the previous case, yet the energy change from monotely to low-tension amphitely and syntely , $\Delta G^0_{ml}$ was eliminated (Figure 2.3E, 1/$k_k$=100 s), thus nascent low-tension amphitely did not revert back to monotely as readily and instead transitioned to high-tension amphitely. Finally, for an overly-prolonged delay before detachment (1/$k_k$=10000 s), the global minimum for the energy change from low-tension amphitely to high-tension amphitely was once again approximately the same as for the previous cases, yet the energy change from monotely to low-tension amphitely and syntely, $\Delta G^0_{ml}$ , was negative, resulting in the emergence of a new minima in the energy change to low-tension syntely (Figure 2.3E, 1/$k_k$=10000 s, $\Delta G^0_{ml}$ blue), thus stabilizing low-tension syntely so that it did not transition to monotely..

The slowest Ipl1 kinase rate constant ($k_k$=0.0001 s-1) was used to simulate *ipl1* mutants with the modifications that initial phosphorylation of the substrates was zero (instead of randomly zero or 1) and the maximum simulation time 10.1 minutes because the Ipl1 kinase is required for the tension-dependent sensitivity of the spindle assembly checkpoint (16). Despite these minor modifications, the same results were obtained (compare Figure 2.3, 1/$k_k$=10000 s to 2.S1).

In summary, we identified a set of conditions that resulted in 0.991 complete amphitely with a single phosphorylation site, which required very weak kinase activity relative to phosphatase activity so that the delay before detachment was long. While

theoretically plausible, this scenario is inconsistent with experimental results that not only show that Ipl1 has multiple phosphorylation sites but that high levels of phosphorylation of Ipl1/Aurora B sites have been observed in early mitosis and when kinetochores lack tension or attachment (15, 46, 52, 56, 78–80). By contrast, the single site phosphorylation model predicts that to consistently achieve complete amphitely, the phosphorylation site will nearly always be dephosphorylated. Therefore, while a single site phosphorylation model is illustrative of the requirements for solving the initiation problem of biorientation, it is unrealistic for reproducing experimental results.

**An optimum of complete amphitely in a multisite phosphorylation model requires a high critical phosphorylation for detachment to solve the initiation problem of biorientation**

Although the single site phosphorylation model was not experimentally supported, it allowed us to discover that a delay before detachment was the key feature to solve the initiation problem of biorientation. This delay allowed monotelic attachments to transition to low-tension amphitelic attachments, rather than unattached kinetochores, and allowed nascent low-tension amphitelic attachments to generate tension to transition to high-tension amphitelic attachments, rather than revert to monotelic attachments.

To make a more realistic transition state model, we considered the kinetochore as having a multiplicity of phosphorylation sites, which we refer to as a "multisite phosphorylation model," with the number of phosphorylation sites defined by N. In the multisite phosphorylation model, we returned to balanced kinase and phosphatase activity (Figure 2.1E) with N=10 Ipl1 phosphorylation sites (substrates), as opposed to N=1 assumed for the single site model (46, 57, 81). Under low chromatin tension, the probability distribution of the number of Ipl1 sites phosphorylated follows a binomial

distribution with N=10 sites where the probability of phosphorylation for each site is p=0.5, because

$$p = \frac{k_k}{k_k + k_{ph}}, \tag{2.4}$$

and thus, the expected number of phosphorylated sites under low tension is

$$\mu = Np = 5, \tag{2.5}$$

(Figure 2.4A).

A key aspect of the multisite phosphorylation model is that the delay in detachment in the low tension/kinase-on state can be achieved by requiring an abnormally high phosphorylation state in order to detach. Thus, we hypothesized that maximal complete amphitely would be achieved with a critical phosphorylation for detachment, $N_{cr}$, in the upper tail of the distribution, such as $N_{cr}$=8-10 (Figure 2.4A). The higher the value of $N_{cr}$, the longer the delay before detachment, which we demonstrated by simulating kinase-mediated phosphorylation and phosphatase-mediated dephosphorylation for a single kinetochore under low chromatin tension (Figure 2.4B). $N_{cr}$=8 was reached infrequently, $N_{cr}$=9 very infrequently, and $N_{cr}$=10 extremely infrequently (Figure 2.4B), indicating that the farther into the tail of the distribution, the longer the delay before reaching $N_{cr}$, as expected. For each $N_{cr}$, the delay before detachment, $\tau_d$, was calculated using the number of steps to reach $N_{cr}$, $N_{steps}$ as a function of $N_{cr}$, the total number of phosphorylation sites, N, and the rate of phosphorylation $k_k$=$k_{ph}$=k=1 $s^{-1}$,

$$\tau_d = \frac{N_{steps}(N_{cr})}{Nk}, \tag{2.6}$$

using the theory of absorbing Markov chains (Figure 2.4C) (details in supplement and Figure 2.S2) (82). In order for nascent low-tension amphitelic attachments to transition to stable high-tension amphitelic attachments rather than revert to monotelic attachments, the delay before detachment needed to exceed the minimum time necessary for amphitelic attachments to build enough tension to exceed the maximal tension for kinase activity ($T_k = 0.5$ pN, Figure 2.1E), $\tau_T$. This minimum time required that both sister kinetochore microtubules depolymerize simultaneously, thus generating tension at a rate inversely proportional to the shortening velocity of microtubules, $V$, and the chromatin spring constant, $k_{chr}$,

$$\tau_T = \frac{T_k}{2Vk_{chrom}} \approx 1s. \quad (2.7)$$

If one or both kinetochore microtubules were growing, then the time to exceed the maximal tension for kinase activity would be even longer. The minimum time to generate tension sufficient to exceed the maximal tension for kinase activity was independent of $N_{cr}$. In all cases, the delays before detachment were longer than $\tau_T$ (Figure 2.4C) indicating that amphitely was expected to be high in all three cases ($N_{cr}$=8, 9, or 10) but that amphitely would be least stable with $N_{cr}$=8 and syntely may also be stable with $N_{cr}$=10 (Figure 2.4C).

An optimum of complete amphitely emerged as the delay before detachment increased (0.721, 0.989, and 0.982, for $N_{cr}$=8 (n=1000 spindles), 9 (n=3600 spindles), and 10 (n=2800 spindles), respectively; $X^2$=1300, df=2, $p<10^{-100}$, Figure 2.4D). Despite the small decrease in complete amphitely between $\tau_d$ = 15 s (0.989) and $\tau_d$ = 118 s (0.982), the difference was statistically significant ($X^2$=20, df=1, $p<10^{-5}$). These results indicate that complete amphitely is very sensitive to small changes in the delay before

detachment when it is near $\tau_T$ (4 s versus 15 s) but less sensitive when it is far from $\tau_T$ (15 s versus 118 s). However, from the single phosphorylation site case, we concluded that when the delay before detachment is very long (1000 s or more) complete amphitely is not achieved because low-tension syntely is stabilized.

The optimum in complete amphitely coincided with the minimum total time to complete mitosis, indicating that tension generation satisfied the spindle assembly checkpoint earliest when complete amphitely was greatest, as expected because amphitelic attachments generate tension while monotelic and syntelic attachments generally do not; all of the times to complete mitosis were statistically different ($p<10^{-85}$ (Kruskal-Wallis), followed by multiple comparisons with α=0.05 (Tukey-Kramer), Figure 2.4E).

The optimum in complete amphitely also coincided with maximal amphitely of the distribution of pooled kinetochore attachment states at anaphase onset ($X^2$=1800, df=2, $p<10^{-100}$ (amphitelic versus not amphitelic), Figure 2.4F). The very small difference in amphitely between $\tau_d$ = 15 s and $\tau_d$ = 118 s was statistically significant ($X^2$=6, df=1, p=0.02).

In all cases, the attachments through time showed that amphitely rose within the first 5 minutes and remained high during the following 5 minutes (Figure 2.4G), thus accounting for the high level of amphitely in all cases (Figure 2.4F). However, insets at 9 to 10 minutes show magnifications of later stage behavior and explain why the optimum in complete amphitely occurred for $\tau_d$ =15 s ($N_{cr}$=9). For $\tau_d$ =4 s ($N_{cr}$=8), monotelic, syntelic, and even unattached kinetochores were still present at later times; for $\tau_d$ =15 s ($N_{cr}$=9), nearly all of the non-amphitelic attachments were zero and for $\tau_d$

=118 s ($N_{cr}$=10), syntelic attachments were falling but not completely zero (Figure 2.4G). Lastly, the standard molar Gibbs free energy changes for each transition showed local minima for the energy change from low-tension amphitely to high-tension amphitely, $\Delta G^0_{lh}$, in all cases, demonstrating that high-tension amphitely was highly favorable in all cases, independent of the delay before detachment (Figure 2.4H). However, as in the single site phosphorylation model (Figure 2.3E), the energy changes from monotely to low-tension attachments served as energy barriers to high-tension amphitely when the delay before detachment was shortest (Figure 2.4H, 4 s). The barrier was reduced when the delay before detachment was longer, facilitating entry to stable high-tension amphitely (Figure 2.4H, 15 s). Finally, the energy changes from monotely to low-tension attachments were reduced further such that they were slightly negative when the delay before detachment was longest (Figure 2.4H, 118 s), which stabilized low-tension syntely and accounted for the small decrease in complete amphitely with the longest delay before detachment (Figure 2.4D, 118 s).

## Discussion

Overall, this spindle-attachment error correction budding yeast model explains how a delay before detachment during low tension episodes and net kinetochore microtubule disassembly solve the initiation problem of biorientation. A delay before detachment not only allows monotelic attachments to transition to low-tension amphitelic attachments rather than transition to unattached kinetochores, but even more importantly it also allows low-tension amphitelic attachments to transition to stable high-tension amphitelic attachments rather than revert to monotelic attachments. The net disassembly of kinetochore microtubules generates tension in amphitelic attachments but not in syntelic attachments, thus, high-tension amphitelic attachments are stable

while high-tension syntelic attachments transition to low-tension syntelic attachments and then on to monotelic attachments where they have another opportunity to biorient. Together, the delay before detachment and net kinetochore microtubule disassembly allow all attachments to transition to stable high-tension amphitelic attachments on a time scale of minutes (Figure 2.5).

A delay before detachment was obtained in two ways. The single site phosphorylation model consisted of a single Ipl1 phosphorylation site where detachment occurred automatically following phosphorylation. Maximal complete amphitely, where 0.991 of all spindles ended the simulation with all amphitelic kinetochore pairs, was obtained when Ipl1 kinase activity was much weaker than Glc7 phosphatase activity to obtain a delay before detachment of 100 s (Figure 2.3A). Although this model obtained high levels of complete amphitely, it is not supported experimentally. The multisite phosphorylation model consisted of balanced Ipl1 kinase and Glc7 phosphatase activity and multiple Ipl1 phosphorylation sites where detachment occurred when a high critical phosphorylation for detachment was reached. Maximal complete amphitely, where 0.986 of spindles ended the simulation with all amphitelic kinetochores, was obtained with a high critical phosphorylation ($N_{cr}$=9) before detachment (Figure 2.4D). Unlike the single site phosphorylation model, this model is supported experimentally because multiple Ipl1 phosphorylation sites have been identified (15, 46, 56).

Both the single site and multisite phosphorylation models demonstrate that a delay before detachment greater than 10 s and less than ~120 s achieves maximal complete amphitely. The fraction of spindles with maximal complete amphitely could be optimized by optimizing the number of Ipl1 phosphorylation sites, N, and the critical phosphorylation for detachment, $N_{cr}$. We chose to start with N=10 sites based on the number of Ipl1 phosphorylation sites on the kinetochore proteins Ndc80 and Dam1 (46,

83). We concede that N=10 sites may underestimate the total number of phosphorylation sites on all molecules; however, an adjustment of this number would require an adjustment of $N_{cr}$, thus, the trends would remain. Despite this, the model predicts that the fraction of kinetochores that are *not* amphitelic by the simulation end in the best case of maximal amphitely is ~$10^{-3}$ (Figure 2.4F, 15 s). This number predicts chromosome loss and is only an order of magnitude greater than the experimentally observed chromosome loss rate of wild-type haploid budding yeast of $10^{-5}$ to $10^{-4}$ (76, 84). Furthermore, the model results still corroborate experimental results where biorientation has been widely confirmed through fluorescence microscopy of kinetochore proteins and centromeres as well as through electron microscopy showing short kinetochore microtubules and long interpolar microtubules (15–17, 19, 20, 42, 61, 62, 85, 86).

This model predicts that a high critical phosphorylation for detachment, $N_{cr}$, results in maximal complete amphitely, in which all kinetochores on a spindle make stable amphitelic attachments before anaphase. Mutating Ipl1 phosphorylation sites on kinetochore proteins Ndc80 and Dam1 to alanine inhibits phosphorylation generating "phosphodeficients" and mutating the same sites to aspartic acid mimics phosphorylation generating "phosphomimics," allowing investigation of the consequences of intermediate levels of phosphorylation (46, 83). *In vivo,* mutations to Dam1 phosphorylation sites to generate phosphodeficients result in a graded response: single mutations do not slow growth, multiple mutations result in chromosome mis-segregation, and mutations of all sites are lethal (46). In the model, this is equivalent to preventing phosphorylation of Ipl1 sites, which increases the time to reach the critical phosphorylation for detachment, $N_{cr}$, results in longer delays before detachment, and thus prevents correction of erroneous attachments. Incremental increases in the delay before detachment, such as what was

obtained by increasing $N_{cr}$ from 9 to 10, result in only a modest decrease in the fraction of spindles with all amphitelic kinetochores (Figure 2.4D, i.e. slow growth from modest levels of chromosome mis-segregation), but larger increases in the delay before detachment result in significant decreases in spindles with amphitelic kinetochores (Figure 2.3A, 100 s to 1000 s, i.e. higher levels of chromosome mis-segregation) until delays are so long that none of the spindles have amphitelic kinetochores (Figure 2.3A, 1000 s to 10000 s, i.e. lethal). Mutations to generate phosphomimics, on the other hand, lead to lagging chromosomes (46). In the model, this is equivalent to basal phosphorylation of Ipl1 sites without the possibility of dephosphorylation, which decreases the time to reach $N_{cr}$, results in shorter delays before detachment and thus promotes too much detachment. Incremental decreases in the delay before detachment by decreasing $N_{cr}$ from 9 to 8 result in a significant reduction in the fraction of spindles with all amphitelic kinetochores (Figure 2.4D) revealed to be due to an increase in the monotelic attachments (Figure 2.4F, 4 s). Further decreases in the delay before detachment result in unattached kinetochores (Figure 2.3C, 1 s, i.e. lagging chromosomes). *In vitro*, mutations to Ndc80 sites to generate phosphodeficients have no effect on the kinetochore's ability to remain attached to a microtubule against a load while mutations of Ndc80 and Dam1 sites to generate phosphomimics both separately and additively weaken the kinetochore's ability to remain attached to microtubules against a load (83). Collectively, these experimental results support a multisite phosphorylation site model with a high critical phosphorylation for detachment, where reduced phosphorylation stabilizes attachments (by increasing the time to reach $N_{cr}$) and increased phosphorylation weakens attachments (by decreasing the time to reach $N_{cr}$). This model also predicts that complete amphitely relies on microtubule dynamics, in particular net kinetochore microtubule depolymerization, to stabilize high-tension amphitelic attachments. High levels of mis-segregation occur in yeast with the C354A

beta-tubulin mutation which increases microtubule stability and decreases microtubule dynamics, indicating that dynamic microtubules are crucial for proper segregation (87).

In addition, this model predicts that an *ipl1* mutant model (reduced Ipl1 activity) is obtained by greatly reducing the Ipl1 kinase relative to the Glc7 phosphatase ($k_{ph}/k_k$=10000), resulting in near complete failure to correct syntelic attachments, such that 24% of all kinetochore attachments are syntelic, 76% are amphitelic, and none of the cells achieve full amphitely (Figure 2.S1). These results reproduce experimental results in three ways. On an individual chromosome level, mis-segregation of tagged chromosomes occurs in 60-85% of *ipl1* mutants indicating that mis-segregation of specific chromosomes is common (15–17, 88). On an all-chromosome segregation level, both FACS sorting and DAPI staining of chromosomes in *ipl1* mutants show a spread of ploidy indicating that segregation is neither equal nor completely asymmetric but rather a combination of both (17, 46, 84). Finally, on an all-cell level, *ipl1* mutants do not grow at the restrictive temperatures, suggesting high levels of aneuploidy (46, 57). Altogether, these experimental results support a model where *ipl1* mutants result from weak Ipl1 kinase relative to Glc7 phosphatase activity, such that the final kinetochore attachments are a mixture of both syntely and amphitely, and none of the cells achieve complete amphitely.

The advantage of this budding yeast error-correction model is that it integrates decades of experimental studies on error correction together with yeast chromosome congression modeling in a very simple model dominated by straight-forward kinase and phosphatase activity with microtubule dynamics. Although simple, the model both reproduces wild-type and *ipl1* mutant experimental results and elegantly demonstrates why attachments are more or less stable through energy diagrams. Improvements of this model could include a more sophisticated relationship between the kinase and

phosphatase, such as kinase-mediated phosphorylation regulating phosphatase localization to the kinetochore (89, 90). In addition, the error correction principles presented in this model can be incorporated into existing mitosis models in higher-level organisms that already include microtubule flux and multiple microtubules per kinetochore (91, 92). Overall, this model provides a better understanding of how kinetochores make the correct attachments to microtubules to yield faithful chromosome segregation and avoid aneuploidy across phylogeny.

**Acknowledgements**

We thank Dr. Yiannis Kaznessis for helpful discussions and Dr. Duncan Clarke, Dr. Melissa Gardner, Dr. Jeremy Chacon, Ms. Aimee Littleton, and Ms. Teahl Banner for technical assistance. This work was supported by the National Institute of General Medical Sciences of the National Institutes of Health under award numbers R01GM071522 and R01GM076177 to D.J.O. and R01GM64386 to S.B. E.T. was a recipient of a University of Minnesota Interdisciplinary Doctoral Fellowship through the Institute for Advanced Study.

**Author Contributions**

E.T. developed the model, analyzed the results, prepared the figures, and wrote the paper. S.B. collaborated in developing the model. D.O., principal investigator, oversaw the project and collaborated in developing the model.

**Simulation methods**

The model was simulated using a Gillespie stochastic simulation algorithm to calculate both the next event and the time until the next event (93). Possible events were microtubule catastrophe, microtubule rescue, Ipl1 kinase-mediated phosphorylation, and Glc7-mediated dephosphorylation, each with its own characteristic rate constant, $k_i$. The time, $\tau_i$, for each event was calculated using a randomly generated number, $rand_i$, and the rate constant for that event

$$\tau_i = \frac{-\ln(rand_i)}{k_i} \tag{2.8}$$

The event associated with the shortest time was executed, and the time was increased by $\tau_i$. This process continued until the requirements for the end of the simulation were met.

## Supplement

### Additional model details

To promote depolymerization of kinetochore microtubules following microtubule capture of free kinetochores on opposite spindle poles, the catastrophe gradient was linear instead of parabolic as in Gardner, *et al.* (62), however the catastrophe rate at the equator and originating poles were equivalent.

To offset the increase in the catastrophe frequency, the tension-dependent rescue frequency was given as

$$k_r = k_{r0} \exp(\rho^* \Delta x), \quad \text{(2.S1)}$$

where $k_{r0}$ =9/min, the basal rescue frequency in the absence of tensional force and $\rho^*$ =0.0009/nm, the spring constant/$F_0$ where $F_0$ is the characteristic force at which rescue frequency increases e-fold (62) instead of

$$k_r = k_{r0} \exp(\rho^* (\Delta x - x_{eq})), \quad \text{(2.S2)}$$

resulting in a 16% decrease in the rescue frequency overall. We verified that using the rescue frequency in Equation 2.S2 resulted in the same trends but with slightly more stable amphitely, because of the stronger catastrophe slope.

To prevent microtubules from shortening below the spindle pole or past the opposite spindle pole, boundary conditions were imposed such that a microtubule that shortened back to the spindle pole switched to growth and a microtubule that grew to the opposite spindle pole switched to shortening. Spindle lengths were 1.5 μm and each spindle contained 20 microtubules/pole (12).

**Calculation of delay before detachment for $N_{cr}$**

For each $N_{cr}$, the times before detachment, $\tau_d$ , were calculated by dividing the number of steps to reach $N_{cr}$, $N_{steps}(N_{cr})$, by the product of the total number of phosphorylation sites, N, and the kinase rate ($k_k=k_{ph}=k=1$),

$$\tau_d = \frac{N_{steps}(N_{cr})}{Nk}. \qquad (2.S3)$$

This required first calculating $N_{steps}(N_{cr})$ and then simulating the phosphorylation of a kinetochore with N=10 phosphorylation sites to verify that the expected times to reach the critical phosphorylation for detachment, $N_{cr}$, were obtained.

1) Calculating $N_{steps}(N_{cr})$

The number of steps to reach each $N_{cr}$ were calculated using the theory of absorbing Markov chains (82). With balanced kinase and phosphatase rates ($k_k=k_{ph}=k=1$) and N sites, the transition between subsequent numbers of sites phosphorylated is

$$\textit{dephosphorylation} \qquad m \underset{\frac{(m+1)k}{N}}{\overset{\frac{mk}{N}}{\rightleftarrows}} m+1 \qquad \textit{phosphorylation} \qquad (2.S4)$$

because there are m sites available for phosphorylation and m+1 sites available for dephosphorylation. For N=10 sites, the transitions are

$$0 \underset{0.1}{\overset{1}{\rightleftarrows}} 1 \underset{0.2}{\overset{0.9}{\rightleftarrows}} 2 \underset{0.3}{\overset{0.8}{\rightleftarrows}} 3 \underset{0.4}{\overset{0.7}{\rightleftarrows}} 4 \underset{0.5}{\overset{0.6}{\rightleftarrows}} 5 \underset{0.6}{\overset{0.5}{\rightleftarrows}} 6 \underset{0.7}{\overset{0.4}{\rightleftarrows}} 7 \underset{0.8}{\overset{0.3}{\rightleftarrows}} 8 \underset{0.9}{\overset{0.2}{\rightleftarrows}} 9 \underset{1.0}{\overset{0.1}{\rightleftarrows}} 10 \qquad \text{(2.S5)}$$

which can be displayed in a transition matrix

$$Tr = \begin{array}{c} \\ 0 \\ 1 \\ 2 \\ 3 \\ 4 \\ 5 \\ 6 \\ 7 \\ 8 \\ 9 \\ 10 \end{array} \begin{array}{c} \begin{array}{ccccccccccc} 0 & 1 & 2 & 3 & 4 & 5 & 6 & 7 & 8 & 9 & 10 \end{array} \\ \begin{pmatrix} 0 & 1.0 & 0 & 0 & 0 & 0 & 0 & 0 & 0 & 0 & 0 \\ 0.1 & 0 & 0.9 & 0 & 0 & 0 & 0 & 0 & 0 & 0 & 0 \\ 0 & 0.2 & 0 & 0.8 & 0 & 0 & 0 & 0 & 0 & 0 & 0 \\ 0 & 0 & 0.3 & 0 & 0.7 & 0 & 0 & 0 & 0 & 0 & 0 \\ 0 & 0 & 0 & 0.4 & 0 & 0.6 & 0 & 0 & 0 & 0 & 0 \\ 0 & 0 & 0 & 0 & 0.5 & 0 & 0.5 & 0 & 0 & 0 & 0 \\ 0 & 0 & 0 & 0 & 0 & 0.6 & 0 & 0.4 & 0 & 0 & 0 \\ 0 & 0 & 0 & 0 & 0 & 0 & 0.7 & 0 & 0.3 & 0 & 0 \\ 0 & 0 & 0 & 0 & 0 & 0 & 0 & 0.8 & 0 & 0.2 & 0 \\ 0 & 0 & 0 & 0 & 0 & 0 & 0 & 0 & 0.9 & 0 & 0.1 \\ 0 & 0 & 0 & 0 & 0 & 0 & 0 & 0 & 0 & 1.0 & 0 \end{pmatrix} \end{array} \qquad \text{(2.S6)}$$

For $N_{cr}$=8, detachment occurs automatically, which is equivalent to an absorption at the N=8 site (note absence of reverse arrow in equation 2.S7).

$$0 \underset{0.1}{\overset{1}{\rightleftarrows}} 1 \underset{0.2}{\overset{0.9}{\rightleftarrows}} 2 \underset{0.3}{\overset{0.8}{\rightleftarrows}} 3 \underset{0.4}{\overset{0.7}{\rightleftarrows}} 4 \underset{0.5}{\overset{0.6}{\rightleftarrows}} 5 \underset{0.6}{\overset{0.5}{\rightleftarrows}} 6 \underset{0.7}{\overset{0.4}{\rightleftarrows}} 7 \xrightarrow{0.3} 8 \qquad \text{(2.S7)}$$

The transition matrix then takes on the form

$$P = \begin{array}{c} \\ Tr \\ Abs \end{array} \begin{array}{c} \begin{array}{cc} Tr & Abs \end{array} \\ \left(\begin{array}{c|c} Q & R \\ \hline 0 & 1 \end{array}\right) \end{array} \qquad \text{(2.S8)}$$

Where the transient states are in the top left corner and the absorbing state in the bottom right

$$P = \begin{array}{c} \\ 0 \\ 1 \\ 2 \\ 3 \\ 4 \\ 5 \\ 6 \\ 7 \\ 8 \end{array} \begin{array}{c} \begin{array}{ccccccccc} 0 & 1 & 2 & 3 & 4 & 5 & 6 & 7 & 8 \end{array} \\ \left(\begin{array}{ccccccccc|c} 0 & 1.0 & 0 & 0 & 0 & 0 & 0 & 0 & 0 \\ 0.1 & 0 & 0.9 & 0 & 0 & 0 & 0 & 0 & 0 \\ 0 & 0.2 & 0 & 0.8 & 0 & 0 & 0 & 0 & 0 \\ 0 & 0 & 0.3 & 0 & 0.7 & 0 & 0 & 0 & 0 \\ 0 & 0 & 0 & 0.4 & 0 & 0.6 & 0 & 0 & 0 \\ 0 & 0 & 0 & 0 & 0.5 & 0 & 0.5 & 0 & 0 \\ 0 & 0 & 0 & 0 & 0 & 0.6 & 0 & 0.4 & 0 \\ 0 & 0 & 0 & 0 & 0 & 0 & 0.7 & 0 & 0.3 \\ \hline 0 & 0 & 0 & 0 & 0 & 0 & 0 & 0 & 1 \end{array}\right) \end{array} \tag{2.S9}$$

The fundamental matrix is

$$F = (1 - Q)^{-1} \tag{2.S10}$$

where the index $f_{ij}$ gives the expected number of times that the phosphorylation visits the phosphorylation state $s_j$ starting from the $s_i$ phosphorylation state. Thus, to calculate the number of steps before the total number of phosphorylated sites reaches $N_{cr}$ starting from any number of phosphorylated sites simply requires summing across the columns or equivalently multiplying the fundamental matrix by a column matrix of ones.

$$\left\langle N_{steps} \right\rangle = Fc; c = \begin{pmatrix} 1 \\ 1 \\ 1 \\ 1 \\ 1 \\ 1 \\ 1 \\ 1 \end{pmatrix} \tag{2.S11}$$

For $N_{cr}$=8,

$$\left\langle N_{steps} \right\rangle = \begin{pmatrix} 0 \to 8 \\ 1 \to 8 \\ 2 \to 8 \\ 3 \to 8 \\ 4 \to 8 \\ 5 \to 8 \\ 6 \to 8 \\ 7 \to 8 \end{pmatrix} = \begin{pmatrix} 51 \\ 50 \\ 49 \\ 47 \\ 45 \\ 42 \\ 37 \\ 27 \end{pmatrix}. \tag{2.S12}$$

Thus the number of steps required to reach $N_{cr}$=8 from the expected number of phosphorylated sites μ=5 is 42. This process was also used to calculate the number of steps required to reach different numbers of phosphorylated sites (phosphorylation levels) X=0,1,2,3,4,6,7,9,10 (where $N_{cr}$ can equal any X) from μ=5 as well as the times to reach μ=5 from X=0,1,2,3,4,6,7,8,9,10 (Analytical, Figure 2.S2 A,B). Additionally, we simulated a single kinetochore pair under low chromatin tension for 1000 simulation minutes (i.e. with only kinase-mediated phosphorylation and phosphatase-mediated dephosphorylation) to verify that the same number of steps to reach X from μ=5 and the number of steps to reach μ=5 from X were obtained (Stochastic, Figure 2.S2 A,B). In

both cases, the stochastic data fell directly on top of the analytical data, providing evidence that the theory of absorbing Markov chains accurately calculates the number of steps before reaching $N_{cr.}$

2) Calculating the time to reach $N_{cr}$

We predicted that the time to reach $N_{cr}$ would be of the form

$$\tau_d = \frac{N_{steps}(N_{cr})}{ak}, \tag{2.S13}$$

however, we were unsure about the constant in the denominator, $a$, and so initially started with the total number of sites, N. Using this equation, we calculated the predicted times before reaching different phosphorylation levels, X=0,1,2,3,4,6,7,8,9,10 (Analytical, Figure 2.S2 C,D). Returning to our simulation we then collected the times to reach X (Stochastic, Figure 2.S2 C,D). As before, the times to reach X fell directly on top of the analytical data, hence we accepted equation 2.S3 to calculate the times to reach $N_{cr}$ from μ=5.

**Tables and Figures**

**Table 1. Error correction model parameters and values**

| Parameter Description | Symbol | Value |
|---|---|---|
| Growth and shortening velocity | V | 20 nm/s[a] |
| Chromatin spring constant | $k_{chrom}$ | 14 pN/μm[b] |
| Chromatin rest length | $x_{eq}$ | 200 nm[c] |
| Maximum tension for Ipl1 activity | $T_{Ipl1}$ | 0.5 pN[d] |
| Maximum distance of MT plus ends for KT capture | $d$ | 17 nm[e] |
| Number of Ip1 substrates, single state phosphorylation model | $N$ | 1 |
| Critical phosphorylation for detachment, single state phosphorylation model | $N_{cr}$ | 1 |
| Number of Ip1 substrates, multistate phosphorylation model | $N$ | 10[f] |
| Critical phosphorylation for detachment, multistate phosphorylation model | $N_{cr}$ | 8-10 |

[a](Gardner, *et al.,* 2005, 2008)
[b](Chacon, *et al.,* 2014)
[c](Gardner, *et al.,* 2005)
[d]estimated value (Dewar, *et al.,* 2004; Tanaka, *et al.,* 2002)
[e] root mean square displacement of KT on chromatin spring (Chacon, *et al.,* 2014)
[f](Cheeseman, *et al.,* 2002)

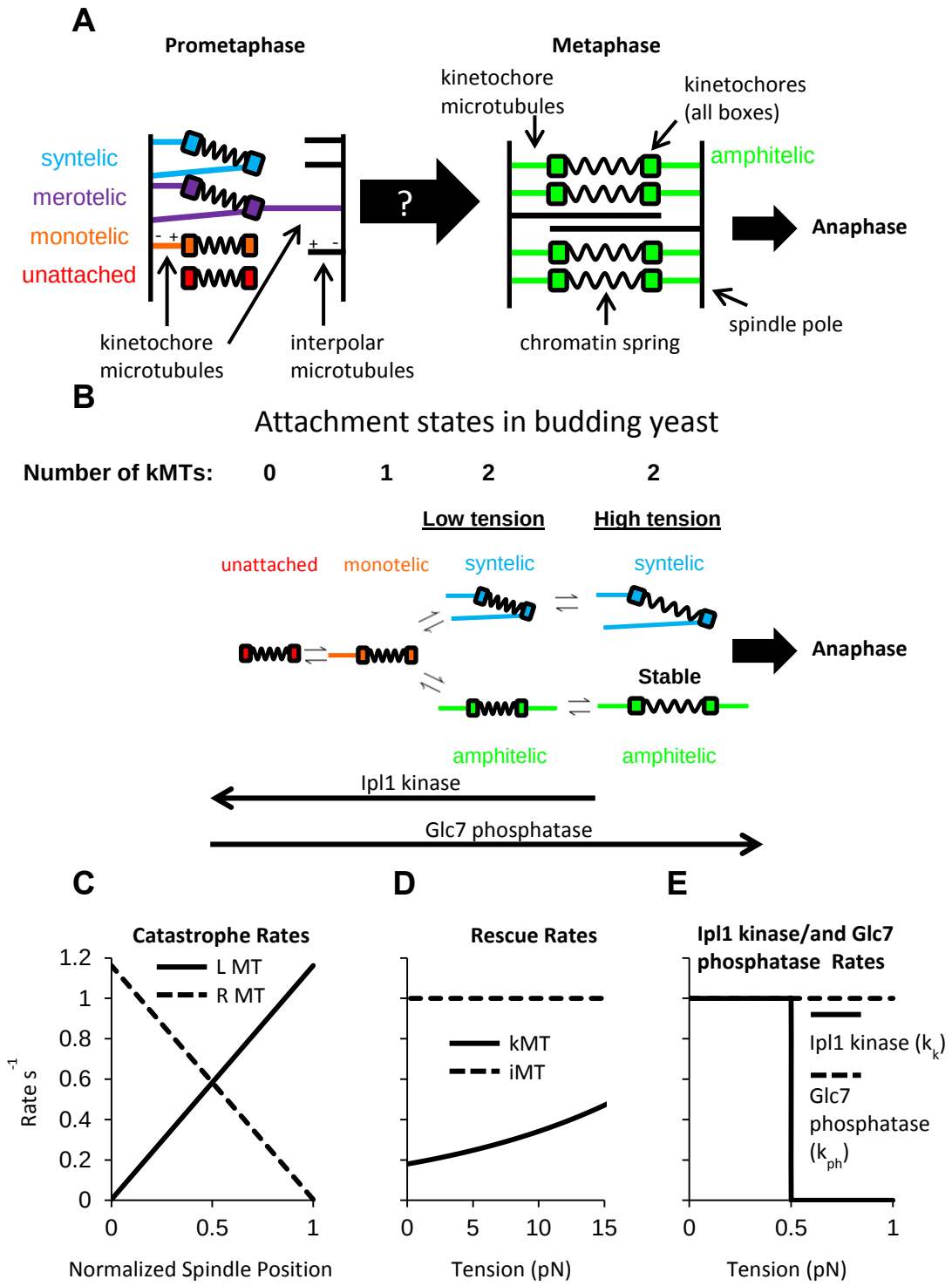


**Figure 2.1. Model for mitotic error correction**

A) Cartoon of prometaphase spindle with erroneous kinetochore-microtubule attachments and metaphase spindle with correct kinetochore-microtubule attachments. Erroneous attachments

must be corrected before anaphase to avoid aneuploidy. B) Attachment states of kinetochores and microtubules in budding yeast spindle. All transitions between attachment states require passage through monotelic attachments, and two-kinetochore attachments are sub-divided by low-tension and high-tension attachments. Only high-tension amphitelic attachments are stable. Ipl1 kinase-mediated phosphorylation promotes kinetochore-microtubule detachment when chromatin lacks tension, and Glc7 phosphatase-mediated dephosphorylation promotes kinetochore-microtubule attachments independent of tension. C) The linear microtubule catastrophe gradient promotes length-dependent depolymerization of microtubules, which generates tension in amphitelic, but not syntelic, attachments. D) The weakly tension-dependent rescue frequency promotes polymerization of kinetochore microtubules when chromatin is under tension, maintaining short kinetochore microtubules. The constant, high rescue frequency of interpolar microtubules promotes growth, maintaining long interpolar microtubules. E) The Ipl1 kinase rate promotes phosphorylation of Ipl1 phosphorylation sites when chromatin tension is low. The Glc7 phosphatase rate is constitutively active and antagonizes Ipl1 kinase-mediated phosphorylation.

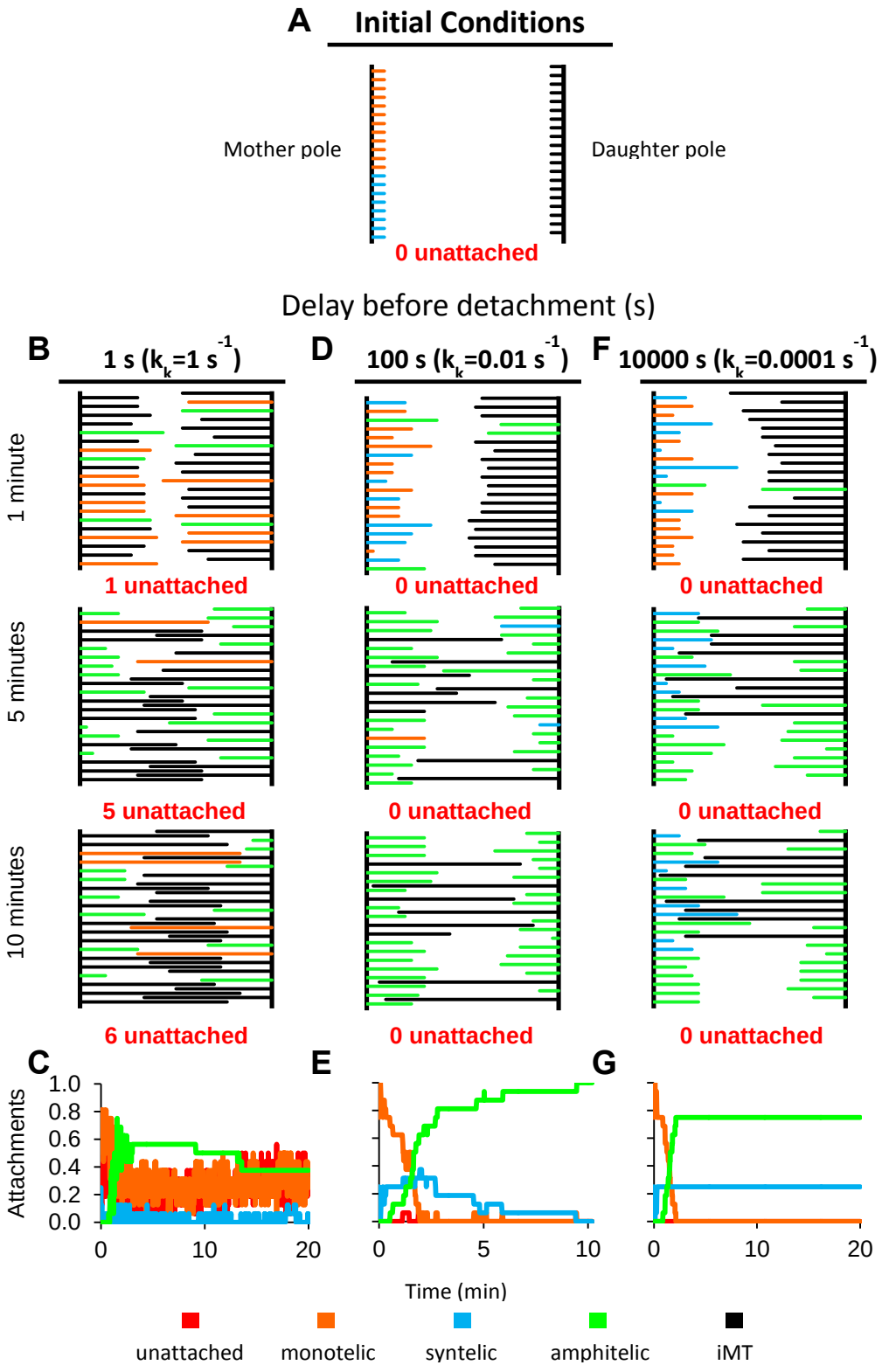


**Figure 2.2. Model output depicting microtubule lengths and kinetochore attachments through time for a single site phosphorylation model**

In subfigures 2A,B,D,F vertical lines represent spindle poles, and horizontal lines represent microtubules, where the length indicates microtubule length and color indicates type of kinetochore attachment. In the case of monotely, a single line represents attachment to a single kinetochore (kinetochore not shown). In the cases of syntely and amphitely, two lines represent attachments to two kinetochores (kinetochores not shown). A) Initially, all microtubules on the left pole, i.e. the mother pole, were attached to kinetochores in monotelic or syntelic attachments and all microtubules on the right pole, i.e. the daughter pole, were interpolar microtubules (iMTs). B) For a kinase rate constant of $k_k=1s^{-1}$, a short delay before detachment of $1/k_k=1$ s led to high levels of detachment, i.e. unattached kinetochores and monotelic attachments with only some amphitelic attachments (Movie 2.S1). C) The time series indicate that kinetochore-microtubule attachment and detachment was extremely dynamic, and amphitelic attachments were unable to maintain stability throughout time. D) For a kinase rate constant of $k_k=0.01s^{-1}$, a longer delay before detachment of $1/k_k=100$ s led to higher levels of attachment, particularly amphitelic attachments because the initiation problem of biorientation was solved as monotelic attachments transitioned to amphitelic attachments rather than reverting to unattached kinetochores, and low-tension amphitelic attachments transitioned to stable high-tension amphitelic attachments rather than low-tension amphitelic attachments (Movie 2.S2). E) The time series indicate that amphitelic attachments replaced initial monotelic and syntelic attachments, and amphitelic attachments maintained stability throughout time. F) For a kinase rate constant of $k_k=0.0001s^{-1}$, an overly-prolonged delay before detachment of $1/k_k=10000$ s led to prevention of correction of improper syntelic attachments (Movie 2.S3). This case effectively mimics Ipl1 mutants that lack kinase activity. G) The time series indicate that after initial failure of monotelic and syntelic attachments due to the random phosphorylation in the initial conditions, syntelic attachments were established with microtubules from the mother pole and amphitelic attachments were established in the remaining kinetochores. Because of the overly-prolonged delay before detachment, the syntelic attachments were not corrected.

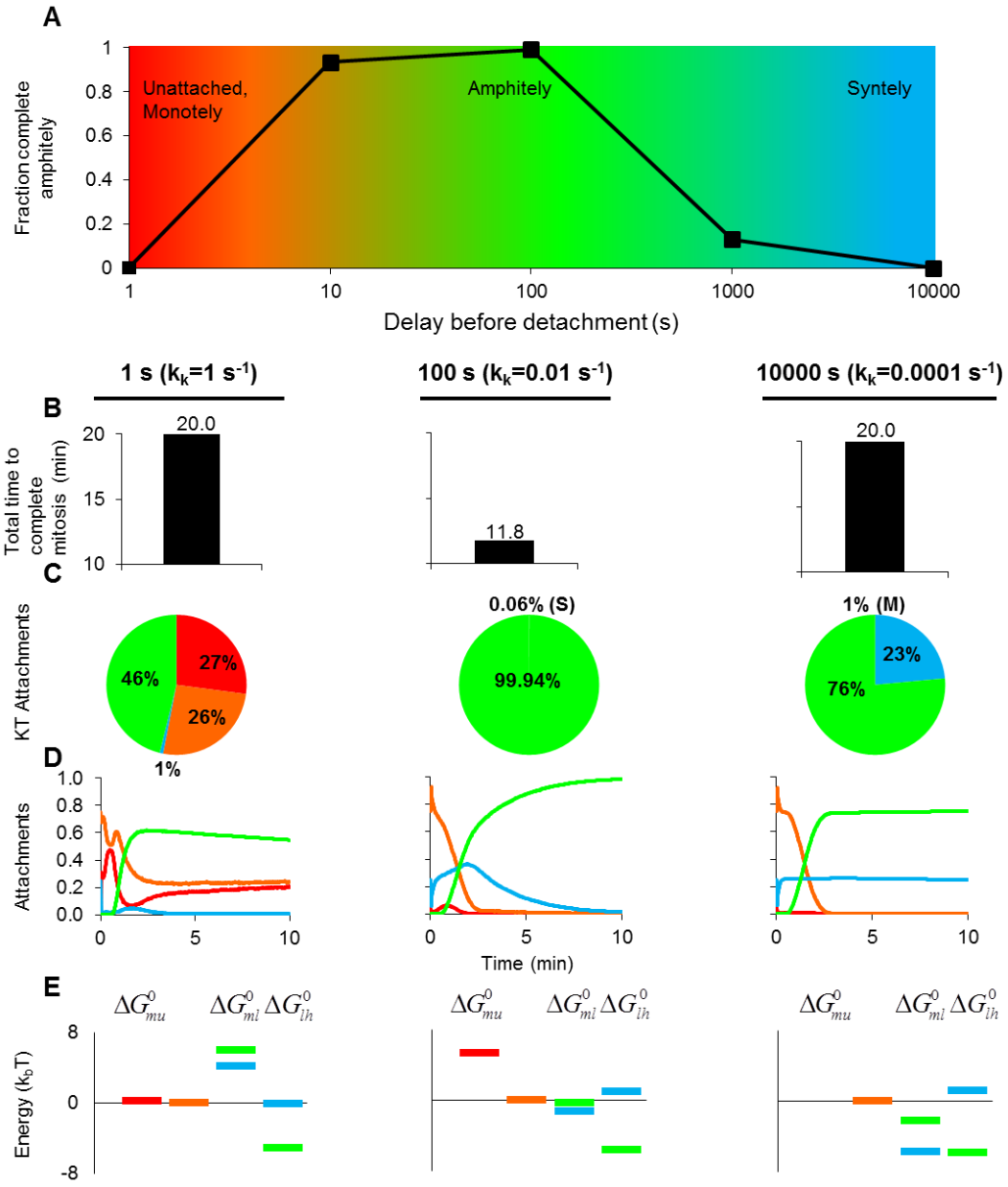


**Figure 2.3. An optimum in complete amphitely requires a delay before detachment**

A) Reducing the kinase rate relative to phosphatase in the single site phosphorylation model results in increased delays before detachment and the emergence of an optimum in the number of spindles that end the simulation with complete amphitely, i.e. where all 16 pairs are amphitelic (n=1000 simulated spindles for each phosphatase/kinase ratio with delays before detachment of 1-10000 s, $X^2$=4000, df=4, $p<10^{-100}$). B) The total time to complete mitosis coincides with maximal complete amphitely ($p<10^{-100}$, (Kruskal-Wallis)). All groups were statistically different (multiple comparisons test (Tukey-Kramer, α=0.05)). C) Distribution of kinetochore attachment states at anaphase onset. For a 1 s delay before detachment, unattached kinetochores and

monotelic attachments were both high because detachment was too fast. For a 100 s delay, amphitelic attachments reached nearly 100% because the delay before detachment was sufficient to solve the initiation problem of bi-orientation, and for a 10000 s delay, syntelic attachments were high because the delay before detachment was too long, ($X^2$=12000, df=2, $p<10^{-100}$ (amphitelic versus not amphitelic)). D) The average attachment states over time for the first ten minutes revealed how kinetochore attachments were obtained. In all cases, amphitelic attachments rose within the first five simulation minutes, but for $1/k_k$=1 s delay before detachment it began to fall as monotelic attachments and unattached kinetochores rose, for a $1/k_k$=100 s delay, it continued to rise, and for a $1/k_k$=10000 s delay it reached a plateau as syntelic attachments persisted, consistent with the final kinetochore attachment distributions at anaphase onset (C). E) The energy diagrams show that the energy change from low-tension amphitely to high-tension amphitely was most favorable in all cases. For a $1/k_k$=1 s delay before detachment the energy change from monotelic to low-tension attachments was an energy barrier to high-tension amphitely, for a $1/k_k$=100 s delay the energy barrier was decreased, facilitating passage to high-tension amphitely, and for a $1/k_k$=10000 s delay the energy barrier transitioned to a new minimum for low-tension syntely, thus stabilizing low-tension syntely.

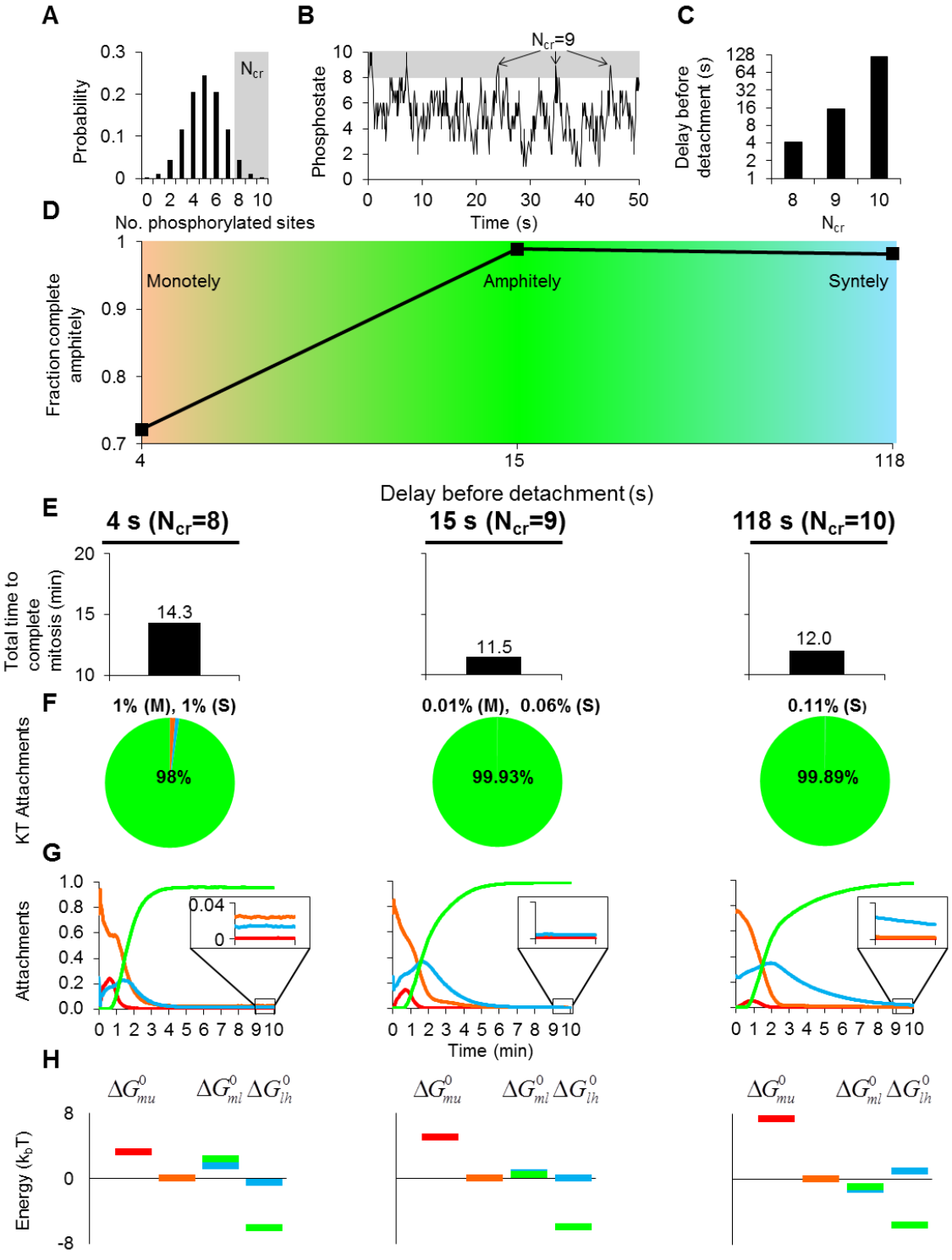
A
Probability
0.3
0.2
0.1
0
$N_{cr}$
0 2 4 6 8 10
No. phosphorylated sites
B
Phosphostate
10
8
6
4
2
0
$N_{cr}$=9
0 10 20 30 40 50
Time (s)
C
Delay before detachment (s)
128
64
32
16
8
4
2
1
8 9 10
$N_{cr}$
D
Fraction complete amphitely
1
0.9
0.8
0.7
Monotely
Amphitely
Syntely
4
15
118
Delay before detachment (s)
E
4 s ($N_{cr}$=8)
15 s ($N_{cr}$=9)
118 s ($N_{cr}$=10)
Total time to complete mitosis (min)
20
15
10
14.3
11.5
12.0
F
KT Attachments
1% (M), 1% (S)
0.01% (M), 0.06% (S)
0.11% (S)
98%
99.93%
99.89%
G
Attachments
1.0
0.8
0.6
0.4
0.2
0.0
0.04
0
0 1 2 3 4 5 6 7 8 9 10
Time (min)
H
$\Delta G^0_{mu}$
$\Delta G^0_{ml}$ $\Delta G^0_{lh}$
Energy ($k_bT$)
8
0
-8

**Figure 2.4. A multisite phosphorylation model solves the initiation problem of biorientation by requiring nearly maximal phosphorylation for detachment**

A) When chromatin lacks tension with 10 Ipl1 phosphorylation sites, the probability of the number of sites phosphorylated follows a binomial distribution with N=10 sites and p=0.5 probability of phosphorylation. A high critical phosphorylation for detachment $N_{cr}$ in the right tail of the distribution ensures a delay before detachment. B) A simulated kinetochore pair under low chromatin tension subject to Ip1 kinase-mediated phosphorylation and Glc7 phosphatase-mediated dephosphorylation demonstrates that the phosphostate of the kinetochore is on average 5 but reaches $N_{cr}$=8 infrequently, $N_{cr}$=9 very infrequently, and $N_{cr}$=10 extremely infrequently. C) As $N_{cr}$ increases, the delay before detachment increases monotonically. D) Increasing the delay before detachment by increasing the critical phosphorylation for detachment $N_{cr}$ results in the emergence of an optimum in spindles that end the simulation with complete amphitely (n=1000, 3600, 2800 simulated spindles for each $N_{cr}$=8,9,10, $X^2$=1300, df=2, $p<10^{-100}$, detachment times of 15 s and 118 s were statistically significant, $X^2$=20, df=1, $p<10^{-5}$), (Movies 2.S4-2.S6). E) The total time to complete mitosis coincides with maximal complete amphitely ($p=10^{-58}$ (Kruskal-Wallis)). All groups were statistically different (multiple comparisons test (Tukey-Kramer, α=0.05)). F) Distribution of kinetochore attachment states at anaphase onset. Although the differences were modest, the highest level of amphitely was achieved with the intermediate delay before detachment ($X^2$=1800, df=2, $p<10^{-100}$ (amphitelic versus not amphitelic), detachment times of 15 s and 118 s were statistically significant $X^2$=6, df=1, p=0.02). G) The average attachments through time for the first ten minutes revealed how kinetochore attachments were obtained. Although the differences appear modest, amphitelic attachments rose more slowly and monotelic and syntelic attachments fell more slowly, as the delay before detachment increased. Insets between 9 and 10 minutes indicate that incorrect attachments were low for the intermediate delay before detachment but higher for the shortest and longest delays before detachment. H) The energy diagrams show that the energy change from low-tension amphitely to high-tension amphitely was most favorable in all cases. Although the differences were modest, as the delay before detachment increased, the energy change of monotelic to low-tension attachments decreased, facilitating passage to high-tension amphitely for the intermediate detachment time (when $N_{cr}$=9) and became negative for the longest detachment time ($N_{cr}$=10) which stabilized syntely and accounts for the small drop in complete amphitely over all spindles (D).

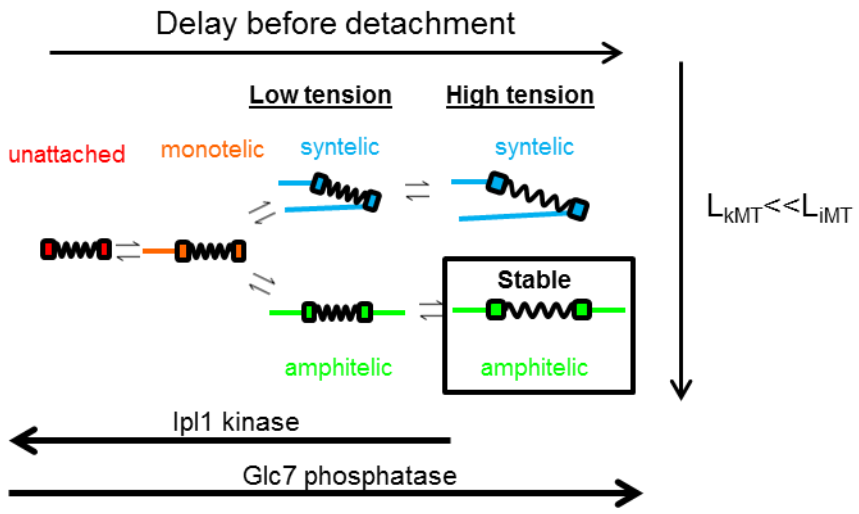


**Figure 2.5. High-tension amphitely is achieved by a combination of a long delay before detachment and net kinetochore microtubule disassembly**

Overall, the model for spindle-attachment error correction in budding yeast revealed that in order to achieve maximal amphitelic attachments, the delay before detachment needed to be sufficiently long to solve the initiation problem of biorientation, so that monotelic attachments transitioned to low-tension amphitelic attachments instead of unattached kinetochores, and low-tension amphitelic attachments transitioned to high tension amphitelic attachments rather than monotelic attachments. Additionally, the net disassembly of kinetochore microtubules generated tension in amphitelic, but not syntelic attachments, which prevented transitions of high-tension amphitelic attachments to low-tension amphitelic attachments thus ensuring stability of high-tension amphitelic attachments.

## Supplemental Figures

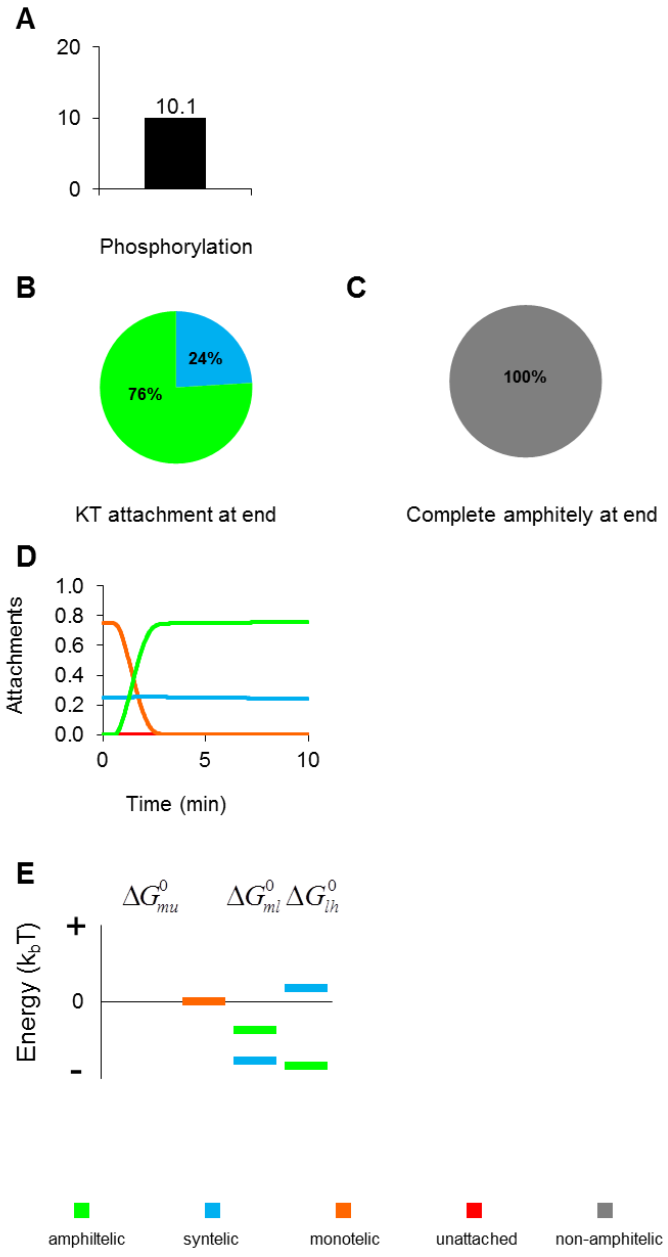


**Figure 2.S1. An *ipl1* mutant maintains high levels of syntely**

(A) An *ipl1* mutant was simulated with $k_{ph}$=1$s^{-1}$ and $k_k$=0.0001$s^{-1}$ with a maximum simulation time of 10.1 seconds and no initial phosphorylation of Ipl1 sites. The simulations ended at the expected times (n=1000 spindles simulated). B) The pooled kinetochore attachments showed that syntelic attachments accounted for ~1/4 of all attachments with the remainder amphitelic attachments, indicating that the initial syntelic attachments were not resolved. C) None of the cells achieved complete amphitely by the end of the simulation, as expected because syntelic

attachments persisted. D) The attachments through time showed that syntelic attachments persisted throughout the simulation while the free kinetochores of monotelic attachments were captured by microtubules and transitioned to amphitelic attachments. E) The energy diagrams show two minima corresponding to low-tension syntely and high-tension amphitely, indicating that both were stabilized.

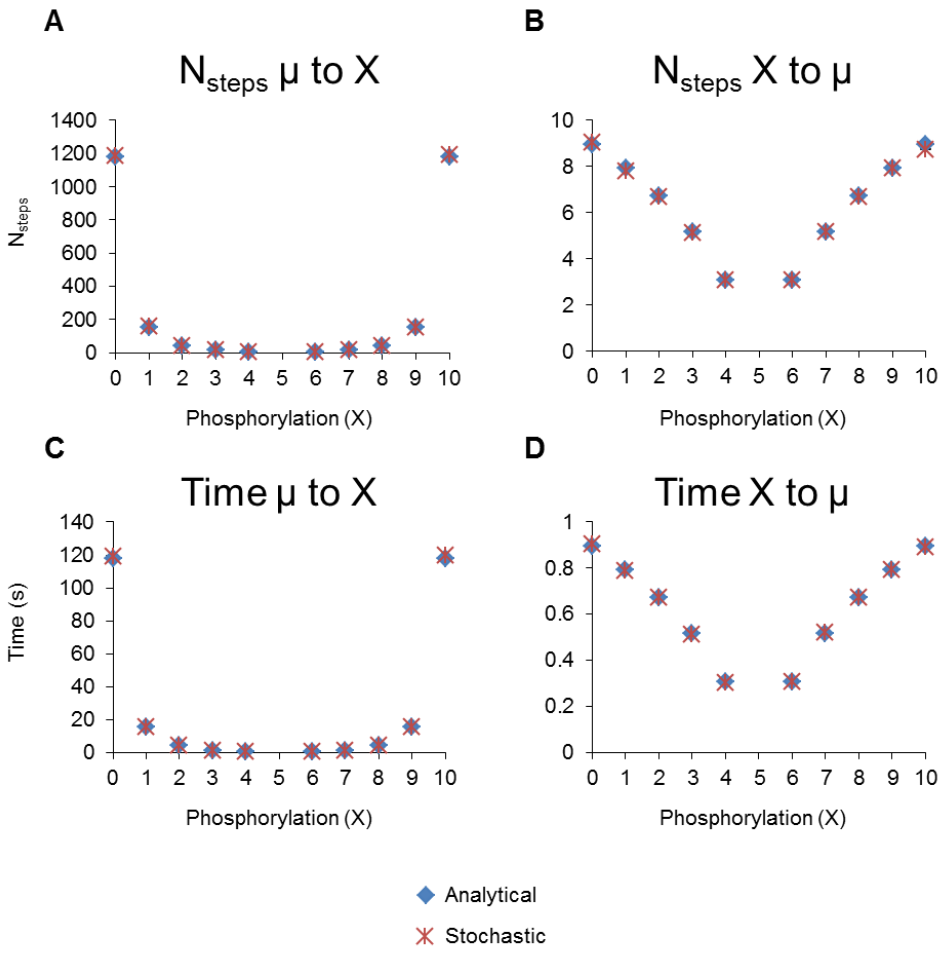


**Figure 2.S2. Number of steps and time to reach specific phosphorylation levels**

A) Analytical and stochastic simulation output of the number of steps to reach different phosphorylation levels X from the expected phosphorylation level, μ=5, shows that the number of steps rises monotonically as X extends into either tail. B) Analytical and stochastic simulation output of the number of steps to reach the expected phosphorylation level, μ=5 from different phosphorylation levels X shows that the number of steps falls monotonically as X approaches μ. C) Analytical and stochastic simulation output of the time to reach different phosphorylation levels X, from the expected phosphorylation level, μ=5, shows that the time rises monotonically as X extends into either tail and is proportional to the number of steps by 1/N. D) Analytical and stochastic simulation output of the time to reach the expected phosphorylation level, μ=5 from different phosphorylation levels X shows that the time falls monotonically as $N_{cr}$ approaches μ, and is proportional to the number of steps by 1/N.

## Supplemental Movie Captions

**In all movies, a simulated spindle with kinetochore microtubules and interpolar microtubules (as in Figure 2.2 B,D,F) is shown on the top, and a plot with attachments through time (as in Figure 2.2 C,E,G) is shown on the bottom.**

**Movie 2.S1: Single site phosphorylation model (N=Ncr=1), $k_{ph}/k_k$=1**
With balanced kinase and phosphatase activity in a single site phosphorylation model, detachment occurs too frequently. The cell does not achieve "complete amphitely" in which all kinetochore pairs are amphitelic by the simulation end.

**Movie 2.S2: Single site phosphorylation model (N=Ncr=1), $k_{ph}/k_k$ =100**
With weak kinase relative to phosphatase activity in a single site phosphorylation model, monotelic and syntelic attachments are replaced by amphitelic attachments which are stabilized because the delay before detachment is longer, allowing low-tension amphitelic attachments to transition to stable, high-tension amphitelic attachments. The cell achieves "complete amphitely."

**Movie 2.S3: Single site phosphorylation model (N=Ncr=1), $k_{ph}/k_k$ =10000**
With very weak kinase relative to phosphatase activity in a single site phosphorylation model, syntelic attachments made early in the simulation are not corrected because the delay before detachment is too long. The cell does not achieve "complete amphitely."

**Movie 2.S4: Multisite phosphorylation model (N=10, Ncr=8), $k_{ph}/k_k$ =1**
With balanced kinase and phosphatase activity in a multisite phosphorylation model with $N_{cr}$=8, amphitelic attachments rise throughout time but the simulation ends without "complete amphitely" because the delay before detachment is too short, preventing stabilization of all amphitelic attachments.

**Movie 2.S5: Multisite phosphorylation model (N=10, Ncr=9), $k_{ph}/k_k$ =1**
With balanced kinase and phosphatase activity in a multisite phosphorylation model with $N_{cr}$=9, amphitelic attachments rise throughout time and the simulation ends with "complete amphitely" because the delay before detachment is longer, allowing stabilization of all amphitelic attachments.

**Movie 2.S6: Multisite phosphorylation model (N=10, Ncr=10), $k_{ph}/k_k$ =1**
With balanced kinase and phosphatase activity in a multisite phosphorylation model with $N_{cr}$=10, amphitelic attachments rise more slowly throughout time (compared to Movie 2.S5) and the simulation ends with "complete amphitely" because the delay before detachment is long, allowing

stabilization of all amphitelic attachments. Note that in this instance complete amphitely was attained, however overall complete amphitely is less common with $N_{cr}$=10 compared to $N_{cr}$=9 because the delay before detachment is too long in some cases (Figure 2.4 D).

# Chapter 3: Kinesin-5 mediated chromosome congression in animal spindles

Authors: Emily Tubman[1], Yungui He[2], Thomas S. Hays[2],* and David J. Odde[1*]

Affiliations:

[1]Department of Biomedical Engineering, University of Minnesota, Minneapolis, MN 55455

[2]Department of Genetics, Cell Biology, and Development, University of Minnesota, Minneapolis, MN 55455

*Co-senior authors

## Summary

The microtubule motor protein kinesin-5 is well known to establish the bipolar spindle by outward sliding of antiparallel interpolar microtubules. In yeast, kinesin-5 also facilitates chromosome alignment at the spindle equator, "chromosome congression," by preferentially depolymerizing long kinetochore microtubules. To determine if kinesin-5 also facilitates chromosome congression in animal spindles, we performed RNAi of the kinesin-5 Klp61F in *Drosophila melanogaster* S2 cells, which resulted primarily in monopolar spindles; however with a weak Klp61F knockdown, approximately half of the spindles transitioned to bioriented spindles before completing mitosis, allowing analysis of congression. Consistent with kinesin-5 length-dependent depolymerase activity, kinetochore microtubules were longer and the kinetochores less congressed compared to control over a range of conditions. RNAi of the kinesin-8 Klp67A revealed that kinetochore microtubules relative to the spindle lengths were not longer compared to control, but rather that the spindles were longer, indicating that Klp67A acts preferentially as a length-dependent depolymerase on interpolar microtubules without significantly affecting kinetochore microtubule length and chromosome congression. These studies show that in addition to establishing the bipolar spindle, kinesin-5 also regulates

kinetochore microtubule length to facilitate chromosome congression in animal spindles, as it does in yeast.

## Introduction

During mitosis, replicated chromosomes attach to the mitotic spindle machinery through their chromosome-associated kinetochores, which attach to the plus ends of dynamic kinetochore microtubules that have their minus ends anchored near the spindle poles (44). Biorientation of chromosomes requires that the kinetochores attach to kinetochore microtubules from opposite spindle poles. A key step in mitotic progression is chromosome congression, the alignment of the bioriented chromosomes at the mitotic spindle equator during metaphase. Although chromosome congression is a well-documented phenomenon in mitosis, the mechanism by which it is achieved is still a subject of debate (94).

A polar ejection force has been proposed in which pushing forces act on chromosome arms to bias movement of chromosomes away from the poles and toward the spindle equator to promote congression. The pushing force is attributed to: 1) plus-end directed chromokinesins (kinesin-4/10) that reside on chromosome arms and walk along spindle microtubules, 2) microtubule "pushing" by polymerizing microtubules at spindle poles, or 3) a dense array of microtubules inhibiting movement into the spindle poles (33, 34, 40, 95–97). However, several lines of evidence argue against a polar ejection force-based mechanism for congression. First, cells injected with antibodies to chromokinesins show only a modest defect in chromosome congression (38). Second, mitotic cells with unreplicated genomes, or "MUGS," which essentially lack chromosome arms, still have congressed kinetochores (36, 37, 39, 98). Finally, experiments in which chromosome arms were removed using lasers did not produce conclusive changes in

the oscillations of the resultant chromosomes sufficient to reject the null hypothesis that the polar ejection force is not involved in chromosome oscillations (see expanded discussion in Materials and Methods). Altogether, these results argue that the polar ejection force is not critical for achieving chromosome congression.

Because the polar ejection force does not adequately explain how chromosomes congress, another mechanism must exist to promote congression. Kinetochores attach to the plus ends of dynamic kinetochore microtubules that shorten or lengthen. The progressive alignment of chromosomes at the spindle equator requires that the plus-end dynamics of the kinetochore microtubules are spatially regulated, so that they grow well from the spindle poles and poorly near the equator (42, 61, 62). The quality of congression can be quantitatively characterized by a signal-to-noise ratio, SNR=<L>/$\sigma$, where the mean kinetochore microtubule length, <L>, is normalized to the standard deviation of lengths, $\sigma$, or, equivalently, by the coefficient of variation, CV=1/SNR, where CV=0 means perfect congression and CV=1 means poor congression (43). Previous studies have reported that mitotic microtubule motor proteins other than chromokinesins mediate chromosome congression by regulating the plus-end dynamics of kinetochore microtubules. Specifically, kinesin-8 is a dimeric, plus-end directed motor protein that promotes disassembly of long microtubules *in vitro*, mediates spindle length, and dampens chromosome oscillations *in vivo* (41, 97, 99, 100, 66, 101–103). Kinesin-5 is a homotetrameric, plus-end directed, motor protein best known for its role in the cross-linking and sliding apart of antiparallel microtubules during bipolar spindle formation (104). In the fungi *Saccharomyces cerevisiae* and *Candida albicans*, the kinesin-5 mutants *cin8Δ* (Cin8p and Kip1p are the only two kinesin-5 genes in *S. cerevisiae*) and *KIP1/kip1Δ* (Kip1p is the only kinesin-5 in diploid *C. albicans*) were still able to form bipolar mitotic spindles; however, in these mutants the kinetochore microtubules were

longer and more variable in length, thus impairing chromosome congression (42, 43). In contrast, kinesin-8 mutants showed no evidence of longer kinetochore microtubules or impaired chromosome congression, but did exhibit an increase in spindle lengths (42, 43). Gardner *et al.* established a model where tetrameric kinesin-5 crosslinks microtubules, which naturally guides it toward kinetochore microtubule plus ends where it promotes kinetochore microtubule disassembly and mediates chromosome congression (42). By contrast, dimeric kinesin-8, unable to crosslink between MTs, tends to remain persistent on the longer interpolar microtubules; therefore, kinesin-8 is guided toward interpolar microtubule plus ends where it promotes interpolar microtubule disassembly and controls spindle length (42). Significantly, kinesin-5 is only known to mediate chromosome congression in fungi, raising the question of whether this motor-based congression mechanism preceded fungal divergence from other eukaryotes during evolution, or emerged as a later elaboration after divergence.

To address whether kinesin-5 drives chromosome congression in animal cells, we examined the function of kinesin-5 in the fly *Drosophila melanogaster* S2 cells. The *Drosophila* kinesin-5, Klp61F, has been reported to mediate bipolar spindle assembly, promote poleward flux, and drive spindle elongation during anaphase B (105–108). We chose the *Drosophila* system because it is very amenable to protein knockdown with RNAi via dsRNA-induced gene silencing (105, 108–110). In previous experiments with near-complete protein reduction, Klp61F RNAi led to monopolar spindles (105, 107, 108). In our experiments, the partial reduction of kinesin-5 allowed us to study bioriented spindles assembled in animal cells, to ask whether kinesin-5 also regulates kinetochore microtubule assembly in a length-dependent manner to facilitate chromosome congression.

## Results

### Klp61F RNAi cells undergo delayed mitosis with asymmetric chromosome segregation in anaphase

Mitotic delay is a typical consequence of impairment of microtubule dynamics, e.g. via mitotic poisons used for cancer treatment, such as paclitaxel, nocodazole, and kinesin-5 inhibitors (111, 112). Outcomes are mitotic slippage (completion of mitosis without satisfaction of the spindle assembly checkpoint), aneuploidy, and eventual apoptosis (111, 112). To determine the longer-term mitotic effects of Klp61F reduction, we performed RNAi of Klp61F (5 µg dsRNA/$10^6$ cells) on days 0 and 3 in S2 cells, indicating up to 50% protein reduction after 3 days (Figure 3.1A) (109, 113). This was completed in S2 cells stably expressing mCherry-Tubulin and GFP-Cid (Centromere identifier, CENP-A histone, a core kinetochore component) (114, 115). We observed cells via time-lapse fluorescence microscopy 2.5 days after the initial transfection (estimated Klp61F reduction 30%) and found that most control spindles were bipolar and Klp61F RNAi spindles were monopolar with approximately half transitioning to bioriented spindles (Figure 3.1B,C). The Klp61F RNAi bioriented phenotype (Figure 3.1C middle row) has been observed previously in S2 cells, and called “monastral bipolars;” it was found that this pathway required Klp61F, indicating that sufficient Klp61F remained to form bioriented spindles (105, 107).

To determine if the cells underwent mitotic delay with reduced Klp61F levels, we measured the time in mitosis, defined as the difference between anaphase onset and nuclear envelope breakdown, observed in 97% of control cells, 64% of Klp61F RNAi bioriented cells, and 20% of Klp61F RNAi monopolar cells (Figure 3.1D). In the remaining cells, only a minimum time was obtained because cells either entered into and

remained in mitosis through the end of the time-lapse imaging or they were already in mitosis at the start of the time-lapse imaging. Overall, time in mitosis correlated with severity of phenotype, with Klp61F RNAi spindles that never bioriented spending the most time in mitosis (Figure 3.1D). Cid distribution in anaphase indicated chromosome segregation and was quantified by taking the ratio of the lower side's fluorescence to the higher side's fluorescence, where a ratio of 1 means perfect symmetry (i.e. high chromosome segregation fidelity) and zero means complete asymmetry (i.e. massive aneuploidy). Again, the trend was increased asymmetry with severity of phenotype, indicating that chromosome segregation was more impaired in Klp61F RNAi spindles than control (Figure 3.1E).

Our results demonstrate that a weak knockdown of Klp61F causes mitotic delay followed by mitotic slippage and asymmetric segregation of chromosomes in S2 cells, similar to aberrant mitoses for cancer cell lines treated with kinesin-5 inhibitors (112).

**Klp61F RNAi bioriented and bipolar spindles have longer kinetochore microtubules and less congressed chromosomes than control bipolar spindles**

In addition to collecting time-lapse images, we also collected single time point images of control and Klp61F RNAi spindles with varying amounts of dsRNA Klp61F (0,1,10 µg dsRNA/$10^6$ cells) transfected and various times following transfection. These experiments were performed in both mCherry-Tubulin/GFP-Cid S2 cells and GFP-Tubulin S2 cells (105, 114, 115). Overall, we found that increased time following transfection of dsRNA led to greater monopolarity, more so than increased dsRNA (Figure 3.2B). This was not surprising because transfecting cells with dsRNA initiates RNAi to inhibit gene expression, but it does not directly target the existing protein level. The low level of monopolarity one day after transfection indicates that the Klp61F protein

level was still high in most cells, but two and three days after transfection the high level of monopolarity indicates that the remaining protein was degraded and not replaced. As in our movie data, we also observed bipolar and bioriented spindles, which again allowed us to investigate congression with reduced kinesin-5.

We measured the tubulin fluorescence distribution, Cid fluorescence distribution, and spindle length in bipolar and bioriented spindles in the time-lapse and single time point data across different dsRNA concentrations, times following transfection, and cell lines, and found the same trends in all experimental conditions; therefore, we pooled the data (for results of individual experiments, see Supplemental Figures 3.S1-3.S2). Cells were defined as being in metaphase when their spindle lengths were within two standard deviations of the mean of control cells' spindle lengths and this criterion was applied to limit our investigation to metaphase spindles (42, 43). A bilobed tubulin fluorescence distribution, in which fluorescence rises from the spindle poles and then decreases at the spindle equator indicates that the mean location of kinetochore microtubule plus ends is where the fluorescence signal decays most rapidly in space, which effectively positions sister kinetochores on either side of the equator (61, 62). This fluorescence distribution is observed experimentally in wild-type yeast (42, 43). The loss of the bilobed fluorescence distribution, characterized by a relatively flat "bar" of fluorescence across the spindle, indicates that the kinetochore microtubules are longer and more variable in length and the chromosomes are not properly congressed (42, 43, 62). This fluorescence distribution is observed experimentally in *S. cerevisiae cin8Δ* and *C. albicans KIP1/kip1* (42, 43). We used this same assay in S2 cells where the majority of minus ends are located at the spindle poles (116). Whereas a bilobed tubulin distribution was observed in control bipolar spindles, a "flattened" bilobed tubulin distribution was observed in Klp61F RNAi bipolar and bioriented spindles, indicating that

the kinetochore microtubules in Klp61F RNAi bipolar and bioriented spindles were longer and more variable in length than kinetochore microtubules in control spindles (Figure 3.2C). Additionally, the aligned fluorescent peaks of the Cid distributions for control and Klp61F RNAi bipolar and bioriented spindles revealed that the Klp61F RNAi Cid fluorescence distribution was broader than control, consistent with a loss of congression (Figure 3.2D). Furthermore, the CV metric was applied to quantify the level of congression (Materials and Methods) (43). The CV for control spindles was 0.22 and for Klp61F RNAi spindles was 0.26, indicating that congression was reduced in Klp61F RNAi spindles compared to control. Lastly, with fewer kinesin-5 motors to force the poles apart, the spindle length is expected to be shorter, and we found that indeed the spindle lengths were 8.5% shorter in Klp61F RNAi bipolar and bioriented spindles compared to control bipolar spindles (Figure 3.2E).

Our results show Klp61F RNAi bipolar and bioriented spindles have longer kinetochore microtubules, less concentrated Cid fluorescence at the spindle equator, and shorter spindles. Taken together with the result that Klp61F RNAi bioriented spindles segregate their chromosomes more asymmetrically than control, this demonstrates that a lack of chromosome congression correlates with poor chromosome segregation and that kinesin-5 has a role in facilitating both proper chromosome congression and segregation. Additionally, Brust-Mascher *et al.* found that in *Drosophila* embryos injected with anti-Klp61F antibodies that had only partial dissociation of kinesin-5 from the spindles (avoiding monopolar spindle collapse), the kinetochores were less concentrated at the spindle equator compared to control cells, although they did not propose a mechanism for this observation (117). Here, we find similar results in *Drosophila* S2 cells using RNAi, namely that kinetochore microtubules are longer and the Cid distribution is broader than control, indicating that chromosome congression is

impaired, verified by a larger CV. Furthermore, because these cells still formed bipolar or bioriented spindles, there was very likely a residual effect of the remaining Klp61F that allowed the spindles to remain somewhat congressed. Thus this means that Klp61F is very likely a strong mediator of congression.

**Klp67A RNAi bipolar spindles have control-like kinetochore microtubule organization but spindles are longer**

Kinesin-8 has shown both length-dependent microtubule depolymerase activity *in vitro* and chromosome congression activity *in vivo,* and kinesin-8 mutant spindles are abnormally long (41–43, 97, 99, 100, 66, 101). In fungi kinesin-8 mutant spindles were longer than control but chromosome congression was not impaired, consistent with kinesin-8 acting preferentially as a length-dependent microtubule depolymerase on interpolar microtubules instead of kinetochore microtubules (42, 43). To test the role of kinesin-8 in S2 cells, we performed RNAi of the kinesin-8 Klp67A using different amounts of dsRNA and took single time point images one and three days following transfection (Figure 3.3A), following the same protocol as single time point measurements for Klp61F RNAi. We found that nearly all spindles were bipolar (Figure 3.3B). As before, we pooled all control spindles and all Klp67A RNAi bipolar spindles; however, unlike before, we did not apply our spindle length criterion because this resulted in eliminating almost 30% of long Klp67A RNAi bipolar spindles (for results with the spindle length criterion, see Supplemental Figure 3.S3). If kinesin-8 affected chromosome congression in S2 cells, we would expect that, like the Klp61F RNAi bipolar and bioriented spindles, the tubulin fluorescence distribution would be flatter for Klp67A RNAi spindles indicating longer kinetochore microtubules; however, the tubulin fluorescence distributions were visibly similar and did not show a statistically significant difference ($p=0.77$, Figure 3.3C), demonstrating that the kinetochore microtubules in

Klp67A RNAi spindles were on average the same length, relative to the spindle, as control. We also found that the spindles in Klp67A RNAi spindles were significantly longer than control (Figure 3.3D), consistent with previous studies of kinsesin-8 mutants (41–43, 97, 99–101). These results are consistent with Klp67A acting as a plus-end directed, length-dependent disassembly promoter that acts primarily on interpolar microtubule s instead of kinetochore microtubules, thus affecting the overall spindle length but not affecting the kinetochore microtubule length and subsequent chromosome congression (42, 43).

## Discussion

Overall these results support a model in which chromosome congression is driven by motor-mediated disassembly of long kinetochore microtubules by tetrameric kinesin-5 motors that act primarily on kinetochore microtubules because of their cross-linking ability, and spindle length is driven by motor-mediated disassembly of interpolar microtubules by dimeric kinesin-8 motors that act primarily on interpolar microtubules because of their inability to crosslink (Figure 3.3E). In cells with modestly reduced levels of kinesin-5 (i.e. enough Klp61F remains to form bipolar or bioriented spindles), kinetochore microtubules are longer and more variable in length, compromising chromosome congression, and spindle lengths are shorter presumably because of decreased outward pushing force (Figure 3.3E). In cells with reduced levels of kinesin-8, kinetochore microtubules are the same length relative to the spindle length as control, maintaining proper chromosome congression, yet the overall spindle length is longer because of longer interpolar microtubules (Figure 3.3E).

Mitotic mechanisms have focused primarily on chromokinesin (kinesin-4/10) mediated polar ejection force to promote chromosome congression, yet kinetochores still

align at the mitotic spindle equator despite the loss of both chromokinesins and the chromosome arms on which the chromokinesins act, demonstrating that neither is indispensable for proper congression (36–40, 98). On the other hand, three separate studies now point to kinesin-5 mediated chromosome congression spanning yeast to animal cells, an alternative model focusing on length-dependent control of kinetochore microtubule dynamics, instead of a poorly-supported polar ejection force (42, 43). Future work is needed to test for kinesin-5 mediated chromosome congression in other eukaryotes, including human cells, and this work must overcome the technical challenge of reducing kinesin-5 while avoiding monopolar spindle collapse, but if it is found that kinesin-5 promotes chromosome congression in higher eukaryotes this will fundamentally change mitotic spindle assembly models, by both replacing the polar ejection force with motor-mediated kinetochore microtubule length regulation and by providing an additional role for kinesin-5, separate from (but not inconsistent with) its role in bipolar spindle assembly and maintenance.

## Acknowledgements

We thank Professor Lawrence Goldstein for providing us with rat-anti-Klp61F antibody. Research reported in this publication was supported by the National Institute of General Medical Sciences of the National Institutes of Health under award numbers R01GM071522 and R01GM076177 to D.J.O. and award RO1GM044757 to T.S.H. E.T. was a recipient of a University of Minnesota Interdisciplinary Doctoral Fellowship through the Institute for Advanced Study.

## Author Contributions

E.T. conducted RNAi experiments, collected images, analyzed results, prepared figures, and wrote the paper. E.T. and Y.H. designed primers, prepared dsRNA, and ran the Western Blot. T.H. and D.O., co-principal investigators, oversaw the project and contributed to intellectual ideas.

## Materials and Methods

### Cell culture and RNA interference

*Drosophila melanogaster* Schneider (S2) cells and plasmids (Addgene) were obtained from Professor Ronald Vale's lab (105, 114, 115). Cells were maintained in T25 flasks at room temperature and passed weekly into normal media consisting of Shields and Sang M3 Media (Sigma-Aldrich #S3652 ), Insect Medium Supplement (Sigma-Aldrich #I7267), and Schneider's *Drosophila* Media (Sigma-Aldrich #S0146) supplemented with 2% fetal bovine serum and penicillin/streptomycin (113).

For RNAi, dsRNAs were prepared following *in vitro* transcription using the Megascript T7 kit (Ambion) (113). PCR was performed using genomic *Drosophila* DNA

as template and with the following primers Klp61F: forward 5'-t7-GCT CTG AGT CAC CTT TTC GAT-3', reverse 5'-t7-CAC-GAT-ATG-GAA-CGT-GAG-GAG-3' Klp67A: forward 5'-t7-AAC-GAA-CAT-GTG-ATG-AAT-CTG-3' reverse 5'-t7-TCT-TCA-CAT-AGA-ACT-CGG-TTG-3', which were designed using published results of the Klp61F sequence from flybase.org (Klp61F) or from published results (Klp67A) (105). PCR products were purified (Qiagen kit) and used as transcription templates in the MEGAScript T7 kit to generate RNA. The RNA was then heated at 65$^{o}$C for 30 minutes to promote annealing and the resulting dsRNA was cooled to room temperature over 4-5 hours, aliquoted, and stored at -20$^{o}$C until use.

RNAi was performed following the methods of Clemens et al. (109). Prior to transfection with dsRNA, 4.5-6 million cells were exchanged from normal media to 1X M3 media supplemented with 1X Insect Medium Supplement and placed in a well of a 6-well plate to obtain a concentration of 2 million cells/mL. DsRNA was added directly to the well (amounts varied according to experiment) and the plate was placed on a rotator at 50 rpm. After one hour an equal volume (to the existing media) of 1X Schneider's *Drosophila* media supplemented with 10% fetal bovine serum was added to the well to obtain a concentration of 1 million cells/mL, and the cells remained in the well until imaging (109). DsRNA was transfected again in the cells three days after the initial transfection in the first experiment to verify protein knockdown (Figure 3.1) but only single transfections were performed in all remaining experiments.

**Immunoblotting**

Antibodies used for immunoblotting were DM1α (mouse-anti-$\alpha$-tubulin) (1:10,000, Sigma-Aldrich #T6199) with goat anti-mouse IgG/IgM Secondary Antibody, AP conjugate (1:10,000, Thermo Fisher Scientific #T2192) and rat-anti-Klp61F (1:5,000, a

gift from Dr. Lawrence Goldstein) with goat anti-rat IgG Secondary Antibody, AP conjugate (1:10,000, Thermo Fisher Scientific #31350) antibodies.

**Microscopy**

Cells were plated on 35-mm dishes with round, 14-mm no.1.5 cover glass bottoms (MatTek P35G-1.5-14C) coated with Concanavalin A (Sigma-Aldrich #C7275) and allowed to adhere to the dishes for 20 minutes before imaging (118). All cells were imaged at room temperature on a Zeiss LSM 7 Live swept-field confocal microscope using a 100X 1.45 NA plan-fluor oil immersion objective with 488 nm and 561 nm lasers and 495-555 nm and 575-615 nm plus longpass 655 nm filter sets for imaging the mCherry-Tubulin, GFP-Cid cells, and longpass 495 nm filter set for imaging the GFP-tubulin cells. Images were collected on a 1 x 512 line scanning 12-bit CCD camera with 60% quantum efficiency scanning 512 lines to obtain 512x512 images of each confocal plane. Time-lapse images of a 10 x 10 array of 512x512 fields tiled together, with 5 z-planes per tile (3.75 µm sections), were collected at 10 minute intervals for 10-12 hours with a zoom of 0.5, which yields a pixel size of 263 nm. Single time-point images with variable numbers of z-planes (typically 1-5 planes) in order to collect images of complete spindles were collected with a zoom of 1.3, which yields a pixel size of 101 nm.

**Image analysis**

Identification of spindle poles and estimation of the fluorescence distribution for tubulin and Cid across the spindle axis were performed using a semi-automated MATLAB (Mathworks) algorithm as previously described (43). Briefly, spindles were rotated to lie along the horizontal axis and the tubulin and Cid fluorescence intensities were collected for each vertical section in a background-subtracted region containing the

spindle and along the axis of the spindle. The tubulin fluorescence decrease near the ends of the spindle were fit to Gaussian survival functions for each half-spindle, and the spindle pole locations were identified as the mean locations of the survival curves (43, 119, 120). The intensities between the centrosomes were then binned with a constant number of bins (24) to allow comparison between different spindle lengths. The left and right halves were averaged to obtain a half spindle fluorescence intensity distribution, and finally the distributions were normalized by dividing each bin position's fluorescence intensity by the sum of all of the bin positions' fluorescence intensities (43). For each spindle, the background-subtracted, binned Cid fluorescence distributions were fit to Gaussian functions centered at the Cid fluorescence peaks with constrained maxima and minima given by the maximum peak fluorescence intensity and minimum tail fluorescence intensity for each Cid fluorescence distribution and unconstrained standard deviations. The standard deviations were then obtained by minimizing the sums of the least-squared fits to the data. A single Cid fluorescence distribution was removed from the data because its peak occurred in the last bin, making a Gaussian fit impossible. The Cid fluorescence distributions were aligned with their peaks at the center to avoid misinterpretation of broad Cid fluorescence due to off-center peaks. Cid distribution in anaphase was collected from movie data by rotating anaphase spindles to lie along the horizontal spindle axis, generating a rectangle sufficiently large to contain the segregated Cid fluorescence, dividing the rectangle in equal thirds, and subtracting the mean signal of the middle third from both the left and right thirds (background subtraction).

**Acceptance criteria for evaluating metaphase cells**

To avoid evaluating prometaphase or anaphase spindles, a spindle length criterion was developed where only spindles with spindle lengths within two standard

deviations of the mean of the control spindle length were analyzed for tubulin fluorescence distribution, Cid fluorescence at the spindle equator, and spindle length for each set of experiments (43).

**Bootstrapping method for comparing tubulin fluorescence distributions**

Tubulin fluorescence distributions were compared using a bootstrapping method implemented with a MATLAB script as previously described (43). Briefly, for N cells of condition A, the mean fluorescence intensity distribution ($mean_A$) was obtained by taking the mean across all N cells at each bin location (12 bins total). The same procedure was followed for obtaining the mean fluorescence intensity distribution of M cells of condition B ($mean_B$). At each bin position, the difference of the means between the two distributions ($mean_A$ and $mean_B$) was squared and the sum of the squared differences gave the value of the experimental sum of squares difference between the distributions. A matrix of size N+M rows by 12 bins columns was then created. The first N rows were populated by the fluorescence distributions of the N cells of condition A and then last M rows were populated by the fluorescence distributions of the M cells of condition B. The rows were then shuffled. The first N rows of the shuffled set became the simulated cells of condition A and the last M rows became the simulated cells of condition B. As before, the mean fluorescence distributions were obtained but now for the simulated cells of each condition. The sum of squares difference for the mean simulated distributions was obtained and stored. The process of preparing simulated distributions and comparing them was repeated 10000 times to obtain 10000 simulated sum of squares differences, and the values were sorted. The experimental sum of squares difference was then ranked within the list of simulated sum of squares and the p-value was calculated by dividing the difference between total number of simulated sum of squares differences and the rank, R, by the total number of simulated sum of squares differences,

$$p = \frac{10000 - R}{10000} \tag{3.1}$$

This boot-strapping method is sensitive to outliers when the sizes of the groups to be compared are very different and thus the fluorescence distributions of outliers must be removed prior to making the comparisons. This was found when comparing the tubulin fluorescence distributions of control (n=83) and Klp61F RNAi bipolar and bioriented spindles (n=16) in single time point measurements of mCherry-Tubulin/GFP-Cid cells (Figure 3.S2) that appeared different but did not give a significant p-value. A single fluorescence distribution in the control spindles where the normalized fluorescence intensity values in 11 out of 12 bins had outlier values (deviating 1.5 times the interquartile range above the third quartile or below the first quartile) was identified, the fluorescence distribution for that spindle was removed, the comparison repeated, and a significant p-value was obtained (121). This was the only case when a tubulin fluorescence distribution was removed from the data set.

**Statistical comparisons**

With the exception of comparing tubulin fluorescence distributions, all groups were compared using the Kruskal-Wallis test, which does not require normality of data, and multiple comparisons (Tukey-Kramer with $\alpha$=0.05) were conducted if the Kruskal-Wallis test revealed that the groups did not all have the same mean ranks. Heights on all bar graphs represent mean values unless stated otherwise. All error bars represent standard error of the mean (SEM).

**Calculation of p-value in laser-cutting chromosome arm experiments**

If one assumes a null hypothesis that PEF does not play a major role in congression, then each of the 16 laser cutting experiments would be equally probable to

exhibit larger oscillations as smaller oscillations. In this case, the probability of larger oscillations in each chromosome cutting experiment is 0.5 (i.e. random chance), and the expected number of chromosomes that would increase oscillations after cutting by chance alone is 8 out of 16. Using a Bernoulli trial calculation with n=16 trials and p=0.5 of success in each trial we obtain the probability of having 11 or more (or 5 or fewer) spindles with increased oscillations by chance alone is 0.21. In other words, the null hypothesis that PEF does not play an important role in congression cannot be rejected from these laser cutting experiments (p=0.21).

**CV calculation for chromosome congression**

The mean kinetochore microtubule lengths are estimated as the location where the normalized tubulin fluorescence is steepest multiplied by the respective mean spindle lengths, (0.75)(8.2 μm)=6.2 μm for control and (0.92)(7.5 μm)=6.9 μm for Klp61F RNAi (43). The standard deviations of kinetochore microtubule lengths are estimated by the product of the normalized Cid Gaussian fit standard deviations and spindle lengths, (0.17)(8.2 μm)=1.4 μm for control and (0.24)(7.5 μm)=1.8 μm for Klp61F RNAi. The CV is calculated by the ratio of the standard deviations of the spindle lengths to the mean kinetochore microtubule lengths, thus, the spindle lengths drop out of the equation. For control spindles, the CV is

$$\frac{(0.17)(8.2)}{(0.75)(8.2)} = 0.22\,. \tag{3.2}$$

For Klp61F RNAi spindles, the CV is

$$\frac{(0.24)(7.5)}{(0.92)(7.5)} = 0.26\,. \tag{3.3}$$

## Figures

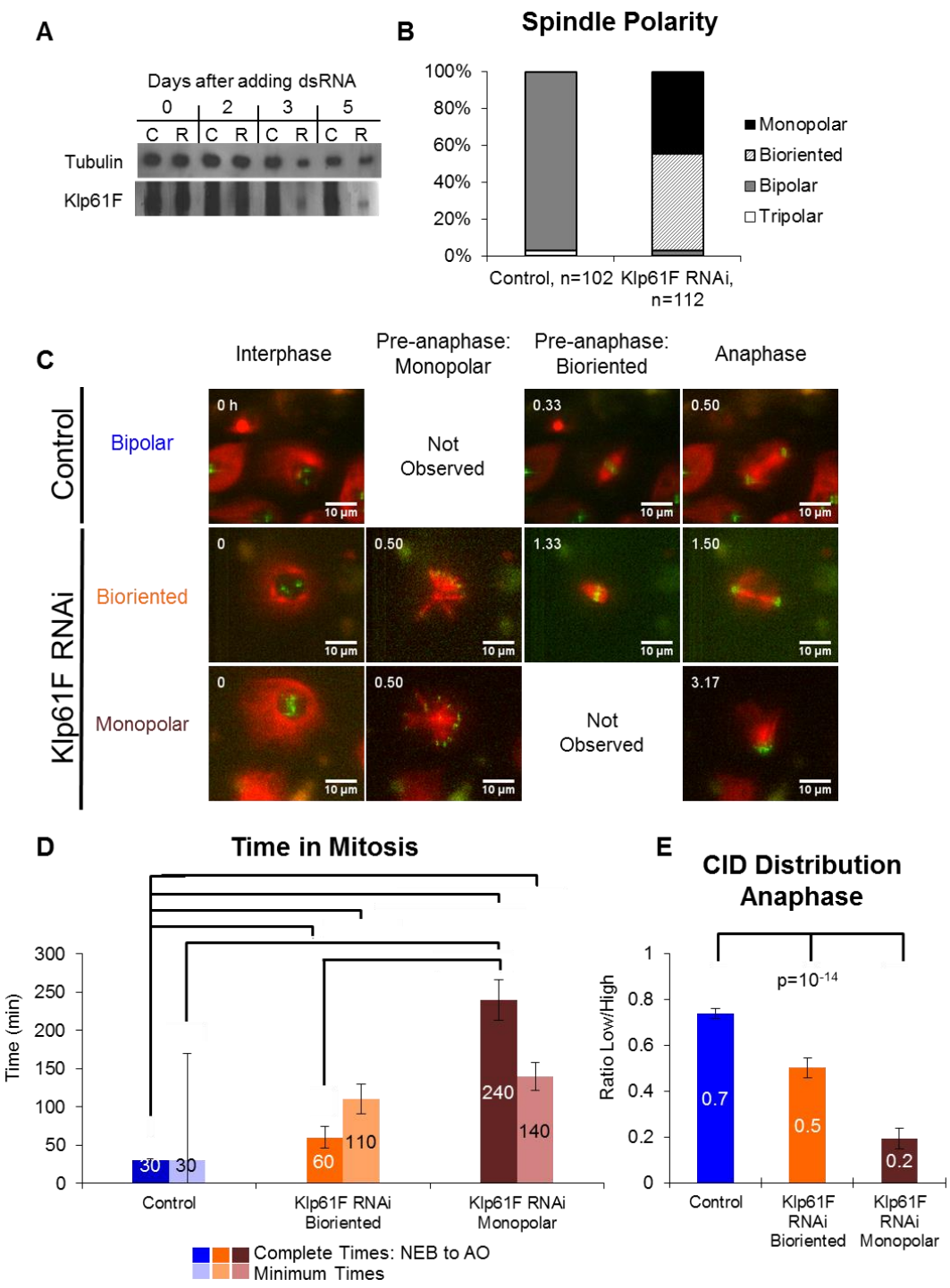


**Figure 3.1: Klp61F RNAi spindles have delayed mitoses with unequal segregation of chromosomes relative to control spindles**

A) Immunoblot of tubulin and Klp61F in control and Klp61F RNAi cells shows reduction of Klp61F throughout time following RNAi Klp61F (C=Control, R=Klp61F RNAi; 10% reduction after 0 and 2 days, 50% reduction after 3 days, and 90% reduction after 5 days, normalized to control Klp61F for each day). Antibodies used were DM1α (mouse-anti-α-tubulin) (1:10,000), goat anti-mouse (1:10,000), rat-anti-Klp61F (1:5,000), and goat anti-rat (1:10,000). B) Spindles were bipolar for control and initially monopolar for Klp61F RNAi, although over half of the monopolar spindles eventually transitioned to bioriented spindles. C) Representative images of mitosis in control and Klp61F RNAi cells obtained from time-lapse fluorescence imaging. D) Klp61F RNAi results in a mitotic delay. Dark bars represent complete times (NEB to AO); light bars represent minimum times (either NEB or AO not observed). Times are not from the same distribution ($p=10^{-22}$, n=96,3,36,26,10,40, respectively). Statistically significant times indicated (α=0.05 by Tukey-Kramer test). Bars are median +/- SEM. E) Klp61F RNAi results in improper kinetochore segregation given by Cid fluorescence in anaphase. Bars represent the ratio (low/high) of the mean fluorescence for the background-subtracted Cid signals in anaphase. Ratios are not from the same distribution ($p=10^{-14}$, n=98,62,40, respectively). Error bars are SEM.

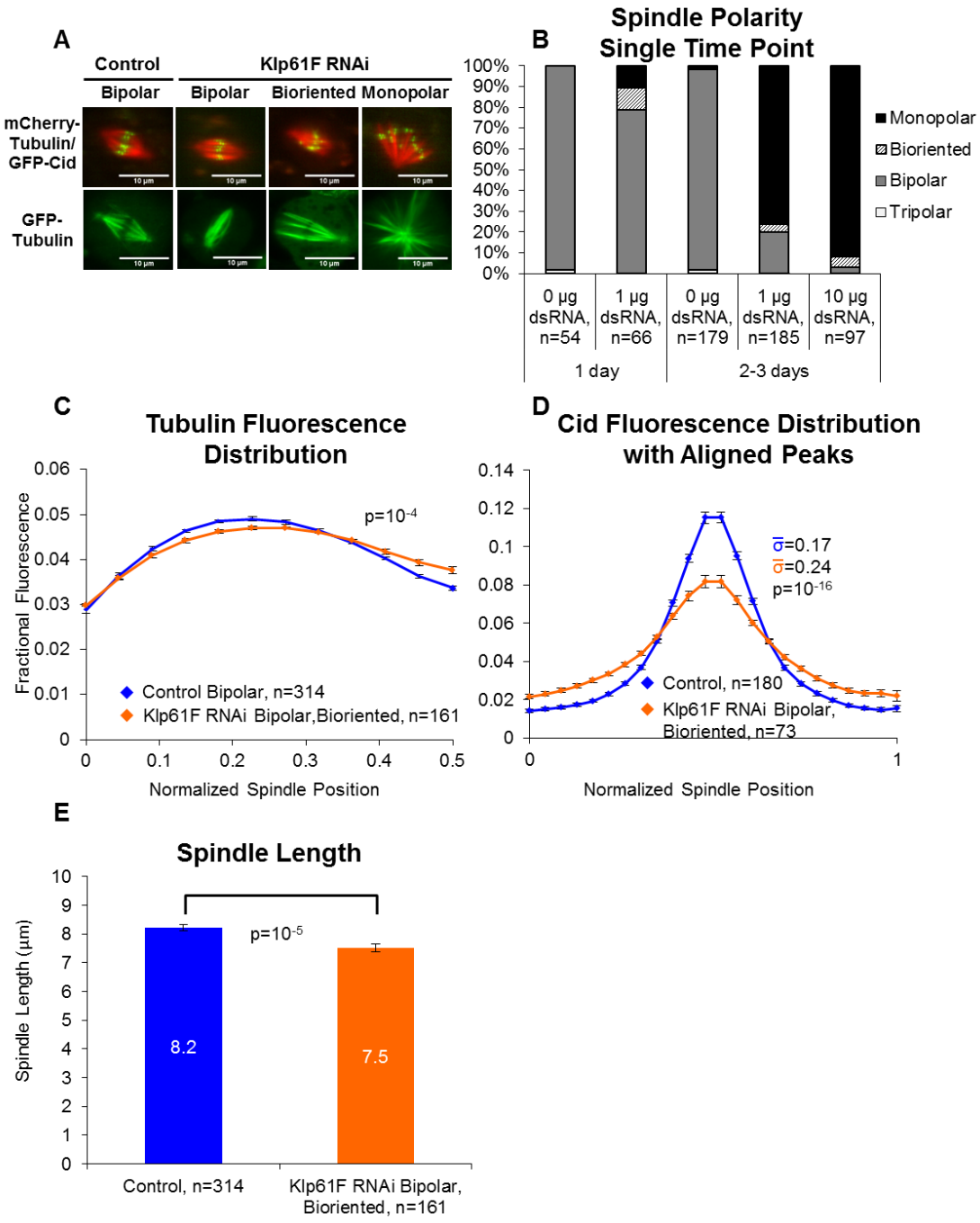


**Figure 3.2: Klp61F RNAi bipolar and bioriented spindles have impaired chromosome congression and shorter spindle lengths relative to control spindles**

A) Representative single time point images of control and Klp61F RNAi spindles. B) Spindles were primarily bipolar for control (0 µg dsRNA) and bipolarity decreased more with longer incubation following transfection of dsRNA rather than more dsRNA transfected. C) Tubulin fluorescence distribution of bipolar and bioriented spindles indicates that kinetochore

microtubules were longer and more variable in length in Klp61F RNAi spindles compared to control. Error bars are SEM. D) Cid fluorescence distribution with aligned peaks indicates that kinetochores were more broadly distributed in Klp61F RNAi bipolar and bioriented spindles compared to control. Error bars are SEM. E) Spindles lengths were shorter for Klp61F RNAi bipolar and bioriented spindles compared to control. Error bars are SEM.

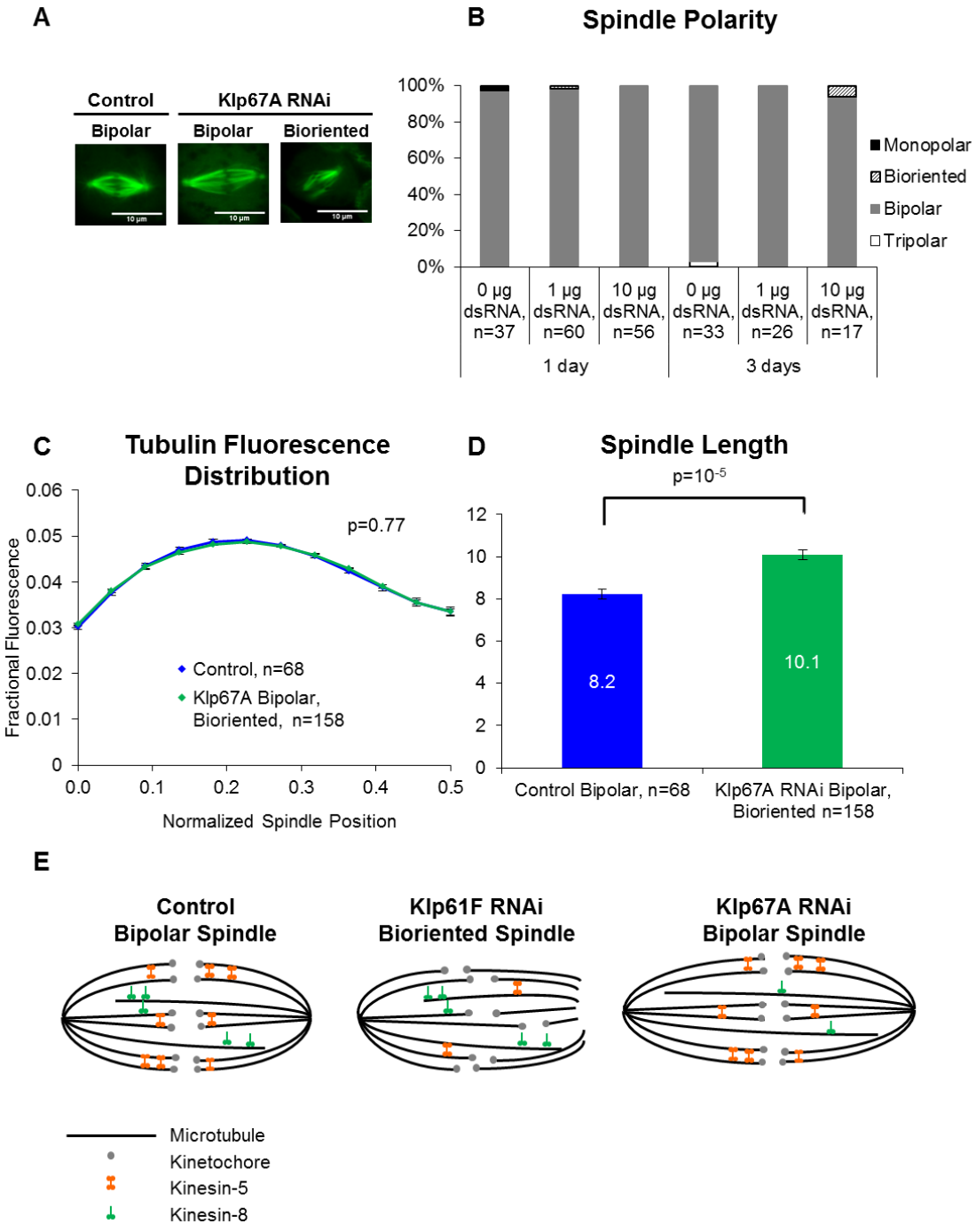


**Figure 3.3. Klp67A RNAi bipolar and bioriented spindles have normal chromosome congression and longer spindle lengths relative to control spindles**

A) Representative single time point images of control and Klp67A RNAi spindles. B) Spindles were predominantly bipolar for both control and Klp67A RNAi cells. C) Tubulin fluorescence distribution indicates that kinetochore microtubules in Klp67A RNAi bipolar and bioriented

spindles were the same length, relative to the spindle length, as kinetochore microtubules in control spindles. Error bars are SEM. D) Spindles lengths were longer for Klp67A RNAi bipolar and bioriented spindles compared to control. Error bars are SEM. E) Model of kinesin-5 mediated length control of kinetochore microtubules and kinesin-8 mediated length control of interpolar microtubules. In control bipolar spindles, tetrameric kinesin-5 crosslinks parallel MTs, promoting catastrophe at the plus ends thus facilitating congression of kinetochores (hence chromosomes), while dimeric kinesin-8, unable to crosslink, remains persistent on interpolar microtubules, promoting catastrophe at the plus ends thus facilitating maintenance of spindle length. In Klp61F RNAi bioriented spindles, reduced kinesin-5 leads to both lack of kinetochore congression because of lack of control of kinetochore microtubule lengths and lack of formation of complete bipolar spindle because of lack of antiparallel MT force generation. In Klp67A RNAi bipolar spindles, reduced kinesin-8 leads to maintenance of congressed kinetochores because of presence of kinesin-5 but longer spindle length because of lack of control of interpolar microtubule lengths.

## Supplemental Figures

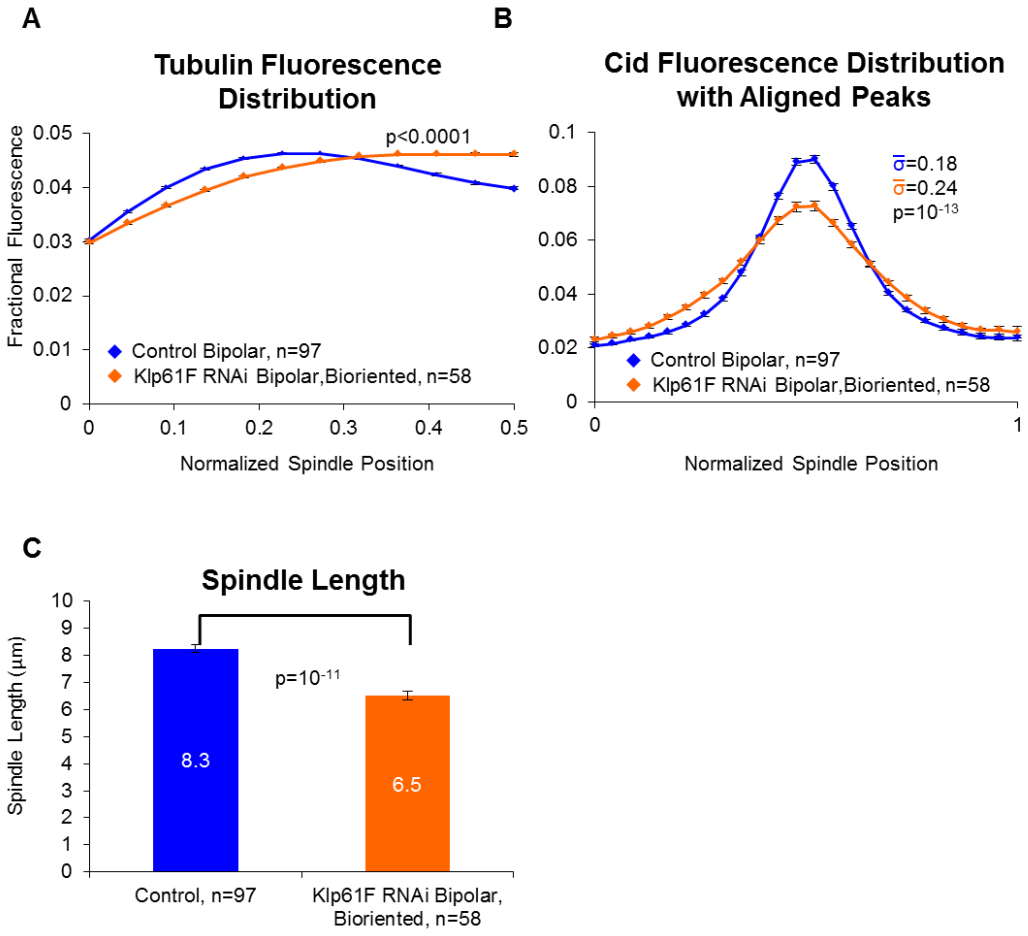


**Figure 3.S1. From time-lapse imaging data, Klp61F RNAi bipolar and bioriented spindles have impaired chromosome congression and shorter spindle lengths relative to control spindles**

A) Tubulin fluorescence distribution of bipolar and bioriented spindles indicates that kinetochore microtubules were longer and more variable in length in Klp61F RNAi spindles compared to control (0 µg dsRNA/$10^6$ cells (control) and 5 µg dsRNA/$10^6$ cells, 2 day incubation). Error bars are SEM. B) Cid fluorescence distribution with aligned peaks indicates that kinetochores were more broadly distributed in Klp61F RNAi bipolar and bioriented spindles compared to control (0 µg dsRNA/$10^6$ cells (control) and 5 µg dsRNA/$10^6$ cells, 2 day incubation). Error bars are SEM. C) Spindle lengths were shorter for Klp61F RNAi bipolar and bioriented spindles compared to control (0 µg dsRNA/$10^6$ cells (control) and 5 µg dsRNA/$10^6$ cells, 2 day incubation). Error bars are SEM.

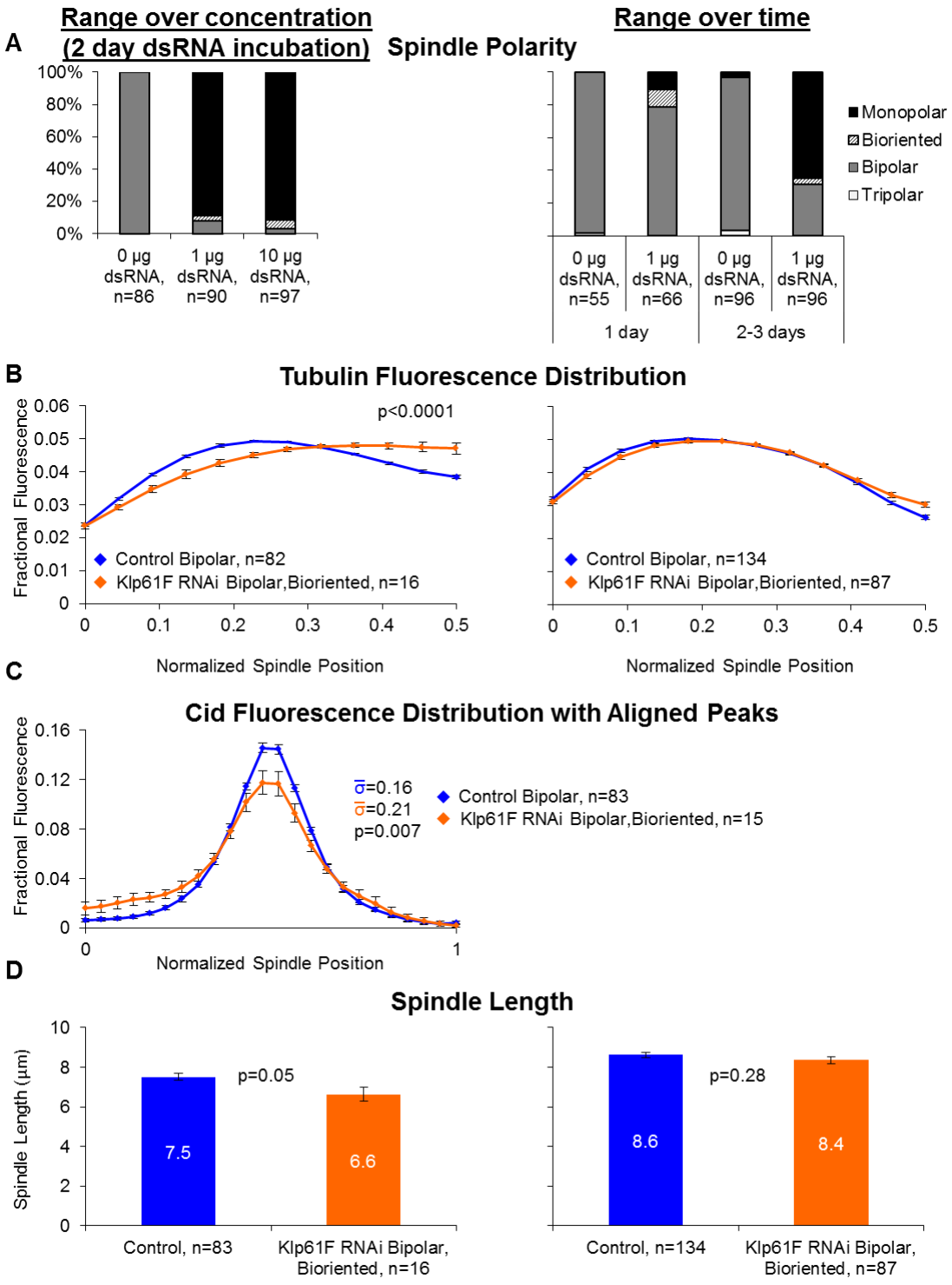


**Figure 3.S2. From single time-point data, transfecting more dsRNA targeting Klp61F leads to only a modest increase in monopolarity, more time following transfection of dsRNA targeting Klp61F leads to higher level of monopolarity, and Klp61F RNAi bipolar and**

**bioriented spindles have flatter tubulin distributions and similar spindle lengths compared to control**

A) Spindle polarity shows that longer incubation of dsRNA (> 1 day), leads to higher level of monopolarity, more so than increase in concentration of dsRNA (in each case dsRNA was transfected per $10^6$ cells, i.e. 0-10 µg dsRNA/$10^6$ cells). B) Tubulin fluorescence distribution of bipolar and bioriented spindles indicates that kinetochore microtubules were longer and more variable in length in Klp61F RNAi spindles compared to control. Error bars are SEM. C) Cid fluorescence distribution with aligned peaks indicates that kinetochores were more broadly distributed in Klp61F RNAi bipolar and bioriented spindles compared to control. Error bars are SEM. D) Spindles lengths were shorter for Klp61F RNAi bipolar and bioriented spindles compared to control, although the statistical significance was marginal or not significant. Error bars are SEM.

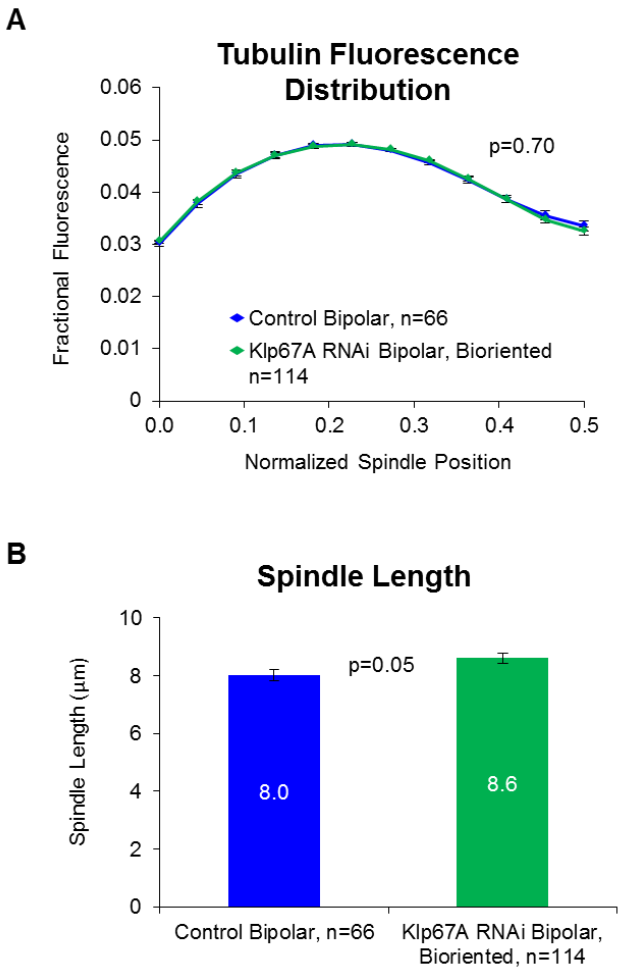


**Figure 3.S3. Applying control spindle length criterion to Klp67A RNAi bipolar spindles does not change tubulin fluorescence distribution but does mask increased spindle length** A) The tubulin fluorescence distribution for Klp67A RNAi bioriented and bipolar spindles is the same as control, implying that kinetochore microtubule lengths relative to the spindle length are not altered. Error bars are SEM. B) Spindle lengths were longer but not statistically different for Klp67A RNAi bioriented and bipolar spindles compared to control when applying the control spindle length criterion. Error bars are SEM. When all of the data is analyzed without application of the length criterion, then Klp67A RNAi spindles are significantly longer than control (see Fig. 3.3C).

# Chapter 4: Summary and Conclusions

Over 120 years ago, Walter Flemming observed evidence of nuclear division on the mitotic spindle (122). Despite the advances that have been made since then, there are still a plethora of unanswered questions regarding how the cell so elegantly divides the genome. This dissertation uses *in silico* computational modeling and experimentation to research two of these questions, which are how kinetochores make proper attachments to microtubules to biorient on the mitotic spindle and how chromosomes align at the mitotic spindle equator in metaphase.

In the first chapter, a spindle-attachment error correction model of kinetochore-microtubule attachments including microtubule dynamics, Ipl1 kinase/Glc7 phosphatase activity, and kinetochore-microtubule attachment and detachment was presented. The model revealed that with multiple phosphostates and a high critical phosphorylation for detachment, a delay before detachment provided the necessary window for nascent amphitelic attachments to generate tension to transition to stable high-tension amphitelic attachments and avoid detachment. This delay before detachment provides a solution to the “initiation problem of biorientation” where Ipl1 kinase-mediated phosphorylation promotes kinetochore-microtubule detachment when chromatin tension is low, yet high tension is required to prevent phosphorylation and subsequent detachment. This mechanism allows all kinetochore pairs to biorient on the mitotic spindle prior to anaphase to ensure that each daughter cell receives the correct number of chromosomes.

In the second chapter, the motor proteins kinesin-5 and kinesin-8 were tested for roles promoting chromosome congression in *Drosophila melanogaster* S2 cells. Knocking down levels of the kinesin-5 protein in cells that were still able to form

bioriented spindles led to kinetochore microtubules that were longer and more variable in length and had more broadly distributed kinetochore distributions, indicating poorer congression. Thus, tetrameric kinesin-5 was found to have a role as a length-dependent depolymerase of kinetochore microtubules to facilitate chromosome congression in S2 cells, as it has been found in fungi (42, 43). Knocking down levels of the kinesin-8 protein in cells did not lead to longer kinetochore microtubules relative to the spindle but instead led to longer spindles overall. Thus, dimeric kinesin-8 was found to have a role as a length-dependent depolymerase of interpolar microtubules to facilitate spindle length in S2 cells, which has also been found in fungi (42, 43). Overall, these results corroborate those in fungi, demonstrating not only that motor proteins have length-dependent depolymerase activity *in vivo*, but also that their preferential activity on kinetochore versus interpolar microtubules is due to their ability to crosslink or not. This is now the third study implicating kinesin-5 in promoting chromosome congression and the first in animal cells, providing further evidence that chromosomes congress due to the spatial control of the kinetochore microtubules to which they are attached, and that kinesin-5 is the molecule that provides such control generally among eukaryotes.

In addition to contributing to the overall understanding of error correction and chromosome congression within mitotic research, these studies are also relevant because they involve proteins that have been identified as targets for anti-cancer drugs, specifically Aurora B and kinesin-5. As mentioned previously, the most successful anti-cancer drugs target microtubules, however, these drugs lead to negative side effects, therefore an effort has been underway to identify alternatives that more specifically target the mitotic machinery of rapidly dividing cancer cells.

Aurora B (human orthologue of Ipl1) is overexpressed in acute myeloid leukemia (AML), colorectal cancer, and anaplastic thyroid carcinoma (123). Barasertib, developed

by AstraZeneca, has been the most widely studied Aurora B inhibitor in clinical trials (123). In phase I and II clinical trials with Barasertib, the most common side effect was neutropenia, suppression of neutrophil production (123). Complete responses (disappearance of all signs of cancer) were obtained in approximately 12-25% of patients with Barasertib alone and 36% of patients with Barasertib in combination with other drugs, and disease stabilization was obtained in approximately 25% of patients with Barasertib alone. The rationale behind anti-Aurora B drugs is that inhibiting Aurora B leads to loss of normal chromosome segregation, incomplete cytokinesis, generation of polyploid cells, and eventual apoptosis of cancer cells (123). However, the spindle-attachment error correction model predicts that strong kinase activity alone leads to mis-segregation, thus inhibiting Aurora B in cells in which it is overexpressed may inadvertently return Aurora B to wild-type levels where amphitelic kinetochore-microtubule attachments are favored, eliminating chromosome mis-segregation and preventing apoptosis of cancer cells. Instead, providing anti-Aurora B drugs to patients with normal levels of Aurora B may be more beneficial to kill cancer cells because the model also predicts that weak kinase activity leads to mis-segregation, which would eventually lead to apoptosis. Therefore, the error correction model is useful in making predictions about which patients would benefit most specifically from Aurora B inhibitors based on Aurora B expression level.

Similarly, the human kinesin-5, Eg5, is overexpressed in many cancers, including renal cell, urothelial, and pancreatic carcinoma (124). Multiple Eg5 inhibitors have been used in both phase I and phase II clinical trials, and, like Aurora B inhibitors, the most common side effect was neutropenia (124). In both phase I and phase II clinical trials, the response rates were highly variable due to the drug administered, type of cancer, and whether the drug was used alone or in combination with other drugs (124). In the

worst case, no objective responses were obtained in a phase II clinical trial following administration of the drug Ispinesib in any patients with melanoma, head and neck squamous cell carcinoma, hepatocellular carcinoma, or prostate carcinoma, and in the best case response rates as high as 42% were obtained in phase I clinical trials following administration of the drug ARRY-520 in combination with other drugs (124). The rationale behind anti-Eg5 drugs is that inhibiting Eg5 causes mitotic arrest with monopolar spindles and eventual apoptosis (112, 125). However, our results indicate that a partial knockdown of kinesin-5 (Eg5) allows cells to progress through mitosis with poorly congressed chromosomes. Thus, if Eg5 inhibitors are not adequately reducing kinesin-5 protein levels, then this may provide an explanation for the low response rates following drug administration. Altogether, the clinical results combined with our experimental results indicate that Eg5 inhibitors may have a promising future in the clinic, but more work is required to ensure that the drug is reaching the cells at the appropriate concentration to sufficiently inhibit Eg5.

Overall, clinical trials of Aurora B and Eg5 inhibitors have demonstrated that more work must be completed to improve the efficacy of these drugs. The problems may be related to a combination of short drug half-life and slow cell doubling time, preventing the drugs from reaching the cells during mitosis (124). However, the problems may also be due to a misunderstanding of how the proteins function. Thus, a greater mechanistic understanding of how proteins are involved in the machinery of mitosis can only lead to improvements in the development of more specific anti-cancer drug targets. Therefore, the work presented in this dissertation regarding how Ipl1/Aurora B promotes correct kinetochore-microtubule attachments and how kinesin-5 facilitates chromosome congression contributes to the knowledge of how the mitotic

spindle segregates chromosomes and provides a foundation for future studies necessary to identify anti-cancer drug targets.

# Bibliography


1. Tilney, L.G., J. Bryan, D.J. Bush, K. Fujiwara, M.S. Mooseker, and D.B. Murphy. 1973. Microtubules : Evidence for 13 Protofilaments. J. Cell Biol. 59: 267–275.
2. Weber, K., R. Pollack, and T. Bibring. 1975. Antibody Against Tubulin: The Specific Visualization of Cytoplasmic Microtubules in Tissue Culture Cells. Proc. Natl. Acad. Sci. U. S. A. 72: 459–463.
3. Olmsted, J.B., and G.G. Borisy. 1973. Microtubules. Annu. Rev. Biochem. 42: 507–540.
4. Castle, B.T., and D.J. Odde. 2016. Dynamics of Microtubule Self-Assembly. Encycl. Cell Biol. 4: 36–43.
5. Mitchison, T., and M. Kirschner. 1984. Dynamic instability of microtubule growth. Nature. 312: 237–242.
6. Kops, G.J.P.L., B.A.A. Weaver, and D.W. Cleveland. 2005. On the road to cancer: aneuploidy and the mitotic checkpoint. Nat. Rev. Cancer. 5: 773–85.
7. Rajagopalan, H., and C. Lengauer. 2004. Aneuploidy and cancer. Nature. 432: 338–341.
8. Sluder, G., and D. McCollum. 2000. The mad ways of meiosis. Science. 289: 254–255.
9. Schmidt, M., and H. Bastians. 2007. Mitotic drug targets and the development of novel anti-mitotic anticancer drugs. Drug Resist. Updat. 10: 162–81.
10. Michaelis, C., R. Ciosk, and K. Nasmyth. 1997. Cohesins: Chromosomal proteins that prevent premature separation of sister chromatids. Cell. 91: 35–45.
11. Peters, J.-M. 2002. The Anaphase-Promoting Complex: Proteolysis in Mitosis and Beyond. Mol. Cell. 9: 931–943.
12. Winey, M., C.L. Mamay, E.T. O'Toole, D.N. Mastronarde, T.H.J. Giddings, K.L. Mcdonald, and J.R. Mcintosh. 1995. Three-Dimensional Ultrastructural Analysis of the Saccharomyces cerevisiae Mitotic Spindle. J. Cell Biol. 129: 1601–1615.
13. Rieder, C.L. 1981. The structure of the cold-stable kinetochore fiber in metaphase PtK1 cells. Chromosoma. 84: 145–158.
14. Cimini, D., L.A. Cameron, and E.D. Salmon. 2004. Anaphase Spindle Mechanics Prevent Mis-Segregation of Merotelically Oriented Chromosomes University of North Carolina at Chapel Hill. Cell. 14: 2149–2155.
15. Biggins, S., F.F. Severin, N. Bhalla, I. Sassoon, A.A. Hyman, and A.W. Murray. 1999. The conserved protein kinase Ipl1 regulates microtubule binding to kinetochores in budding yeast. Genes Dev. 13: 532–544.
16. Biggins, S., and A.W. Murray. 2001. The budding yeast protein kinase Ipl1 / Aurora allows the absence of tension to activate the spindle checkpoint. Genes Dev. 15: 3118–3129.
17. Tanaka, T.U., N. Rachidi, C. Janke, G. Pereira, M. Galova, E. Schiebel, M.J.R. Stark, and K. Nasmyth. 2002. Evidence that the Ipl1-Sli15 (Aurora kinase-INCENP) complex promotes chromosome bi-orientation by altering kinetochore-spindle pole connections. Cell. 108: 317–29.
18. Hauf, S., R.W. Cole, S. LaTerra, C. Zimmer, G. Schnapp, R. Walter, A. Heckel, J.

Van Meel, C.L. Rieder, and J.M. Peters. 2003. The small molecule Hesperadin reveals a role for Aurora B in correcting kinetochore-microtubule attachment and in maintaining the spindle assembly checkpoint. J. Cell Biol. 161: 281–294.

19. Dewar, H., K. Tanaka, K. Nasmyth, and T.U. Tanaka. 2004. Tension between two kinetochores suffices for their bi-orientation on the mitotic spindle. Nature. 428: 93–97.

20. Chacón, J.M., S. Mukherjee, B.M. Schuster, D.J. Clarke, and M.K. Gardner. 2014. Pericentromere tension is self-regulated by spindle structure in metaphase. J. Cell Biol. 205: 313–324.

21. Nicklas, R.B., and C.A. Koch. 1969. Chromosome micromanipulation. 3. Spindle fiber tension and the reorientation of mal-oriented chromosomes. J. Cell Biol. 43: 40–50.

22. Akiyoshi, B., K.K. Sarangapani, A.F. Powers, C.R. Nelson, S.L. Reichow, H. Arellano-Santoyo, T. Gonen, J.A. Ranish, C.L. Asbury, and S. Biggins. 2010. Tension directly stabilizes reconstituted kinetochore-microtubule attachments. Nature. 468: 576–579.

23. Kalantzaki, M., E. Kitamura, T. Zhang, A. Mino, B. Novák, and T.U. Tanaka. 2015. Kinetochore–microtubule error correction is driven by differentially regulated interaction modes. Nat. Cell Biol. 17: 421–433.

24. Zhang, T., R.A. Oliveira, B. Schmierer, and B. Novak. 2013. Dynamical scenarios for chromosome bi-orientation. Biophys. J. 104: 2595–2606.

25. Lampson, M.A., and I.M. Cheeseman. 2011. Sensing centromere tension: Aurora B and the fregulation of kinetochore function. Trends Cell Biol. 21: 133–40.

26. Zaytsev, A. V, and E.L. Grishchuk. 2015. Basic mechanism for biorientation of mitotic chromosomes is provided by the kinetochore geometry and indiscriminate turnover of kinetochore microtubules. Mol. Biol. Cell. 26: 3985–98.

27. Gay, G., T. Courtheoux, C. Reyes, S. Tournier, and Y. Gachet. 2012. A stochastic model of kinetochore-microtubule attachment accurately describes fission yeast chromosome segregation. J. Cell Biol. 196: 757–774.

28. Nicklas, R.B., and P. Arana. 1992. Evolution and the meaning of metaphase. J. Cell Sci. Sci. 102: 681–690.

29. Pinsky, B.A., and S. Biggins. 2005. The spindle checkpoint: Tension versus attachment. Trends Cell Biol. 15: 486–493.

30. Hays, T.S., D. Wise, and E.D. Salmon. 1982. Traction force on a kinetochore at metaphase acts as a linear function of kinetochore fiber length. J. Cell Biol. 93: 374–382.

31. Hays, T.S., and E.D. Salmon. 1990. Poleward force at the kinetochore in metaphase depends on the number of kinetochore microtubules. J. Cell Biol. 110: 391–404.

32. Sharp, D.J., G.C. Rogers, and J.M. Scholey. 2000. Roles of motor proteins in building microtubule-based structures: A basic principle of cellular design. Biochim. Biophys. Acta - Mol. Cell Res. 1496: 128–141.

33. Rieder, C.L., E.A. Davison, L.C. Jensen, L. Cassimeris, and E.D. Salmon. 1986. Oscillatory movements of monooriented chromosomes and their position relative to the spindle pole result from the ejection properties of the aster and half-spindle.

J. Cell Biol. 103: 581–91.

34. Cassimeris, L., C.L. Rieder, and E.D. Salmon. 1994. Microtubule assembly and kinetochore directional instability in vertebrate monopolar spindles: implications for the mechanism of chromosome congression. J. Cell Sci. 107: 285–97.

35. Heald, R., and A. Khodjakov. 2015. Thirty years of search and capture: The complex simplicity of mitotic spindle assembly. J. Cell Biol. 211: 1103–1111.

36. Brinkley, B., R. Zinkowski, W. Mollon, F. Davis, M. Pisegna, M. Pershouse, and P. Rao. 1988. Movement and segregation of kinetochores experimentally detached from mammalian chromosomes. Nature. 336: 251 – 254.

37. Wise, D.A., and B.R. Brinkley. 1997. Mitosis in cells with unreplicated genomes (MUGs): spindle assembly and behavior of centromere fragments. Cell Motil. Cytoskeleton. 36: 291–302.

38. Levesque, A.A., and D.A. Compton. 2001. The chromokinesin Kid is necessary for chromosome arm orientation and oscillation, but not congression, on mitotic spindles. J. Cell. Biol. 154: 1135–1146.

39. O'Connell, C.B., J. Loncarek, P. Hergert, A. Kourtidis, D.S. Conklin, and A. Khodjakov. 2008. The spindle assembly checkpoint is satisfied in the absence of interkinetochore tension during mitosis with unreplicated genomes. J. Cell Biol. 183: 29–36.

40. Ke, K., J. Cheng, and A.J. Hunt. 2009. The distribution of polar ejection forces determines the amplitude of chromosome directional instability. Curr. Biol. 19: 807–15.

41. Stumpff, J., G. von Dassow, M. Wagenbach, C. Asbury, and L. Wordeman. 2008. The Kinesin-8 Motor Kif18A Suppresses Kinetochore Movements to Control Mitotic Chromosome Alignment. Dev. Cell. 14: 252–262.

42. Gardner, M.K., D.C. Bouck, L. V. Paliulis, J.B. Meehl, E.T. O'Toole, J. Haase, A. Soubry, A.P. Joglekar, M. Winey, E.D. Salmon, K. Bloom, and D.J. Odde. 2008. Chromosome Congression by Kinesin-5 Motor-Mediated Disassembly of Longer Kinetochore Microtubules. Cell. 135: 894–906.

43. McCoy, K.M., E.S. Tubman, A. Claas, D. Tank, S.A. Clancy, E.T. O'Toole, J. Berman, and D.J. Odde. 2015. Physical limits on kinesin-5 mediated chromosome congression in the smallest mitotic spindles. Mol. Biol. Cell . 26: 3999–4014.

44. Inoué, S., and E.D. Salmon. 1995. Force generation by microtubule assembly/disassembly in mitosis and related movements. Mol. Biol. Cell. 6: 1619–40.

45. Guacci, V., D. Koshland, and A. Strunnikov. 1997. A direct link between sister chromatid cohesion and chromosome condensation revealed through the analysis of MCD1 in S-cerevisiae. Cell. 91: 47–57.

46. Cheeseman, I.M., S. Anderson, M. Jwa, E.M. Green, J.S. Kang, J.R. Yates, C.S.M. Chan, D.G. Drubin, and G. Barnes. 2002. Phospho-regulation of kinetochore-microtubule attachments by the Aurora kinase Ipl1p. Cell. 111: 163–172.

47. Meraldi, P., R. Honda, and E.A. Nigg. 2004. Aurora kinases link chromosome segregation and cell division to cancer susceptibility. Curr. Opin. Genet. Dev. 14: 29–36.

48. Katayama, H., and S. Sen. 2010. Aurora kinase inhibitors as anticancer molecules. Biochim. Biophys. Acta. 1799: 829–39.

49. Goldenson, B., and J.D. Crispino. 2015. The aurora kinases in cell cycle and leukemia. Oncogene. 34: 537–45.

50. Tanaka, K., N. Mukae, H. Dewar, M. van Breugel, E.K. James, A.R. Prescott, C. Antony, T.U. Tanaka, V. Breugel, E.K. James, A.R. Prescott, C. Antony, and T.U. Tanaka. 2005. Molecular mechanisms of kinetochore capture by spindle microtubules. Nature. 434: 987–94.

51. Lampson, M. a, K. Renduchitala, A. Khodjakov, and T.M. Kapoor. 2004. Correcting improper chromosome-spindle attachments during cell division. Nat. Cell Biol. 6: 232–7.

52. Liu, D., G. Vader, M.J.M. Vromans, M.A. Lampson, and S.M.A. Lens. 2009. Sensing chromosome bi-orientation by spatial separation of Aurora B Kinase from kinetochore substrates. Science. 323: 1350–1353.

53. Liu, D., and M.A. Lampson. 2009. Regulation of kinetochore-microtubule attachments by Aurora B kinase. Biochem. Soc. Trans. 37: 976–80.

54. DeLuca, J.G., W.E. Gall, C. Ciferri, D. Cimini, A. Musacchio, and E.D. Salmon. 2006. Kinetochore Microtubule Dynamics and Attachment Stability Are Regulated by Hec1. Cell. 127: 969–982.

55. Francisco, L., W. Wang, and C.S. Chan. 1994. Type 1 protein phosphatase acts in opposition to IpL1 protein kinase in regulating yeast chromosome segregation. Mol. Cell. Biol. 14: 4731–40.

56. Hsu, J.Y., Z.W. Sun, X. Li, M. Reuben, K. Tatchell, D.K. Bishop, J.M. Grushcow, C.J. Brame, J. a Caldwell, D.F. Hunt, R. Lin, M.M. Smith, and C.D. Allis. 2000. Mitotic phosphorylation of histone H3 is governed by Ipl1/aurora kinase and Glc7/PP1 phosphatase in budding yeast and nematodes. Cell. 102: 279–291.

57. Pinsky, B.A., C. V Kotwaliwale, Y. Sean, S.Y. Tatsutani, C.A. Breed, and S. Biggins. 2006. Glc7 / Protein Phosphatase 1 Regulatory Subunits Can Oppose the Ipl1 / Aurora Protein Kinase by Redistributing Glc7. Mol. Cell. Biol. 26: 2648–2660.

58. Khodjakov, A., and J. Pines. 2010. Centromere tension: a divisive issue. Nat. Cell Biol. 12: 919–23.

59. Pearson, C.G., E. Yeh, M. Gardner, D. Odde, E.D. Salmon, and K. Bloom. 2004. Stable Kinetochore-Microtubule Attachment Constrains Centromere Positioning in Metaphase University of North Carolina at Chapel Hill. Curr. Biol. 14: 1962–1967.

60. Marco, E., J.F. Dorn, P. Hsu, K. Jaqaman, P.K. Sorger, and G. Danuser. 2013. S. cerevisiae chromosomes biorient via gradual resolution of syntely between S phase and anaphase. Cell. 154: 1127–39.

61. Sprague, B.L., C.G. Pearson, P.S. Maddox, K.S. Bloom, E.D. Salmon, and D.J. Odde. 2003. Mechanisms of microtubule-based kinetochore positioning in the yeast metaphase spindle. Biophys. J. 84: 3529–46.

62. Gardner, M.K., C.G. Pearson, B.L. Sprague, T.R. Zarzar, K. Bloom, E.D. Salmon, and D.J. Odde. 2005. Tension-dependent Regulation of Microtubule Dynamics at Kinetochores Can Explain Metaphase Congression in Yeast. Mol. Biol. Cell. 16: 3764 –3775.

63. Maddox, P.S., K.S. Bloom, and E.D. Salmon. 2000. The polarity and dynamics of microtubule assembly in the budding yeast Saccharomyces cerevisiae. Nat. Cell Biol. 2: 36–41.

64. Gardner, M.K., and D.J. Odde. 2010. Stochastic simulation and graphic visualization of mitotic processes. Methods. 51: 251–6.

65. Gupta, M.L., P. Carvalho, D.M. Roof, and D. Pellman. 2006. Plus end-specific depolymerase activity of Kip3, a kinesin-8 protein, explains its role in positioning the yeast mitotic spindle. Nat. Cell Biol. 8: 913–923.

66. Varga, V., J. Helenius, K. Tanaka, A.A. Hyman, T.U. Tanaka, and J. Howard. 2006. Yeast kinesin-8 depolymerizes microtubules in a length-dependent manner. Nat. Cell Biol. 8: 957–62.

67. Skibbens, R. V., V.P. Skeen, and E.D. Salmon. 1993. Directional instability of kinetochore motility during chromosome congression and segregation in mitotic newt lung cells: A push-pull mechanism. J. Cell Biol. 122: 859–875.

68. Skibbens, R. V, C.L. Rieder, and E.D. Salmon. 1995. Kinetochore motility after severing between sister centromeres using laser microsurgery: evidence that kinetochore directional instability and position is regulated by tension. J. Cell Sci. 108: 2537–48.

69. Maddox, P., A. Straight, P. Coughlin, T.J. Mitchison, and E.D. Salmon. 2003. Direct observation of microtubule dynamics at kinetochores in Xenopus extract spindles: Implications for spindle mechanics. J. Cell Biol. 162: 377–382.

70. Brown, G.C., and B.N. Kholodenko. 1999. Spatial gradients of cellular phospho-proteins. FEBS Lett. 457: 452–4.

71. Guacci, V., E. Hogan, and D. Koshland. 1997. Centromere position in budding yeast: evidence for anaphase A. Mol. Biol. Cell. 8: 957–72.

72. Jin, Q.W., J. Fuchs, and J. Loidl. 2000. Centromere clustering is a major determinant of yeast interphase nuclear organization. J. Cell Sci. 113: 1903–12.

73. O'Toole, E.T., M. Winey, and J.R. McIntosh. 1999. High-Voltage Electron Tomography of Spindle Pole Bodies and Early Mitotic Spindles in the Yeast. Mol. Biol. Cell. 10: 2017–2031.

74. Li, X., and R.B. Nicklas. 1995. Mitotic forces control a cell-cycle checkpoint. Nature. 373: 630–632.

75. Stern, B.M., and A.W. Murray. 2001. Lack of tension at kinetochores activates the spindle checkpoint in budding yeast. Curr. Biol. 11: 1462–1467.

76. Li, R., and A.W. Murray. 1991. Feedback control of mitosis in budding yeast. Cell. 66: 519–531.

77. Walker, R.A., O. Brien, K. Pryer, M.E. Soboeiro, W.A. Voter, H.P. Erickson, and E.D. Salmon. 1988. Dynamic Instability of Individual Microtubules. J. Cell Biol. 107: 1437–1448.

78. Keating, P., N. Rachidi, T.U. Tanaka, and M.J.R. Stark. 2009. Ipl1-dependent phosphorylation of Dam1 is reduced by tension applied on kinetochores. J. Cell Sci. 122: 4375–4382.

79. Welburn, J.P.I., M. Vleugel, D. Liu, J.R. Yates, M.A. Lampson, T. Fukagawa, and I.M. Cheeseman. 2010. Aurora B Phosphorylates Spatially Distinct Targets to

Differentially Regulate the Kinetochore-Microtubule Interface. Mol. Cell. 38: 383–392.

80. DeLuca, K.F., S.M.A. Lens, and J.G. DeLuca. 2011. Temporal changes in Hec1 phosphorylation control kinetochore-microtubule attachment stability during mitosis. J. Cell Sci. 124: 622–34.

81. Akiyoshi, B., C.R. Nelson, J.A. Ranish, and S. Biggins. 2009. Analysis of Ipl1-mediated phosphorylation of the Ndc80 kinetochore protein in Saccharomyces cerevisiae. Genetics. 183: 1591–1595.

82. Grinstead, C.M., and J.L. Snell. 2006. Introduction to Probability. Second Edi. American Mathematical Society.

83. Sarangapani, K.K., B. Akiyoshi, N.M. Duggan, S. Biggins, and C.L. Asbury. 2013. Phosphoregulation promotes release of kinetochores from dynamic microtubules via multiple mechanisms. Proc. Natl. Acad. Sci. U. S. A. 110: 7282–7.

84. Chan, C.S., and D. Botstein. 1993. Isolation and characterization of chromosome-gain and increase-in-ploidy mutants in yeast. Genetics. 135: 677–91.

85. Pearson, C.G., P.S. Maddox, E.D. Salmon, and K. Bloom. 2001. Budding yeast chromosome structure and dynamics during mitosis. J. Cell Biol. 152: 1255–66.

86. Indjeian, V.B., and A.W. Murray. 2007. Budding Yeast Mitotic Chromosomes Have an Intrinsic Bias to Biorient on the Spindle. Curr. Biol. 17: 1837–1846.

87. Gupta, M.L., C.J. Bode, C.A. Dougherty, R.T. Marquez, and R.H. Himes. 2001. Mutagenesis of β-tubulin cysteine residues in Saccharomyces cerevisiae: Mutation of cysteine 354 results in cold-stable microtubules. Cell Motil. Cytoskeleton. 49: 67–77.

88. Kim, J., J. Kang, and C.S.M. Chan. 1999. Sli15 associates with the Ipl1 protein kinase to promote chromosome segregation in saccharomyces cerevisiae. J. Cell Biol. 145: 1381–1394.

89. Akiyoshi, B., C.R. Nelson, J.A. Ranish, and S. Biggins. 2009. Quantitative proteomic analysis of purified yeast kinetochores identifies a PP1 regulatory subunit. Genes Dev. 23: 2887–2899.

90. Liu, D., M. Vleugel, C.B. Backer, T. Hori, T. Fukagawa, I.M. Cheeseman, and M. a Lampson. 2010. Regulated targeting of protein phosphatase 1 to the outer kinetochore by KNL1 opposes Aurora B kinase. J. Cell Biol. 188: 809–20.

91. Joglekar, A.P., and A.J. Hunt. 2002. A simple, mechanistic model for directional instability during mitotic chromosome movements. Biophys. J. 83: 42–58.

92. Civelekoglu-Scholey, G., D.J. Sharp, a Mogilner, and J.M. Scholey. 2006. Model of chromosome motility in Drosophila embryos: adaptation of a general mechanism for rapid mitosis. Biophys. J. 90: 3966–82.

93. Gillespie, D.T. 1977. Exact Stochastic Simulation of Coupled Chemical Reactions. J. Phys. Chem. 81: 2340–2361.

94. Ault, J.G., and C.L. Rieder. 1994. Centrosome and kinetochore movement during mitosis. Curr. Opin. Cell Biol. 6: 41–49.

95. Funabiki, H., and A.W. Murray. 2000. The Xenopus chromokinesin Xkid is essential for metaphase chromosome alignment and must be degraded to allow anaphase chromosome movement. Cell. 102: 411–424.

96. Brouhard, G.J., and A.J. Hunt. 2005. Microtubule movements on the arms of mitotic chromosomes: polar ejection forces quantified in vitro. Proc. Natl. Acad. Sci., USA. 102: 13903–8.

97. Stumpff, J., M. Wagenbach, A. Franck, C.L. Asbury, and L. Wordeman. 2012. Kif18A and chromokinesins confine centromere movements via microtubule growth suppression and spatial control of kinetochore tension. Dev. Cell. 22: 1017–29.

98. O'Connell, C.B., J. Lončarek, P. Kaláb, and A. Khodjakov. 2009. Relative contributions of chromatin and kinetochores to mitotic spindle assembly. J. Cell Biol. 187: 43–51.

99. Straight, A.F., J.W. Sedat, and A.W. Murray. 1998. Time-lapse microscopy reveals unique roles for kinesins during anaphase in budding yeast. J. Cell Biol. 143: 687–694.

100. Savoian, M.S., M.K. Gatt, M.G. Riparbelli, G. Callaini, and D.M. Glover. 2004. Drosophila Klp67A is required for proper chromosome congression and segregation during meiosis I. J. Cell Sci. 117: 3669–77.

101. Mayr, M.I., S. Hümmer, J. Bormann, T. Grüner, S. Adio, G. Woehlke, and T.U. Mayer. 2007. The Human Kinesin Kif18A Is a Motile Microtubule Depolymerase Essential for Chromosome Congression. Curr. Biol. 17: 488–498.

102. Wargacki, M.M., J.C. Tay, E.G. Muller, C.L. Asbury, and T.N. Davis. 2010. Kip3, the yeast kinesin-8, is required for clustering of kinetochores at metaphase. Cell Cycle. 9: 2581–2588.

103. Savoian, M.S., and D.M. Glover. 2010. Drosophila Klp67A binds prophase kinetochores to subsequently regulate congression and spindle length. J. Cell Sci. 123: 767–76.

104. Ferenz, N.P., A. Gable, and P. Wadsworth. 2010. Mitotic functions of kinesin-5. Semin. Cell Dev. Biol. 21: 255–259.

105. Goshima, G., and R.D. Vale. 2003. The roles of microtubule-based motor proteins in mitosis: comprehensive RNAi analysis in the Drosophila S2 cell line. J. Cell Biol. 162: 1003–16.

106. Brust-Mascher, I., G. Civelekoglu-Scholey, M. Kwon, A. Mogilner, and J.M. Scholey. 2004. Model for anaphase B: role of three mitotic motors in a switch from poleward flux to spindle elongation. Proc. Natl. Acad. Sci. USA. 101: 15938–43.

107. Goshima, G., R. Wollman, N. Stuurman, J.M. Scholey, and R.D. Vale. 2005. Length control of the metaphase spindle. Curr. Biol. 15: 1979–88.

108. Goshima, G., R. Wollman, S.S. Goodwin, N. Zhang, J.M. Scholey, R.D. Vale, and N. Stuurman. 2007. Genes required for mitotic spindle assembly in Drosophila S2 cells. Science. 316: 417–21.

109. Clemens, J.C., C. a Worby, N. Simonson-Leff, M. Muda, T. Maehama, B. a Hemmings, and J.E. Dixon. 2000. Use of double-stranded RNA interference in Drosophila cell lines to dissect signal transduction pathways. Proc. Natl. Acad. Sci., USA. 97: 6499–503.

110. Maiato, H., C.E. Sunkel, and W.C. Earnshaw. 2003. Dissecting mitosis by RNAi in Drosophila tissue culture cells. Biol. Proced. Online. 5: 153–161.

111. Rieder, C.L., and H. Maiato. 2004. Stuck in division or passing through: What

happens when cells cannot satisfy the spindle assembly checkpoint. Dev. Cell. 7: 637–651.

112. Orth, J.D., Y. Tang, J. Shi, C.T. Loy, C. Amendt, C. Wilm, F.T. Zenke, and T.J. Mitchison. 2008. Quantitative live imaging of cancer and normal cells treated with Kinesin-5 inhibitors indicates significant differences in phenotypic responses and cell fate. Mol. Cancer Ther. 7: 3480–3489.

113. Mische, S., Y. He, L. Ma, M. Li, M. Serr, and T.S. Hays. 2008. Dynein Light Intermediate Chain : An Essential Subunit That Contributes to Spindle Checkpoint Inactivation. Mol. Biol. Cell. 19: 4918–4929.

114. Henikoff, S., K. Ahmad, J.S. Platero, and B. van Steensel. 2000. Heterochromatic deposition of centromeric histone H3-like proteins. Proc. Natl. Acad. Sci., USA. 97: 716–721.

115. Vale, R.D., J.A. Spudich, and E.R. Griffis. 2009. Dynamics of myosin, microtubules, and Kinesin-6 at the cortex during cytokinesis in Drosophila S2 cells. J. Cell Biol. 186: 727–738.

116. Goodwin, S.S., and R.D. Vale. 2010. Patronin regulates the microtubule network by protecting microtubule minus ends. Cell. 143: 263–74.

117. Brust-Mascher, I., P. Sommi, D.K. Cheerambathur, and J.M. Scholey. 2009. Kinesin-5 – dependent Poleward Flux and Spindle Length Control in Drosophila Embryo Mitosis. Mol. Biol. Cell. 20: 1749–1762.

118. Rogers, S.L., G.C. Rogers, D.J. Sharp, and R.D. Vale. 2002. Drosophila EB1 is important for proper assembly, dynamics, and positioning of the mitotic spindle. J. Cell Biol. 158: 873–884.

119. Demchouk, A.O., M.K. Gardner, and D.J. Odde. 2011. Microtubule Tip Tracking and Tip Structures at the Nanometer Scale Using Digital Fluorescence Microscopy. Cell. Mol. Bioeng. 4: 192–204.

120. Seetapun, D., B.T. Castle, A.J. McIntyre, P.T. Tran, and D.J. Odde. 2012. Estimating the Microtubule GTP Cap Size In Vivo. Curr. Biol. 22: 1681–1687.

121. Moore, D.S., and G. McCabe. 2009. Introduction to the practice of statistics. Sixth Edit. New York: WH Freeman and Company.

122. Paweletz, N. 2001. Walther Flemming: pioneer of mitosis research. Nat. Rev. Mol. Cell Biol. 2: 72–75.

123. Falchook, G.S., C.C. Bastida, and R. Kurzrock. 2015. Aurora Kinase Inhibitors in Oncology Clinical Trials: Current State of the Progress. Semin. Oncol. 42: 832–848.

124. Rosenfeld, S.S. 2015. Clinical Trials of Mitotic Kinesin Inhibitors. In: Kozielski F, editor. Kinesins and Cancer. Springer Netherlands. pp. 63–76.

125. Tang, Y., J.D. Orth, T. Xie, and T.J. Mitchison. 2011. Rapid induction of apoptosis during Kinesin-5 inhibitor-induced mitotic arrest in HL60 cells. Cancer Lett. 310: 15–24.

126. Kim, J., and P. Sudbery. 2011. Candida albicans, a Major Human Fungal Pathogen. J. Microbiol. 49: 171–177.

127. Sudbery, P., N. Gow, and J. Berman. 2004. The distinct morphogenic states of Candida albicans. Trends Microbiol. 12: 317–24.

128. Noble, S.M., and A.D. Johnson. 2007. Genetics of Candida albicans, a diploid human fungal pathogen. Annu. Rev. Genet. 41: 193–211.

129. Kojic, E.M., and R.O. Darouiche. 2004. Candida Infections of Medical Devices. Clin. Microbiol. Rev. 17: 255–267.

130. Kim, K., L. Zilbermintz, and M. Martchenko. 2015. Repurposing FDA approved drugs against the human fungal pathogen, Candida albicans. Ann. Clin. Microbiol. Antimicrob. 14: 1–11.

131. Joglekar, A.P., D. Bouck, K. Finley, X. Liu, Y. Wan, J. Berman, X. He, E.D. Salmon, and K.S. Bloom. 2008. Molecular architecture of the kinetochore-microtubule attachment site is conserved between point and regional centromeres. J. Cell Biol. 181: 587–94.

132. Burrack, L.S., S.E. Applen, and J. Berman. 2011. The requirement for the Dam1 complex is dependent upon the number of kinetochore proteins and microtubules. Curr. Biol. 21: 889–96.

# Appendix: Simulations of kinesin-5 mediated length control of kinetochore microtubules in *Candida albicans*

Portions of this appendix were reprinted with permission from *Molecular Biology of the Cell* (43). This appendix describes my contribution to the modeling section of:

McCoy, K.M., E.S. Tubman, A. Claas, D. Tank, S.A. Clancy, E.T. O'Toole, J. Berman, and D.J. Odde. 2015. Physical limits on kinesin-5 mediated chromosome congression in the smallest mitotic spindles. Mol. Biol. Cell. 26: 3999–4014.

*Candida* albicans is an infectious yeast that resides in the gastrointestinal tract and oral mucosa of most people (126). It is capable of switching morphological form from yeast to pseudohyphae to hyphae (believed to be the virulent form) under different environmental conditions (127). Under normal circumstances, *C. albicans* is harmless; however, bloodstream infections of *C. albicans* are extremely serious for immune-compromised individuals such as those with concurrent infection, malignancy, or inherited disease, causing death in up to 50% of cases (128). Additionally, *C. albicans* adhere to synthetic materials and thus are problematic for patients with medical devices (129). Infections due to *C. albicans* are the fourth most common hospital-acquired infection in the United States, and Medicare costs due to *C. albicans* exceed $1 billion annually (127, 130). Overall, infections from *C. albicans* are a huge public health concern, and better anti-fungals are critical to prevent death from infection in immune-compromised patients.

Besides *C. albicans'* clear clinical ramifications, it also serves as an excellent organism for comparison to the budding yeast *Saccharomyces cerevisiae*. Like *S. cerevisiae,* the *C. albicans* spindle is relatively simple, with only 16 chromosomes (32 kinetochores in diploid *C. albicans*) and a single kinetochore microtubule per kinetochore (131, 132). However, the *C. albicans* spindle at ~840 nm is just over half the length of

the *S. cerevisiae* spindle at ~1500 nm (12, 43). Despite the short *C. albicans* spindle, chromosome congression is still achieved, and like *S. cerevisiae,* kinesin-5 was found to facilitate chromosome congression by promoting length-dependent depolymerization of long kinetochore microtubules (43). In both fungi, partial knockdown of kinesin-5 results in longer and more variable kinetochore microtubules, thus impeding chromosome congression. In haploid *S. cerevisiae,* which has two kinesin-5 motors, Kipl1 and Cin8, *cin8Δ* mutants resulted in longer and more variable kinetochore microtubules (42). While in diploid *C. albicans,* which only has one kinesin-5 motor, Kip1, *KIP1/kip1Δ* mutants resulted in longer and more variable kinetochore microtubules (43). Thus, these results suggested that the same model of kinesin-5-mediated, length-dependent depolymerization of kinetochore microtubules to facilitate chromosome congression that was developed in *S. cerevisiae* could be applied to *C. albicans* with a few minor modifications, including a shorter spindle length. Therefore, we applied the model to both systems.

The simulation of the model included microtubule dynamics of kinetochore and interpolar microtubules and kinesin-5 motor binding and unbinding. All kinetochores remained attached to the kinetochore microtubules (no attachment or detachment); thus microtubules remained either kinetochore or interpolar microtubules throughout the simulation. Kinetochore microtubule rescue was tension-dependent and interpolar microtubule rescue was constant and high (61, 62). Kinesin-5 motors were allowed to bind and unbind microtubules and walk towards the plus ends of microtubules where they promoted catastrophe; thus both kinetochore and interpolar microtubule catastrophe was dependent on the number of motors present at the microtubule plus end (42). All parameters were obtained from the original *S. cerevisiae* simulation then

adjusted to fit the *C. albicans* spindle length and kinetochore microtubule distribution (Table X). We simulated both wild type and kinesin-5 mutant spindles of both fungi.

The catastrophe and rescue frequencies along the spindle were obtained as outputs of the simulation then averaged for the right and left halves, where zero is the spindle pole and 0.5 is the equator (Figure X). The intersection of catastrophe and rescue indicates the location where there is neither net growth nor net shortening of kinetochore microtubules; thus it forms attractor zones on either side of the equator that are the expected locations of kinetochore microtubule plus ends (Figure X). In *S. cerevisiae* wild type spindles, with a large number of kinesin-5 motors causing a steep catastrophe gradient, the intersection of catastrophe and rescue is approximately midway between the spindle pole and spindle equator and the histogram of kinetochore microtubule plus ends shows that the plus ends cluster at the expected attractor zones, ~0.3 from both spindle poles (Figure XA). In *S. cerevisiae cin8Δ* spindles, the number of kinesin-5 motors is reduced, resulting in both a weaker catastrophe gradient and rescue gradient where the intersection of catastrophe and rescue is closer to the equator (Figure XB). Not only is this expected to result in longer kinetochore microtubules but it is also expected to result in kinetochore microtubules with a larger variance in length. As expected, the histogram or kinetochore microtubule plus ends shows that the distribution of plus ends are on average closer to the equator and more spread within the spindle, indicating that the kinetochore microtubules are longer and more variable in length in *S. cerevisiae cin8Δ* spindles (Figure XB). The same trends in the catastrophe gradient and kinetochore microtubule plus-end locations are observed with *C. albicans* wild type (more motors, Figure XC) and *KIP1/kip1Δ* spindles (reduced motors, Figure XD) even though the *C. albicans* spindle is nearly half the length of the *S. cerevisiae* spindle. Altogether, these results corroborate experimental results, demonstrating that

kinesin-5-mediated, length-dependent depolymerization of kinetochore microtubules controls kinetochore microtubule length to facilitate chromosome congression and that reduced kinesin-5 levels result in longer and more variable kinetochore microtubules and impaired chromosome congression, consistent across both *S. cerevisiae* and *C. albicans* (42, 43).

**Simulation methods**

Simulations were run using MATLAB based on methods described previously (42, 61, 62). The only difference was that rather than using a Monte Carlo method with a constant time step allowing multiple events, a Gillespie first reaction method was used with a variable time step in which the event with the shortest time step was executed (93). Briefly, for *C. albicans* spindles, 32 kinetochore microtubules (16 from each spindle pole body) were simulated to allow each of the eight diploid chromosomes (i.e., 16 replicated chromosomes, for a total of 32 sister chromatids) a single attachment to each pole, and four total interpolar microtubules (two from each spindle pole body) were simulated (131). The spindle length was fixed at 840 nm to match the observed experimental mean spindle length (840 for wild type and 766 nm for the *KIP1/kip1Δ* simulation). As described in Sprague *et al.* (2003), only the plus ends of the microtubules were allowed to undergo dynamic instability because the majority of kinetochore microtubule dynamics take place at the plus ends (63), and the minus ends were fixed at the spindle pole bodies. Thirty motors were used to simulate wild type conditions and 10 to simulate *KIP1/kip1Δ* conditions. All simulations started with no initial motor attachments. All parameters for both conditions are given in Table X. Parameters for the *S. cerevisiae* simulations were taken directly from Gardner *et al.* (2008). All other simulation details were previously described (42, 61, 62).

**Table and Figure**

| Parameter description | Symbol | *C. albicans* WT parameter values | *C. albicans KIP1/kip1Δ parameter values* | *S. cerevisiae* WT parameter values | *S. cerevisiae cin8Δ* Parameter values | Units |
|---|---|---|---|---|---|---|
| Growth velocity | $V_g$ | 1.2 | 1.2 | 1.2 | 1.9 | $\mu$m/min |
| Shortening velocity | $V_s$ | 1.2 | 1.2 | 1.2 | 1.9 | $\mu$m/min |
| Chromatin spring constant | $\rho$ | 0.9 | 0.9 | 0.9 | 0.9 | $\mu m^{-1}$ |
| Basal rescue frequency | $k_{r,0}$ | 9 | 9 | 9 | 9 | $min^{-1}$ |
| Basal rescue frequency (iMTs) | $k_{r,0}$_iMT | 60 | 60 | 60 | 60 | $min^{-1}$ |
| Basal catastrophe frequency | $k_{c.0}$ | 2 | 2 | 2 | 2 | $min^{-1}$ |
| Catastrophe sensitivity factor | $\beta_m$ | 20 | 20 | 20 | 20 | $min^{-1}$ |
| Number of motors | $N_m$ | 30 | 10 | 90 | 20 | -- |
| Unloaded motor velocity | $\square_u$ | 100 | 100 | 100 | 100 | nm/sec |
| Motor stall force | $F_{stall}$ | 6 | 6 | 6 | 6 | pN |
| Motor spring constant | $\rho_m$ | 0.5 | 0.5 | 0.5 | 0.5 | pN/nm |
| Unloaded motor off-rate constant | $k_{off}$ | 0.3 | 0.3 | 0.3 | 0.3 | $sec^{-1}$ |

| | | | | | | |
|---|---|---|---|---|---|---|
| Motor on-rate constant | $k_{on}$ | 1 | 1 | 1 | 1 | $\mu M^{-1}sec^{-1}$ |
| Radius of 2nd motor head attach point relative to 1st motor head | $r_M$ | 40 | 40 | 40 | 40 | Nm |
| Critical force | $F_c$ | 6 | 6 | 6 | 6 | pN |
| Spindle length | -- | 0.84 | 0.77 | 1.6 | 1.4 | $\mu$m |

**Table X. Kinesin-5 model simulation parameters and values.** Reprinted with permission from Molecular Biology of the Cell and following the Attribution-Noncommercial-Share Alike 3.0 Unported Creative Commons License (http://creativecommons.org/licenses/by-nc-sa/3.0).

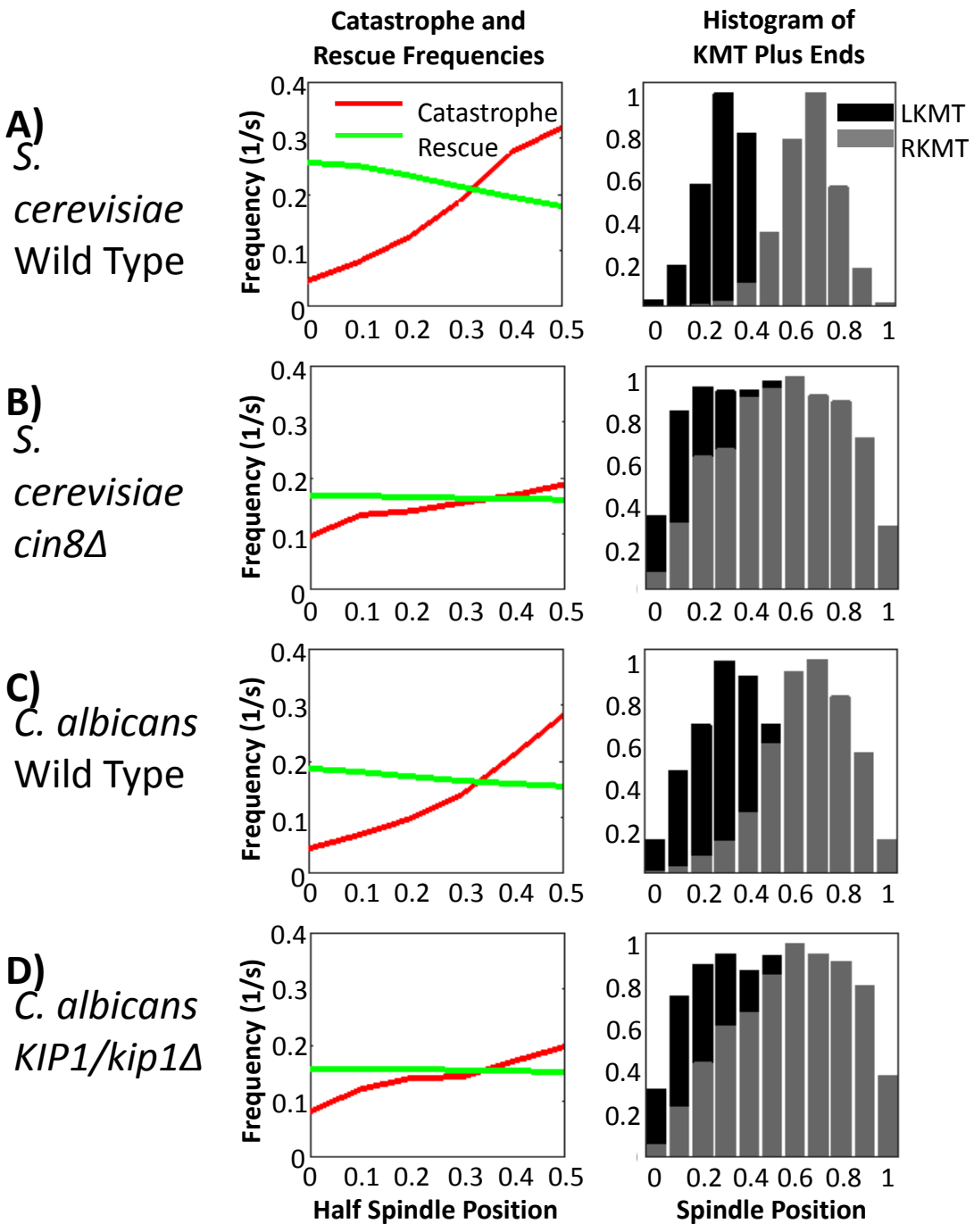


**Figure X. Simulated kinetochore microtubule catastrophe and rescue frequencies based on spindle position and histogram of plus-end positions.** Attractor zones formed by the intersection of catastrophe and rescue frequencies indicate the approximate mean location of kinetochore microtubule plus ends. LKMT denotes plus ends of kinetochore microtubules that grow from the left spindle pole; RKMT denotes plus ends of kinetochore microtubules that grow from the right spindle pole. A) *S. cerevisiae* WT shows an attractor zone located midway between

the spindle pole and the equator and tight clustering of plus ends at this location on either side of the spindle equator. B) *S. cerevisiae cin8*Δ shows a weaker catastrophe gradient relative to WT, which leads to a weaker attractor zone, longer and more variable kinetochore microtubule lengths, and thus weaker clustering of plus ends. C) *C. albicans* WT shows an attractor zone located slightly closer to the spindle equator compared with *S. cerevisiae* WT, leading to clustering of plus ends closer to the equator. D) *C. albicans KIP1/kip1*Δ shows a weaker catastrophe gradient relative to WT, which leads to a weaker attractor zone, longer and more variable kinetochore microtubule lengths, and thus weaker clustering of plus ends, as in *S. cerevisiae cin8*Δ**.** Reprinted with permission from Molecular Biology of the Cell and following the Attribution-Noncommercial-Share Alike 3.0 Unported Creative Commons License (http://creativecommons.org/licenses/by-nc-sa/3.0).